

NORTHWESTERN UNIVERSITY

Theory and Simulation of Polymer and Polyelectrolyte Self-Assembly

A DISSERTATION

SUBMITTED TO THE GRADUATE SCHOOL  
IN PARTIAL FULFILLMENT OF THE REQUIREMENTS

for the degree

DOCTOR OF PHILOSOPHY

Field of Materials Science and Engineering

By

Sharon Loverde

EVANSTON, ILLINOIS

June 2007

© Copyright by Sharon Loverde 2007

All Rights Reserved

## ABSTRACT

Theory and Simulation of Polymer and Polyelectrolyte Self-Assembly

Sharon Loverde

Polymers and polyelectrolytes are ideal tools for the development of novel self-assembled materials. The ability to control the length-scales of self-assembly, and thus the properties, for soft materials lies in the understanding and subsequent manipulation of competing intermolecular interactions, such as hydrophobicity, hydrogen bonding, van der Waals, electrostatics. In this thesis, computer simulation and theory describe two separate phenomena in soft condensed matter—polymer gelation, as well as pattern formation at interfaces by charged macromolecules.

A mean field theory of thermoreversible gelation is outlined, that incorporates a chemical approach to intermolecular interactions. For example, gels that form due to hydrogen bonding between polymer chains. Using Monte Carlo, the processes of chemical interactions, as well as physical interactions are used to describe gelation. Physical interactions refer to hydrogels, or gels that are formed through hydrophobic interactions. It is found that the mean field theory can be extended to describe physical gelation, by incorporating a concentration dependent association constant.

The self-assembly of oppositely charged, immiscible molecular components at interfaces is introduced. The theoretical behavior is outlined at low temperatures, by assuming the formation of finite, strongly segregated lamellar or hexagonal domains. At high temperatures, density fluctuations are examined to determine the transition from the disordered to microphase region.

Molecular dynamics simulations are designed to explore the phase behavior of this model at intermediate temperatures. The formation of lamellar and hexagonal domains are characterized. It is shown that the strength of the electrostatic interactions in competition with short range interactions determines the degree of interfacial ordering between the domains, and the periodicity, illustrating the transition between low and high temperatures. In addition, it is shown that for asymmetrically charged molecular components, increased electrostatic interactions can decrease the fluctuations in the local inter-domain structure. Molecular dynamics results are then be used in complement to theory, to describe the possibility of phase coexistence of the previous phases with a low charge density gas phase. It is found that the periodicity of the structure at intermediate temperatures can be well described, by accounting for the solid phase swelling at low densities.

## Acknowledgements

To begin with, I would like to acknowledge my advisor, Prof. Monica Olvera de la Cruz, most of all for her intuition, on so many levels, personal and scientific. Not only has she encouraged my scientific aspirations by encouraging me to travel, interact, and question those around me, but she has also shown me that creativity and logical deduction are inherently tied with science. Thank you, Monica. Next, I would like to thank the members of my committee, Prof. Ken Shull, Prof. Mark Asta, and Prof. Chris Wolverton, for their help and guidance.

I would like to thank various postdoctoral researchers whom have passed through the Olvera group. Primarily, Dr. Yuri Velichko, without whose help I would be lost in the world of programming syntax, defunct hard drives, and altogether frustrated. It will come from the sky, Yuri. Thank you. As well as Dr. Graziano Vernizzi, for a perpetual smile, eternal patience, and help in understanding numerous theoretical aspects of research. In addition, I would also like to thank Dr. Min Sun Yeom, for his initial computational guidance, as well as for his creative windows videos, Dr. Aleksander Ermoshkin, for an in-depth understanding of statistical mechanics of gelation and his notes on the Random Phase Approximation. In addition, Dr. Alex Kudlay, Dr. Hongxia Guo, Dr. William Kung, Dr. Dongsheng Zhang.

In addition, I would like to thank Dr. Francisco Solis. For his Mathematica knowledge, Murakami insights, and creative mathematical jokes. In addition, I would like to thank Dr. Mark Stevens for inspiring me to tackle some more complicated problems close to the end

of my thesis. I would like to thank Dr. Christian Holm, as well as his group members, Axel Arnold, Bernward Mann (†2006), for their expertise in Espresso. Also, Mehmet Sayar, Pim Schraven, and other members at the MPIP who acted as my guides.

Also, Olvera group members, in particular Dr. Michelle Lefebvre, Dr. Kurt Smith, Dr. Hao Cheng, Megan Greenfield and Kevin Kohlstedt, and recently Aurora Zinck. I wish all of them the best of luck in their research endeavors. Also, Aleta Hagman and Nelson Nunalee, from the Shull group. And Michelle again. Michelle for her eternal presentation guidance and open ears, Aleta for her eternal margaritas, and both of them for their friendship.

I would like to thank Mark Seniw, who will help guide all graduate students through their own maze in this department, and has been my angel on various occasions. In addition, Sharon Jacknow, Peggy Adamson, other members of the staff.

I would like to thank Katie Hamada, who has been a great friend and a simultaneous degree pursuer since we were both five, studying the art of piano performance. Jennifer Loudon, and Julia Carlson, for their miscellaneous advice over the years. Without meeting these intelligent women, I could not have maintained my motivation over the years.

And finally I would like to thank my family, Mike, Joyce, Gina, and David Loverde. My mom and dad for their endless encouragement and continuously positive attitudes. My brother and sister for exploring their own individual passions. Also, my Aunt Joan for her words of wisdom close to the end of my endeavors.

And, of course, I would like to thank Murat Guvendiren, who will hopefully always help me understand this world through his beautiful analogies. He and I would be nowhere in this world, and neither would science, without river currents, rootbeer, vegetable soup, holding your ear the hard way and, of course, apples on trees.

## Table of Contents

ABSTRACT	3
Acknowledgements	5
List of Tables	11
List of Figures	12
Chapter 1. Introduction	16
1.1. Research motivation	16
1.2. Thesis organization	19
Chapter 2. Selected Background	21
2.1. Polymer and polyelectrolyte theory	21
2.1.1. Flory theory for a single polymer chain	22
2.1.2. Poisson Boltzmann and Debye Hückel theory	25
2.1.3. An introduction to the Random Phase Approximation	27
2.2. Essential simulation techniques	29
2.2.1. Monte Carlo method	30
2.2.2. Molecular dynamics simulations	31
2.2.3. Common intermolecular potentials	33
2.2.4. Periodic boundaries	35

2.2.5. Efficient calculations of charged interactions	36
Chapter 3. Thermoreversible Polymer Gels	40
3.1. Introduction and background	40
3.1.1. Overview of gelation theory	42
3.1.2. Mean field theory	46
3.2. Monte Carlo for ideal gels	50
3.2.1. Thermoreversible chemical equilibrium	52
3.2.2. Diffusion limited case	59
3.3. Summary and conclusions	61
3.4. Acknowledgements	63
Chapter 4. A Model for Charged, Incompatible Mixtures at an Interface	64
4.1. Introduction and background	64
4.1.1. Experimental review	65
4.1.2. Theoretical overview	69
4.2. Development of a model for pattern formation	71
4.2.1. Scaling analysis at low temperatures	71
4.2.2. Scaling analysis at high temperatures	76
4.3. Summary and conclusions	79
4.4. Acknowledgements	79
Chapter 5. Molecular Dynamics of Pattern Formation	80
5.1. Introduction	80
5.2. Molecular dynamics of pattern formation at the interface	81

5.2.1.	Formation of lamellar phase	84
5.2.2.	Formation of hexagonal phase	91
5.2.3.	Asymmetric charge ratios and the Lindemann Criterion	98
5.3.	Summary and conclusions	103
5.4.	Acknowledgements	103
Chapter 6. Effects of Salt		105
6.1.	Introduction	105
6.2.	Salt effects on pattern formation	107
6.2.1.	Low temperature Debye Hückel limit	107
6.2.2.	High temperature limit	108
6.2.3.	Melting of the lamellar phase using molecular dynamics	109
6.3.	Multivalent ion condensation on patterned surfaces	114
6.3.1.	Theory of condensation	114
6.3.2.	Adsorbed ion phases using simulation	115
6.4.	Summary and conclusions	117
6.5.	Acknowledgements	118
Chapter 7. Phase Segregation on the Surface		119
7.1.	Introduction	119
7.2.	Theoretical model of phase segregation on the surface	122
7.2.1.	Free energy of the solid phase	123
7.2.2.	Free energy of the gas phase	125
7.2.3.	Construction of the two phase coexistence boundaries	130

	10
7.3. Molecular dynamics of phase coexistence	134
7.3.1. Phase coexistence and scaling	136
7.4. Summary and conclusions	140
7.5. Acknowledgements	141
Chapter 8. Summary and Extension of Work to More Complex Systems	142
8.1. Summary	142
8.2. Extension of work to more complex systems	145
8.3. Acknowledgements	148
References	149
Appendix. Vita	160

## List of Tables

4.1	Experimental systems that display pattern formation	69
5.1	Interparticle potentials	82

## List of Figures

2.1	Two polymers from chemistry and physics point of view	22
2.2	Gaussian distribution for polymer chain	23
2.3	Common intermolecular potentials for coarse-grained simulation	36
3.1	Schematic polymer gel phase diagram	41
3.2	Illustration of percolation model	43
3.3	Illustration of classical gelation theory	44
3.4	Gelation simulation snapshot	53
3.5	Thermodynamic results from simulation	54
3.6	Chain distribution function deviates from Gaussian	55
3.7	Molecular weight of clusters	56
3.8	Percent difference between theory and simulation	56
3.9	Fraction of chains in loops	57
3.10	Loop probability	60
3.11	Values of fitting parameter for physical gelation	61
4.1	AFM images of absorbed surfactant structures on silica	66
4.2	Fluorescence micrographs of a mixed phospholipid system	68

		13
4.3	Phase diagram for a ferromagnetic system	71
4.4	Cartoon of molecules strongly adsorbed to the interface	72
4.5	Schematic phase diagram	75
5.1	Mean square displacement	84
5.2	Diffusion constant	84
5.3	Snapshots of lamellar formation	85
5.4	Thermodynamic quantities during lamellar formation	86
5.5	Peak wave vector for lamellar case	87
5.6	Interfacial order parameter for lamellar case	89
5.7	Equilibrium domain shapes and size distribution for hexagonal case	92
5.8	Structure factor for hexagonal case	94
5.9	Structure factor finite size effects	95
5.10	Root mean square displacement for domain spacing	96
5.11	Mean square displacement for asymmetric charge ratio 3:1	97
5.12	Snapshots of hexagonal systems with different charge asymmetries	98
5.13	Ratio of the asymmetry of the domains as a function of the charge ratio	99
5.14	Root mean square displacement as a function of asymmetry	100
5.15	Heat capacity as a function of the charge ratio of the components	101
5.16	Mean square displacement for asymmetric charge ratios	102
5.17	Structure factor for different charge asymmetries	102

6.1	Cartoon illustrating salt surrounding the interface	105
6.2	Phase diagram with external screening	108
6.3	Behavior of peak wavevector from linear response theory	110
6.4	Simulation snapshots with external screening	111
6.5	Peak wavevector indicates a continuous melting of the system	111
6.6	Peak wavevector indicates macroscopic segregation	112
6.7	Possible phases for condensed ions	116
6.8	Molecular dynamics of condensed ion phases	117
7.1	Schematic phase diagram for phase coexistence	120
7.2	Rafts of charged particles adsorbed to the surface of a vesicle	121
7.3	Schematic of charge particle adsorption to the surface of an interface	123
7.4	Thermodynamic representation of two phase coexistence on the surface	130
7.5	Sample free energy plot, including short range and electrostatic terms.	132
7.6	Solid gas coexistence curves for symmetric mixtures	133
7.7	Solid gas coexistence curves for asymmetric mixtures	134
7.8	Solid gas coexistence curves for external screening	135
7.9	Molecular dynamics snapshots of phase coexistence	137
7.10	Thermodynamics quantities during segregation	138
7.11	Solid phase density for a wide range of parameters	139
7.12	Scaling of the peak wavevector	140

8.1	Schematic phase diagram	144
-----	-------------------------	-----

## CHAPTER 1

# Introduction

### 1.1. Research motivation

The principles of self-assembly are intrinsic to the development of unique, thermodynamically stable, and highly organized soft materials. Polymers and polyelectrolytes are essential tools to the field of self assembly. Just as imaging and characterization techniques improve down to smaller and smaller length scales, the ability to intelligently design bulk and surface organizational properties is simultaneously improving.

The classical picture of self-assembly is based on simple packing ratios of the amphiphilic molecules involved. By changing the shape of the molecule, such as the relative size of the hydrophilic portion of the molecule, or head group, to the tail length, one might predict a shift in the phase behavior of the solution. A simple surfactant can form a range of structures from spherical micelles to bilayers to vesicles [1]. For example, sodium dodecyl sulfate (SDS), a single chained surfactant with a large head group area, would be expected to pack in a spherical micelle, while other single chained lipids with smaller head group areas might be expected to pack into cylindrical micelles.

Surfactants are of widespread importance in the detergent industry and are well known for their use as emulsifying agents, lubricants, and for the stabilization of colloids in solution. One property of SDS is that the head group contains a charged sulfate group. When mixed with oil and water, this can change the phase behavior of the surfactant relative to other

nonionic surfactants [?]. However, the effect of increasing the ionic surfactant content on the relative elastic properties of these microemulsions in hydrophobic films is still not completely understood [?]. One unknown consists of the phase behavior of the charged surfactant at the oil water interface. This is just one example of how a simple property at the molecular level, in this case, the charged group on the head group of a surfactant, can influence the bulk properties of the system.

In many cases, it is the electrostatic interactions that promote the self-assembly of the system, such as in polyelectrolyte hydrogels. Depending on the polyelectrolyte concentration, pH, or solvent, an interconnected polymer network can be formed. The applications of hydrogels are diverse and range from scaffolds for tissue engineering [?] to smart materials that act as actuators or sensors [?]. In addition to synthetic gels, polymer gels are also found in the human body. As an example, the cytoskeleton that supports the cellular plasma membrane is a beautifully varied mechanical network. Its properties are based on the complexation of F-actin with other proteins [2].

Polyelectrolyte complexes, that is, complexes of cationic and anionic polyelectrolytes have long been studied for self-organization behaviors in aqueous solutions into complex ionic structures. Recently, complexes of polyelectrolytes with surfactants are showing more prominence in the engineering field, especially for their potentiality as pharmaceutical drug carriers [3] or in gene therapy [4]. The structure of oppositely charged biomolecular co-assemblies such as DNA-proteins in nucleosomes [5] and the actin-protein complexes in the cytoskeleton [6], are the result of the competition of short range interactions, including excluded volume, and electrostatics. Moreover, the complexation of proteins onto hydrophobic

or hydrophilic surfaces has exhibited the possibility of surface patterning due to electrostatic interactions [7]. Understanding the surface assembly of a complex group of charged components may lead to a greater deal of understanding concerning the stability of self-assembled aggregates, as well as give insight into the complex behavior of lipid rafts and their contribution towards protein sorting and cell signaling [8].

Cationic and anionic mixtures of lipids or peptide amphiphiles co-assembled into vesicles [9, 10] or cylindrical micelles [11, 12, 13] are examples of co-assemblies stabilized by hydrophobic interactions and electrostatics. The surfaces of such complexes of oppositely charged molecules may not be homogenous if the chemically co-assembled structures have net repulsive short range interactions among them, or if the charged surface components have different degrees of compatibilities with water. In this thesis, an ideal model of immiscible and oppositely charged molecular components at an interface will be developed theoretically, and explored with molecular dynamics simulations. This model will explore the possibility of charge heterogeneities at interfaces, with respect to temperature and concentration.

Theoretical techniques can examine the effects of simple changes in molecular architecture on the resulting interfacial concentration. While the variety of theoretical techniques, such as self consistent field theory [14] and mean field theory [15], continue to evolve and specialize to describe the nature of the system in question, computer simulation oftentimes provides additional insight into the problem. Simulation is the ideal tool that will bridge the gap between macroscopic continuum theory and the experimental systems. Within the construction of a simulation model, molecular details can be introduced at a coarse-grained level, without losing the ability to capture the underlying physics of the problem. Computer

simulation techniques will provide insight into the intelligent design of soft materials for a wide range of mechanical, chemical, and biological applications.

## 1.2. Thesis organization

The following chapter begins with an introduction to topics in polymer and polyelectrolyte theory that will be utilized during the course of this thesis. It covers necessary background information for simulation techniques, including Monte Carlo and molecular dynamics as applied to soft systems. Special attention will be given in an overview of current electrostatics techniques in simulation methods.

In Chapter 3, a theoretical model of polymer association and gelation is presented. The analytic results from this mean field theory are then compared with the results of coarse-grained Monte Carlo simulations. Within the simulations, two underlying mechanisms for gelation are considered—physical and chemical thermoreversible association. It is shown that, even at a very simple level, the classical mean field models must be modified to correctly describe the processes of physical gelation.

Next, the idea of self-assembly of oppositely charged, immiscible molecular components at interfaces is introduced in Chapter 4. This model system is described using strong segregation theory at low temperatures, as well as linear response theory at high temperatures. Molecular dynamics simulations are designed to test this model in intermediate temperature regimes. The complete phase diagram will be explored, in Chapters 5, 6, and 7. The formation of well-organized lamellar and hexagonal domains are characterized. It is shown that the strength of the electrostatic interactions determines the degree of interfacial ordering

between the domains. In addition, it is shown that for asymmetrically charged molecular components, the electrostatic interactions can even freeze the local domain structure. Molecular dynamics results will then be used in complement to analytical theory, in order to describe the possibility of phase coexistence of these patterned phases with a low charge density gas phase. Many systems display phase segregation on the interface due to competing interactions. This is of particular significance because the contribution of electrostatics to this possibility has not yet been thoroughly investigated.

## CHAPTER 2

### **Selected Background**

In this chapter, selected background to topics in basic polymer and polyelectrolyte theory are given that will be utilized in the course of this thesis. This is followed with a brief overview of Monte Carlo and molecular dynamics simulations. A basis for mean field gelation theory, presented in Chapter 3, is the Flory theory for an ideal polymer chain. This is introduced in Section 2.1.2. In Section 2.1.2, an introduction to electrostatic interactions is given in Section 2.1.3, a general overview of nonlinear and linear Poisson Boltzmann theory is given. Next, an outline for the Random Phase Approximation is presented in Section 2.1.3, as well as a discussion of its applicability to soft condensed matter systems. After these selected topics in polymer and polyelectrolyte theory, the conceptual basis behind Monte Carlo (Section 2.2.1) and molecular dynamics algorithms (Section 2.2.2) is discussed. Common intermolecular potentials for coarse-grained systems are given in Section 2.2.3. This is followed with a discussion of periodic boundaries in the simulation box in Section 2.2.4. The development of efficient methods to calculate electrostatic energy are critical to the simulation of soft condensed matter systems. An overview of current techniques will be discussed in Section 2.2.5.

#### **2.1. Polymer and polyelectrolyte theory**

A polyelectrolyte is a polymer that contains ionizable groups. In polar solvents, such as water, the polymer backbone dissociates from its respective counterions, which gain entropy

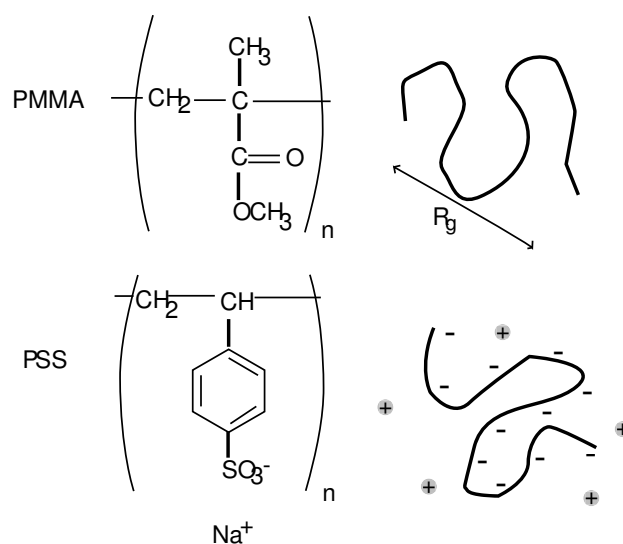


Figure 2.1. Illustration of Polymethyl methacrylate (PMMA) and Sodium polystyrene sulfonate (PSS) showing the chemical structure of the repeat unit. The physics point of view considers a polymer as a gaussian chain, with radius of gyration,  $R_g$ . The polymer is considered to have a uniform line charge, with counterions in solution.

upon interaction with the polar solvent. An example of a polyelectrolyte, Sodium Polystyrene Sulfonate (PSS), is illustrated in Fig. 2.2. PSS is used as a medication to treat Hyperkalemia, or high Potassium levels in the bloodstream. Other examples of polyelectrolytes include biological molecules, such as DNA, RNA, or polypeptides. One common attribute of water soluble polyelectrolytes is that they are associative. Furthermore, they have a propensity for forming polymer gels.

### 2.1.1. Flory theory for a single polymer chain

The properties and structure of polymers such as uncharged Polymethyl methacrylate (PMMA) and charged PSS are very diverse. From a chemical point of view, each bond and angle

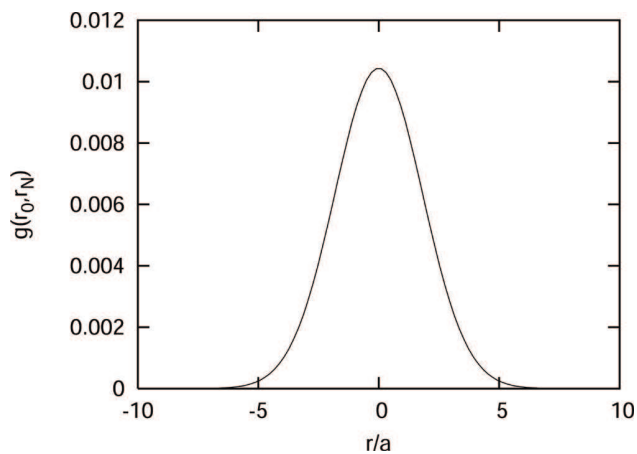


Figure 2.2. Distribution function between positions of monomer 0 and monomer  $N$  for a 10 unit length chain.

must be represented to differentiate the structure, and subsequent properties, of each polymer. However, simple models such as the standard Gaussian model of the polymer chain, as well as lattice models, reproduce many universal properties of polymer chains. Additionally, they are the easiest to investigate theoretically. If one considers a polymer chain of length  $N$  as the pathway of a random walk of steps  $a$ , the elastic or entropic energy can be written as

$$(2.1) \quad F_{ent}(r) = \frac{3k_B T r^2}{2Na^2}.$$

$k_B$  is the Boltzmann constant,  $T$  is the temperature, and  $r$  is the distance between the positions of monomer 0 and  $N$ . The distribution function,  $g(r_0, r_N)$  between the positions of monomer 0 and  $N$  is Gaussian

$$(2.2) \quad g(r_0, r_N) = \left( \frac{3}{2\pi Na^2} \right)^{\frac{3}{2}} e^{-\frac{3r^2}{2a^2N}}.$$

In a real polymer solution, one must take into account the polymer solvent interactions. Also, the molecules cannot interpenetrate one another. The Flory [16] theory of a single polymer chain is based upon a competition between the internal volume interactions of the monomers, as well as the entropic nature of a polymer chain.

$$(2.3) \quad F = F_{int} + F_{ent}$$

The internal free energy can be expanded in terms of the virial interaction coefficients,

$$(2.4) \quad F_{int} = Nk_B T(vB + v^2C + \dots)$$

$$(2.5) \quad B = \int_0^\infty 1 - \exp(-U(r)/k_B T) d^3r.$$

Here,  $B$  is the second virial coefficient,  $C$  is the third order virial coefficient, and  $v$  represents the excluded volume between two monomers [?]. The virial coefficient between two monomers  $i$  and  $j$  is proportional to  $1 - 2\chi$  where  $\chi$  represents the net chemical incompatibility between two monomer types,

$$(2.6) \quad \chi k_B T = \frac{1}{2}(2\varepsilon_{ij} - \varepsilon_{ii} - \varepsilon_{jj}).$$

Here,  $\varepsilon_{ij}$  is the magnitude of the attraction between components  $i$  and  $j$ . In particular solvents, for a value of  $\chi = 1/2$  at the theta temperature ( $\theta_T$ ), the value of the second order virial coefficient,  $B$  vanishes. In this limit, the ideal Gaussian chain is recovered. In Chapter 3, the ideal model of thermoreversible gelation is presented is based on this concept.

### 2.1.2. Poisson Boltzmann and Debye Hückel theory

The behavior of a single chain must be modified for the case when it contains ionizable groups. The electrostatic repulsion between the charged groups increases the persistence length of the polymer chain. Scaling analysis can be extended, as in the neutral polymer case, to incorporate the electrostatic energy of a polymer coil and determine the lengthscale at which the polymer can essentially be treated as a rigid rod. This limit can be used as an accurate model for polymers with a large persistence length, such as actin filaments where the persistence length is in the range of  $10 - 20 \mu m$  or DNA where the persistence length is  $50 nm$  [2].

Consider a rigid rod of line charge density  $\lambda$  with a surrounding counterion or salt distribution in a cylindrical shell. If the configuration of the polymer is assumed to be fixed, one can examine the counterion as well as the salt distribution in solution. Two main approaches involve the linear and nonlinear solutions to the Poisson Boltzmann (PB) equation. The approach assumes a mean counterion density,  $n(r)$ , based on the Boltzmann distribution.

$$(2.7) \quad n(r) = n(R) \exp(-e\psi(r)/k_B T)$$

where  $\psi(r)$  is the electrostatic surface potential, and, in a particular geometry of boundary  $R$ , in this example a cylindrical shell, one finds the solution to the Poisson equation,

$$(2.8) \quad \nabla^2 \psi(r) = \frac{d^2}{dr^2} + \frac{1}{r} \frac{d}{dr} = -\frac{1}{\epsilon_0} n(r).$$

The potential is normalized so that  $\psi(R) = 0$ . Here,  $e$  is the unit of electronic charge and  $\epsilon$  is the dielectric permittivity of the medium. For a detailed discussion of a solution to the

PB equation in cylindrical and other geometries, for both salt-free and salt cases, please see Ref. [17]. The fundamental lengthscale of the electrostatic strength is the Bjerrum length,  $l_B$ , given by,

$$(2.9) \quad l_B = \frac{e^2}{4\pi\epsilon_0 k_B T}.$$

In water, the Bjerrum length, or lengthscale over which the electrostatic interactions is equivalent to  $k_B T$ , is approximately 7 Å. The Manning parameter,  $\xi$ ,

$$(2.10) \quad \xi = \lambda l_B / e$$

is a dimensionless quantity that measures the relative strength of the line charge density. For values of  $\xi$  more than 1, the solution to the PB equation describes a condensed layer on the surface of the macromolecule. This is known as Manning condensation. PB theory fails most noticeably in the following cases—when considering multivalent counterions, at high charge densities, and high values of the surface potential. In these cases, some corrections can be accounted for by allowing for correlation effects within the free energy density.

Nevertheless, at physiological conditions, there is a screening effect due to the salt ions in solution. The distribution of salt ions can be written as

$$(2.11) \quad \rho(r) = \sum_i z_i n_i(R) \exp(-ez_i \psi_i(r)/k_B T)$$

It is possible to consider a linearized version to the PB equation. In this case, the exponent can be expanded when the surface potential is low compared with  $k_B T$ , so that

$$(2.12) \quad \rho(r) = \frac{\sum_i z_i^2 n_i(R) \psi(r) e^2}{\epsilon_0 k_B T}$$

where  $\kappa$  is the Debye length of the solution defined by the concentration of ions in solution,

$$(2.13) \quad \kappa = \left( \frac{4\pi l_B \sum_i z_i^2 n_i(R)}{\epsilon_0 k_B T} \right)^{\frac{1}{2}}$$

The spherical solution to the Poisson equation in this case gives the well known Debye Hückel potential,

$$(2.14) \quad \psi(r) = l_B \frac{\exp(-\kappa r)}{r}.$$

With the integration of this potential, the Debye Hückel correction to the free energy is obtained as

$$(2.15) \quad \frac{F_{el}}{k_B T} = \frac{-\kappa^3}{12\pi}.$$

### 2.1.3. An introduction to the Random Phase Approximation

The Random Phase Approximation (RPA) is a linear response theory, used for polymer solutions, for example, semi-dilute polyelectrolyte solutions [18], or polymer blends [19], in which polymer chains are treated as Gaussian and ideal, and then a small perturbation is added, such as electrostatics or net interaction between monomers. This is a general technique that works well when the system is at high temperatures and fluctuations in the system dominate. All density fluctuations are considered in an isotropic manner. To begin

with, the free energy is expanded in terms of the density fluctuations over all space.

$$\begin{aligned}
 F &= \int f(\rho(r)) d^3r \\
 (2.16) \quad &= \int \left( f(\bar{\rho}) + \frac{1}{2} \frac{\partial^2 f}{\partial \rho^2} \Big|_{\bar{\rho}} (\rho(r) - \bar{\rho})^2 + \frac{1}{3!} \frac{\partial^3 f}{\partial \rho^3} \Big|_{\bar{\rho}} (\rho(r) - \bar{\rho})^3 \right) d^3r
 \end{aligned}$$

Next, the free energy is expanded in the Fourier components of the density, so that

$$(2.17) \quad \rho_k = \int \rho(r) \exp(ikr) d^3r$$

$$(2.18) \quad \rho(r) = \frac{1}{V} \rho_k \exp(-ikr).$$

In this case, we can write the free energy up to the second order terms, which is what the RPA limit refers to, as

$$(2.19) \quad F = F(\bar{\rho}) + \frac{1}{2V} \sum_k U_k \rho_k \rho_{-k} + \dots$$

where  $U_k$  is the fourier representation of the interaction energies. If the free energy is expanded to higher order terms and solved self-consistently this is known as the Hartree Approximation, which can be applied to dilute polyelectrolyte solutions, but also works for other polymer systems, such as block copolymer polymer melts [20, 21]. Upon substitution

in the partition function we obtain,

$$(2.20) \quad Z = \int \exp(-F(\bar{\rho} + \dots)) \prod_k d\rho_k$$

$$(2.21) \quad = Z_0 \prod_{k>0} \left( \frac{U_k + \rho^{-1}}{\rho^{-1}} \right)^{-1}$$

$$(2.22) \quad = Z_0 \prod_{k>0} S(k)^{-1}$$

where  $S(k)$  is the structure factor and  $Z_0$  represents the  $k = 0$  contributions and other constants. In three dimensions, calculation of the free energy from the above partition function gives the same correction to the free energy as in Eq. 2.15. This same technique will be applied in Chapter 7 to obtain the correction to the free energy, but for charges at a surface or an interface.

## 2.2. Essential simulation techniques

To understand the full thermodynamic behavior of the system, one needs the complete partition function. However, obtaining an accurate representation of all the configurations of the system is nearly impossible for complex polymeric and biological systems. The simulation technique used to study the phenomenon of interest should be chosen based on the length-scales and time scales of interest—ab initio methods, atomistic simulations, or else coarse-grained simulations. For the scientific field of self-assembly, since one is interested in how microscopic behavior affects the bulk thermodynamic and structural quantities, larger lengthscales—on the range of several hundred nanometers to micrometers—are necessary, so one appropriate method consists of using coarse-grained molecular simulation, in order to

incorporate the essential physical parameters of the model, without including all atomistic levels of detail.

In this section, a general overview of Monte Carlo and molecular dynamics simulations are given in Section 2.2.1 and 2.2.2. The basic principles behind Monte Carlo and molecular dynamics simulations are discussed briefly, followed by some classic examples of intermolecular pair potentials common in soft systems in Section 2.2.3. Section 2.2.4 continues with a discussion of the calculation of the electrostatic contribution to the energy.

### 2.2.1. Monte Carlo method

The Monte Carlo simulation method is an efficient method to sample all the configurations, or else the phase space, of the components in your system. Efficient Monte Carlo techniques are based on the principle of importance sampling [22, 23, 24] meaning that the frequency with which a configuration state is sampled is weighted by how important the state is, or else, what the associated energy of the state is. If one is to write this mathematically, the average value of  $A$  at some point in space  $r^N$  is given by

$$(2.23) \quad \langle A \rangle = \frac{\int dr^N \exp\left(\frac{U(r^N)}{k_B T}\right) A(r^N)}{\int dr^N \exp\left(\frac{U(r^N)}{k_B T}\right)}$$

where the partition function is

$$(2.24) \quad Z = \int dr^N \exp\left(\frac{U(r^N)}{k_B T}\right)$$

and

$$(2.25) \quad P(r^N) = \exp\left(\frac{U(r^N)}{k_B T}\right) / Z$$

represents the probability density to find the system in state  $r^N$ . In order to derive the classic Metropolis algorithm, the idea of importance sampling can be combined with the principle of detailed balance. Detailed balance implies that the probability to go from state 0 to state  $n$ ,  $W(0 \rightarrow n)$  given that one is in state 0,  $P(0)$ , must be equivalent to the probability to go from state  $n$  to state 0,  $W(n \rightarrow 0)$  given that one is in state  $n$ ,  $P(n)$ . Or else,

$$(2.26) \quad W(0 \rightarrow n)P(0) = W(n \rightarrow 0)P(n).$$

From this, one can derive the acceptance probability for one Monte Carlo step.

$$(2.27) \quad W(0 \rightarrow n) = \begin{cases} \exp\left(-\left(\frac{U(n)}{k_B T} - \frac{U(0)}{k_B T}\right)\right) & \Delta U > 0 \\ 1 & \Delta U < 0 \end{cases}$$

Thus, if the change in energy associated with the move is negative, the move is always accepted, else, if the change in energy is positive, a random number in the range  $(0, 1)$  is generated. If this random number is less than the above acceptance ratio, the move is accepted.

### 2.2.2. Molecular dynamics simulations

Molecular dynamics simulations offer a unique way to investigate the dynamical properties of classical systems. The microscopic state of the system is defined in terms of the positions and the velocities of the ions. The principle calculation of molecular dynamics is the calculation of

the force acting on every particle, in order to best approximate Newton's equations of motion. Since the force is the derivative of the potential, the more complicated the intermolecular potentials, the more time-consuming this step is. For this reason, coarse-grained potentials are kept as simple as possible while still capturing the basic physics of the system.

The most common algorithm for generating equilibrium dynamics of the system in a microcanonical ensemble (NVE) involves a Taylor expansion of the positions and momentums of a particle with respect to time, and it is referred to as the velocity Verlet algorithm. This algorithm has the special characteristics that it is both time reversible and area preserving in phase space [22], meaning that there is a smaller error for long term energy conservation. The position and momentum at time  $t'$  with a timestep  $\delta t$  from the initial time  $t$  can be written as

$$\begin{aligned}
 r(t + \delta t) &= 2r(t) - r(t - \delta t) + 2v(t)\delta t + \frac{f}{m}(\delta t)^2 \\
 v(t) &= \frac{r(t + \delta t) - r(t - \delta t)}{2\delta t}
 \end{aligned}
 \tag{2.28}$$

The goal of molecular dynamics simulations is to generate a simulation long enough to ensure good statistical averages. In addition, useful molecular dynamics often involves ensembles other than the microcanonical ensemble—for instance, NVT or else NPT ensembles. For thermostats, there are several choices based on different approaches. The Nosé-Hoover thermostat is based on an extended Lagrangian approach by adding an additional coordinate to the classical equations. Another approach is to use the Langevin thermostat, which is based on the principle that the system is coupled to an external heat bath, which keeps it at a constant temperature. Another approach is to use dissipative particle dynamics

(DPD) [25], that obeys both conservation of momentum, as well as incorporates the correct hydrodynamics.

The Langevin thermostat [26] incorporates a frictional force, as well as a random force as follows

$$(2.29) \quad m_i \ddot{r}_i = -\nabla U(i,r) - \Gamma \dot{r}_i + \xi_i(t)$$

where  $\xi_i$  is a Gaussian noise source supplied by the heat bath.

$$(2.30) \quad \langle \xi_i(t) \rangle = 0$$

$$(2.31) \quad \langle \xi_i(t) \xi_i(t') \rangle = \delta_{ij} \delta(t - t') 6k_B T \Gamma$$

### 2.2.3. Common intermolecular potentials

Some common intermolecular pair potentials for coarse-grained simulations are illustrated in Fig. (2.3, including the square well potential (a), Lennard Jones 6 – 12 potential (b), finite extensible nonlinear elastic (FENE) potential [?] (c), Coulomb potential (d), and Debye Hückel potential. A square well potential between two particles  $i$  and  $j$  is simply

$$(2.32) \quad U_{ij} = \begin{cases} \infty & r_{ij} < \sigma \\ -\varepsilon & \sigma < r_{ij} < r_c \\ 0 & r_{ij} > r_c \end{cases}$$

Oftentimes it is referred to as a sticky potential. Another classic potential is the Lennard Jones potential, which is used in a variety of systems, to explore solid liquid phase diagrams [27], as well as to represent van der Waals interactions for soft systems. The Lennard Jones

potential is

$$(2.33) \quad U_{ij} = \begin{cases} 4\varepsilon \left( \left( \frac{\sigma}{r_{ij}} \right)^{12} - \left( \frac{\sigma}{r_{ij}} \right)^6 \right) & r_{ij} < r_c \\ 0 & r_{ij} > r_c \end{cases}$$

In molecular dynamics simulations, it is important that this potential, in addition to being truncated at  $r_c = 2^{1/6}\sigma$  is also shifted, so that the intermolecular forces are always finite. Another common intermolecular potential for soft systems is the finite extensible nonlinear elastic, or Fene, potential. This is often used to model polymer chains, as it incorporates the excluded volume of each polymer bead with a finite bonded lengthscale. The Fene potential is as follows

$$(2.34) \quad U_{ij} = -0.5KR_0^2 \ln \left( 1 - \frac{r_{ij}^2}{R_0^2} \right) + 4\varepsilon \left( \left( \frac{\sigma}{r_{ij}} \right)^{12} - \left( \frac{\sigma}{r_{ij}} \right)^6 \right) + \varepsilon$$

For this potential, the finite length of the bond is represented by  $R_0$  while the Lennard Jones type interaction is cut at  $r_c = 2^{1/6}\sigma$ . The stiffness of the bond is determined by the magnitude of  $K$ . Two more potentials of interest consist of the Coulomb potential, as well as the Debye Hückel potential. The Coulomb potential

$$(2.35) \quad U_{ij} = \frac{l_B q_i q_j}{r_{ij}}$$

where the Bjerrum length,

$$(2.36) \quad l_B = \frac{e^2}{4\pi\epsilon k_B T}$$

and  $\epsilon$  is the dielectric constant of the medium. The Debye Hückel potential is a correction to the Coulomb potential

$$(2.37) \quad U_{ij} = \frac{l_B q_i q_j \exp(-\kappa r)}{r_{ij}}$$

where  $\kappa^{-1}$  represents the Debye screening length, determined by the concentration of salt in the medium,  $c_{salt}$ .

$$(2.38) \quad \kappa^2 = 4\pi z^2 l_B c_{salt}.$$

$z$  represents the valency of  $z : z$  salt. At physiological conditions,  $c_{salt}$  is around 0.1M, which corresponds to a screening length,  $\kappa^{-1}$ , of 1 – 2 nm.

#### 2.2.4. Periodic boundaries

As the goal of simulation is to represent the microscopic particles to the macroscopic properties of the system, every simulation is fundamentally limited by the sheer number of particles or atoms or molecules represented. In order to more accurately represent a bulk sample, the boundaries of the simulation box may be treated as periodic. In this case, each simulation box is reproduced and translated to obtain a number of neighboring boxes so that every particle has a corresponding twenty six images for three dimensional periodic boundaries, nine images for a two dimensional simulation. The energy is calculated by summing over every pair within the original cell, as well as the interaction of the particle with its images.

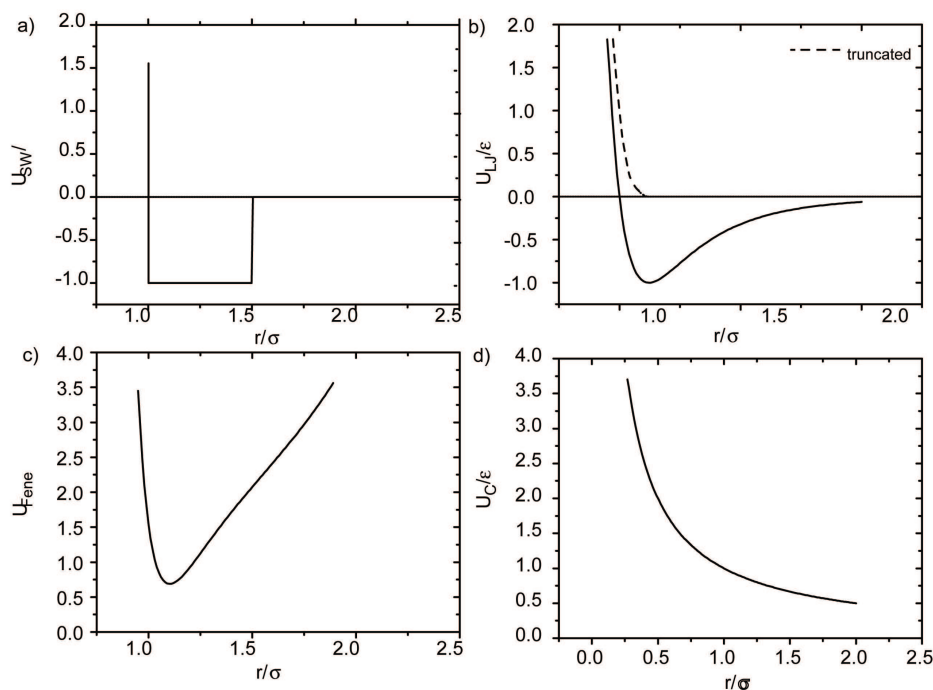


Figure 2.3. Common intermolecular potentials for coarse-grained simulation. a) Square well potential. b) Lennard Jones 6-12 potential. Dashed line represents the truncated and shifted version, including only the repulsive portion of the potential. c) Fene potential d) Repulsive  $1/r$  Coulomb potential.

### 2.2.5. Efficient calculations of charged interactions

While at first glance the calculation of the electrostatic energy from the partition function may at first seem to be fundamentally simple, since the electrostatic energy is additive and is the pairwise sum of all the charged particles in the system. However, there are several complications involved including the distribution of counterions in the system, the effects of the salt in the medium, and the long-range nature of the interaction. Most polyelectrolytes are dissolved in water, certain charged groups disassociate. In addition, the water molecules

themselves carry a dipole moment. Both of these effects can interact and change the local dielectric constant close to an interface.

While computational techniques accounting for these complexities exist, efficient methods are still within their infancy. Computational methods incorporating discontinuities in the dielectric constant exist, in which the image charge is modelled explicitly for two dielectric media [28]. However, this method fails when the charges approach the boundary between the two dielectrics. For ionic solutions, methods have been introduced that accounts for the salt concentration dependence of the dielectric permittivity [29]. In addition, recent algorithms have been investigated for both Monte Carlo [30] and molecular dynamics [31] that incorporate electrodynamic equations on a local scale. In general, it is agreed that incorporation of efficient algorithms into molecular dynamics is more effective than with Monte Carlo [30], simply because the electrostatic interactions between components are calculated simultaneously with molecular dynamics. In Monte Carlo the interactions need to be calculated before and after every Monte Carlo step for each individual particle.

Considering a set of  $N$  particles with charges  $q_i$  in a cubic simulation box of length  $L$  and volume  $L^3$ , including the periodic boundary conditions, the total electrostatic energy is

$$(2.39) \quad E = \frac{1}{2} \sum_{i,j=1}^N \sum'_{n \in Z^3} \frac{q_i q_j}{f_{ij} + nL}$$

The case  $n = 0$  for  $i = j$  is not included in the sum. This is denoted by the ' in the second summation. This sum is conditionally convergent [32] and is dependent on the shape of the simulation box, as well as the electrostatic properties of the outside medium, whether it is a vacuum, dielectric, conductor. The motivation for Ewald summation [33] lies in the separation of the potential into real and fourier terms at a particular cutoff, allowing

for faster convergence of this sum. This is conventionally done by considering a Gaussian screening function of opposite charge around each point charge. The interaction of the point charge and its screening function of opposite charge is included in the real space sum,  $E_r$ , along with a correction due to the self energy of the charges,  $E_s$ . The fourier term,  $E_k$ , then consists of a long range correction for the screening function. In addition, there is a dipole correction term,  $E_d$ , that is dependent on the dielectric constant of the outside medium,  $\epsilon$ .

More explicitly,

$$(2.40) \quad E_r = \frac{1}{2} \sum_{i,j} \sum_{m \in Z^3} q_i q_j \frac{\text{erfc}(\alpha|r_{ij} + mL|)}{r_{ij} + mL}$$

$$(2.41) \quad E_k = \frac{1}{2L} \sum_{k \neq 0} \frac{4\pi}{k^2} e^{-k^2/4\alpha^2} |\rho(k)|^2$$

$$(2.42) \quad E_s = -\frac{\alpha}{\sqrt{\pi}} \sum_i q_i^2$$

$$(2.43) \quad E_d = \frac{2\pi}{(1 + 2\epsilon)L^3} \left( \sum_i q_i r_i^2 \right)^2$$

The inverse length,  $\alpha$ , determines the point at which the sum switches from real space to fourier space, and can be used to tune the accuracy of the summation.

While splitting the sum into real and fourier parts allows for the faster convergence of the electrostatic energy, the algorithm still scales like  $N^{3/2}$ , where  $N$  is the number of particles in the simulation box. Some additional techniques involve the transformation of the charge density onto a grid so that fast fourier transformation (FFT) techniques can be used to

calculate the  $k$  space term. The methodology is known as particle mesh Ewald (*PME*) [34], which reduces the scaling to  $N\log(N)$ .

For many materials science problems, such as membranes, absorption onto surfaces, interfaces, etc, the relevant system of interest is periodic in only two of the three dimensions. While an analog to the three dimensional Ewald technique exists in two dimensions [35], this method is much slower due to the decoupling of the directions parallel to the surface or interface ( $x, y$  directions) and perpendicular ( $z$ ) directions. Two alternatives to this method are convergence techniques [36] (MM2D), and also a correction to the mesh summation discussed previously by subtracting out the periodic contribution due to the images in the third ( $z$ ) direction. This is also known as the electrostatic layer correction [37] (ELC) and will be the technique used in later chapters to sum the electrostatic energy. In this technique, the charged particles are confined within a central slab within the simulation box. The efficiency can be compared to other two dimensional techniques, and it is found that ELC is more efficient for larger systems [38].

## CHAPTER 3

**Thermoreversible Polymer Gels****3.1. Introduction and background**

Associative polymers possess many unique applications in the field of materials science—cosmetics, pharmaceuticals, coatings, treatment and recovery for environmental issues. Supramolecular assembly and new polymer synthesis techniques have greatly increased potential engineering capabilities [39, 40]. The possibility of synthesizing chains with end groups capable of forming thermoreversible links by means of hydrogen bonding [41, 42, 43], physical bonding [44, 45, 46, 47], fluorinated endgroups [48], or DNA-based monomers [49] has led to the discovery of new materials with thermoreversible associating properties, which can be useful for designing novel biological or smart materials [50].

The nature of the polymer-polymer interactions, in addition to the polymer-solvent interactions, determines the polymer chain conformation, and thus the microscopic structure of the solution. However, the resulting macroscopic behavior for associative polymers is generally similar [19]. After a certain concentration, these molecules form an interconnected polymer network or gel. This network coincides with an associated increase in the shear modulus of the polymer gel. Together, this corresponding change in the microscopic ordering of the molecules, in addition to the following macroscopic behavioral change, is known as the sol-gel transition [51]. A schematic phase diagram is illustrated in Fig. 3.1. The dashed line corresponds to the sol-gel transition. Generally, polymer gels are divided into

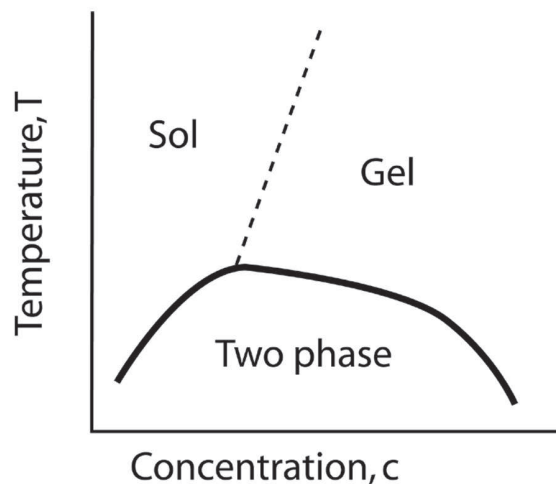


Figure 3.1. Schematic phase diagram for a polymer gel versus temperature and concentration.

two types. A chemical gel, such as vulcanized rubber, is formed by polymerization of the units, or else an epoxy resin, is formed by cross-linking an entangled melt of polyisoprene. A physical gel, such as a triblock copolymer hydrogel, forms upon changing the nature or concentration of the solvent or else the temperature of the system. While both chemical and physical gels maintain a long history in the field of materials science and self-assembly, physical gels, or self-assembled gels, are gaining momentum due to their increased propensity for biological applications. While physical gel formation may be characterized by the strength of the hydrophobic interactions and possesses a diffusion limited nature, chemical gel formation lies in a distinct quantum mechanical probability of association. Yet, from a theoretical standpoint, how the nature of these interactions should be distinguished in their theoretical approach is unclear. In order to gain insight into this question, a Monte Carlo simulation was developed to test how mean field theory describes the thermodynamic properties, as well as the microscopic aggregation behavior, of simple polymer gels in both

the chemical and physical gelation regime. In this model, a polymer molecule is treated as a phantom telechellic—only the ends of the molecule can associate and there are no excluded volume effects. It has been suggested that, should the effects of excluded volume interactions be small, mean field behavior should still be observed [52]. In the manner, by consistently varying the potential of short range interaction, several fundamental questions concerning the sol-gel transition can be addressed.

The chapter is organized as follows. To begin with, a general overview of gelation theory, including percolation theory, classical gelation theory introduced by Flory and Stockmayer, as well as more current approaches. Next, a mean field theoretical approach of thermoreversible gelation that includes the possibility of loop-like structures is outlined. A model is developed for Monte Carlo simulations that can be directly compared with analytic results, incorporating different algorithms for chemical and physical association. In the conclusion, limitations of this model and other current models are discussed.

### 3.1.1. Overview of gelation theory

A simple model that captures the basic characteristics of polymer gelation is percolation theory as shown Fig. 3.2. Percolation theory is a lattice model where each site has a certain probability,  $p$ , of being occupied. If two nearest neighbor sites are both occupied, they are defined as a cluster. When the cluster spans the entire dimensions of the lattice, this is considered the gel transition point [53]. However, percolation theory does not accurately capture certain characteristics of gelation [54]. First of all, molecules in a gel possess a certain degree of disorder, which cannot be captured by a lattice. Secondly, a real gel exists

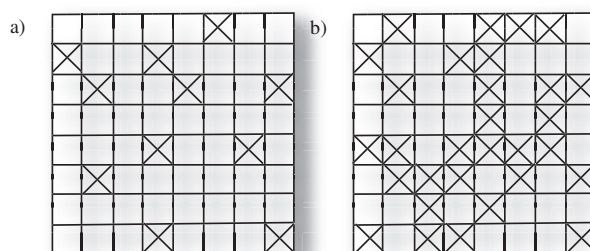


Figure 3.2. a) In the percolation model, each site has a probability,  $p$ , of being occupied. An occupied site is denoted by an  $x$ . b) When a cluster reaches across the dimensions of the lattice, percolation has occurred.

in a solvent, which has no contribution in percolation theory. Consequently, its scaling laws are very different from those predicted by classical theory.

Flory and Stockmayer are acknowledged as the parents of classical gelation theory [55, 56]. Classical gelation theory is considered a tree-like approximation, meaning that all structural conformations of connected polymers are statistically included except for those that include loops (see Fig. 3.3). The polymer chain is also ideal and thus it obeys Rouse statistics (See equations 3.2 and 3.3). Stockmayer was the first to include the effects of loops or rings in a simple model of classical theory, although he did not extend it to his more complete classical theory [57]. Flory introduced the idea that gelation is determined by the formation of an infinitely large network [58]. He statistically found the weight fraction of gel as a function of reacted monomers, although he neglects intramolecular reactions [56]. The critical value of the fraction of reacted monomers,  $\alpha_c$ , at the gel transition temperature as a function of molecular functionality,  $f$ , is found to be

$$(3.1) \quad \alpha_c = 1/(f - 1).$$

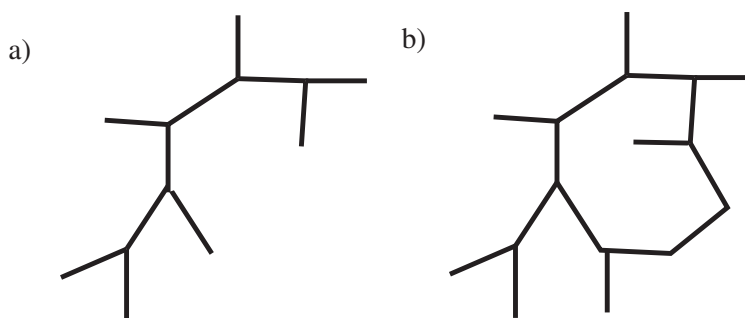


Figure 3.3. a) An illustration of a tree-like structure within classical gelation theory. b) An illustration of a loop-like structure that would not be included in classical gelation theory.

Flory's mean field approximation is often found to be closer to experimental values, even though Stockmayer's theory, at first, seems more general and mathematically complete [55]. This is most likely due to the unintentional inclusion of intramolecular reactions (loops) within Flory's expression for the free energy, which was later recognized and examined further by Stockmayer and Semenov [55, 59]. One of the more recent models to examine the gel transition is attributed to Tanaka [60]. Although still a mean field model, Tanaka extended it to predict the gel transition temperature for specific concentrations and temperatures. Directly after Tanaka, Semenov extended the classical theory to examine even more thermodynamic quantities around the gel point [59]. He predicts that the sol-gel transition is not actually a thermodynamic transition, and is quite critical of Tanaka's earlier theory. He finds that phase separation is found at or near the gelation regime, except in the case when strong excluded volume interactions are included. While Semenov accepts and continues the initial Flory approach to the gelation problem, a recent mathematically intense theory proposed by Erukhimovich, specifically includes loops and loop-like structures in the bonding portion of the free energy [61, 62].

With this simplified model the structure and thermodynamics of the solution can be analyzed and compared directly with Monte Carlo simulations. Important controversial questions regarding the properties of multifunctional associating chains at and below the gelation point cannot be directly addressed. However, determining the applicability or failure of the theory in simpler situations can help to construct more accurate models for complex systems and/or shed light into some controversial issues. For example, extensions of the gelation Flory approach [56, 58, 55, 57] to examine thermodynamic properties lead to contradictory conclusions concerning the order of the sol-gel transition [63, 59]. More recent analysis specifically includes the effect of cyclical structures on resulting thermodynamic and structural quantities [64, 61, 65] and concludes that under certain conditions the sol-gel transition is first order [62]. Competition when specific interactions are added have been addressed in the case of pairwise interactions [66, 67]. Additionally, mean field theory has been expanded to include effects of differing polymer chain conformations and density analytically [68]. It is therefore important to determine the validity of mean field in simpler systems.

There have been multiple computer simulations examining the phase behavior [69, 70] and dynamical properties [71] of telechelic polymers. There have been several on and off-lattice Monte Carlo studies of these sorts of living polymers [72, 73, 74]. However, all simulations treat the bonding potential of the polymer as a physical interaction and do not address its chemical nature. It is generally concluded that the presence of rings does not significantly affect the equilibrium distribution of chains, for the case of unbranched structures [75, 76]. It has also been noted that there exist strong finite size effects on the average chain length formed. The fraction of loops is determined by chain rigidity, as well

as the energy of interaction. A full theoretical understanding of the fraction of loops even in the simplest of cases, as well as effects on thermodynamic quantities, is given here.

### 3.1.2. Mean field theory

Assuming that the ends of the telechelic chains can only associate in pair aggregates, we calculate the free energy of the system. We also assume that the chains possess no excluded volume, so that the statistics of the chains is Gaussian. This assumption, as it applies to the formation of cyclical structures relative to experimental systems, has been addressed by Flory [77]. In addition, contributions of fluctuation correlations to the free energy are neglected, following Lifshitz [78].

For one chain, the probability distribution function  $g(r_0, r_1)$  of having one telechelic end at position  $r_0$  and the other end at  $r_1$ , is given as a function of  $N$ , the length of the chain, and  $a$ , the intermonomer distance, by

$$(3.2) \quad g(r_0, r_1) = \left( \frac{3}{2\pi Na^2} \right)^{\frac{3}{2}} e^{-\frac{3r^2}{2a^2N}}$$

In the case of linear association of  $n$  chains, the distribution function is an integral of the product of the distribution function of the individual chains, integrated over all positions except for the ends:

$$(3.3) \quad \begin{aligned} g(r_0, r_n) &= \int g(r_0, r_1)g(r_1, r_2)\dots g(r_{n-1}, r_n)d^3r_1\dots d^3r_{n-1} \\ &= \left( \frac{3}{2\pi nR_o^2} \right)^{\frac{3}{2}} e^{-\frac{3(r_0-r_n)^2}{2nR_o^2}} \end{aligned}$$

where,  $R_o^2 = Na^2$ . To obtain the partition function we multiply  $g(r_0, r_n)$  by  $k^{n-1}$ , where  $k$  is the reaction constant of pair formation. The reaction constant is defined in terms of  $\varepsilon$ , the energy gained upon formation of a pair,  $\sigma$ , the size of a pair, and its explicit expression will be given in Section IV.

$$(3.4) \quad z(r_0, r_n) = g(r_0, r_n)k^{n-1}$$

Integrating  $z(r_0, r_n)$  over the positions of the end monomers, we get the partition function of a line of associated chains:

$$(3.5) \quad \begin{aligned} Z_n^{line} &= \frac{1}{2} \int z(r_0, r_n) d^3 r_0 d^3 r_n \\ &= \frac{1}{2} \int \left( \frac{3}{2\pi n R_o^2} \right)^{\frac{3}{2}} k^{n-1} e^{-\frac{3(r_0-r_n)^2}{2nR_o^2}} d^3 r_0 d^3 r_n \\ &= \frac{1}{2} V k^{n-1} \end{aligned}$$

The factor  $\frac{1}{2}$  out in front of the integral in Eq. (5) takes into account the symmetry of the line.

For a ring of associated chains, the partition function is comparably:

$$(3.6) \quad \begin{aligned} Z_n^{ring} &= \frac{1}{2n} k \int z(r_0, r_n) \delta(r_0 - r_n) d^3 r_0 d^3 r_n \\ &= \int \frac{1}{2n} \left( \frac{3}{2\pi n R_o^2} \right)^{\frac{3}{2}} \delta(r_0 - r_n) k^n e^{-\frac{3(r_0-r_n)^2}{2nR_o^2}} d^3 r_0 d^3 r_n \\ &= \frac{1}{2n} V k^n \left( \frac{3}{2\pi n R_o^2} \right)^{\frac{3}{2}} \end{aligned}$$

where  $2n$  is the symmetry index of a ring. We can use separate notations for the symmetry indices and define weight indices for linear fragments (lines) and rings in order to simplify the above expressions. We can then write the partition function for a ring and a linear chain as  $Z_n^{ring} = V \frac{w_{nr}}{s_{nr}}$  and  $Z_n^{line} = V \frac{w_{nl}}{s_{nl}}$  where for a ring the weight index  $w_{nr} = (\frac{3}{2\pi n R_0^2}) k^{n-1}$  and the symmetry index  $s_{nr} = 2n$ . For a linear chain, the weight index  $w_{nl} = k^{n-1}$  and the symmetry index  $s_{nl} = 2$ .

The total partition function of the system can then be written as:

$$(3.7) \quad Z = \prod_{n=1}^{\infty} \frac{(Z^{ring})^{N_n}}{N_n!} \prod_{n=1}^{\infty} \frac{(Z^{line})^{Q_n}}{Q_n!}$$

where  $N_n$  represents the number of rings of size  $n$  and  $Q_n$  represents the number of linear fragments of size  $n$ .

Also, define  $A_n$  as the concentration of rings of size  $n$  and  $B_n$  as the concentration of lines of size  $n$ . The free energy rewritten in terms of these parameters is:

$$(3.8) \quad F = -T \ln Z = -T \left[ \sum_{n=1}^{\infty} \ln \frac{(Z^{ring})^{N_n}}{N_n!} + \sum_{n=1}^{\infty} \ln \frac{(Z^{line})^{Q_n}}{Q_n!} \right]$$

Using Sterling's approximation, the above expression reduces to:

$$(3.9) \quad \frac{F}{TV} = \sum_{n=1}^{\infty} \left( A_n \ln \frac{A_n s_{nr}}{w_{nr} e} + B_n \ln \frac{B_n s_{nl}}{w_{nl} e} \right)$$

We add a Lagrange multiplier to ensure that the total concentration of chains,  $C = \sum_n (A_n + B_n)n$ , is constant.

$$(3.10) \quad \tilde{F} = \frac{F}{TV} + \mu \left( \sum_n (A_n + B_n)n - C \right)$$

Minimizing with respect to  $A_n$  and  $B_n$ , we get

$$(3.11) \quad \begin{aligned} A_n &= \frac{w_{nr}}{s_{nr}} e^{-\mu n} = \frac{w_{nr}}{s_{nr}} z^n \\ B_n &= \frac{w_{nl}}{s_{nl}} e^{-\mu n} = \frac{w_{nl}}{s_{nl}} z^n \end{aligned}$$

where  $z$  represents the fugacity of the polymer chain. The equilibrium free energy is then:

$$(3.12) \quad \frac{F}{TV} = \rho \ln z - \sum_{n=1}^{\infty} (A_n + B_n)$$

where  $\rho$  is represented by,

$$(3.13) \quad \begin{aligned} \rho &= \sum_{n=1}^{\infty} \left( \frac{z^n k^{n-1}}{2} + \frac{(zk)^n}{2n} \left( \frac{3}{2\pi n} \right)^{\frac{3}{2}} \right) n \\ &= \frac{1}{2} \frac{z}{(1-zk)^2} + \frac{1}{2} \left( \frac{3}{2\pi} \right)^{\frac{3}{2}} \sum_{n=1}^{\infty} \frac{(zk)^n}{n^{\frac{3}{2}}} \end{aligned}$$

At a given density and temperature we can numerically solve for  $z$  using the previous equation for  $\rho$ . Then, plugging  $z$  back into the expression for the free energy, we can numerically evaluate the energy per chain, the heat capacity per volume, and the fraction of chains participating in rings and lines. Finite difference derivatives are used to evaluate  $U$ , the internal energy of the system, and  $\frac{C_v}{V}$ , the heat capacity per volume, using the following thermodynamic relations.

$$(3.14) \quad U = -T \left( \frac{\partial F}{\partial T} \right)_{V,N} + F$$

$$(3.15) \quad C_v = \left( \frac{\partial U}{\partial T} \right)_{V,N}$$

We also evaluate the fraction of chains that belong to rings,  $f$ ,

$$(3.16) \quad f = \frac{\sum_{n=1}^{\infty} A_n n}{\rho} = \frac{\sum_{n=1}^{\infty} \left( \frac{(zk)^n}{2n} \left( \frac{3}{2\pi n} \right)^{\frac{3}{2}} \right) n}{\rho}$$

### 3.2. Monte Carlo for ideal gels

A standard Metropolis Monte Carlo Algorithm is used with a Canonical Ensemble (constant N,V,T). All described simulations are off lattice, and periodic boundary conditions are enforced with a Verlet linked list methodology when calculating the internal energy of the system. The reduced density is defined by  $\rho^* = \frac{N_m \sigma^3}{V} = \frac{N_s \sigma^3}{2V}$ , where  $N_m$  represents the number of polymer molecules or chains,  $N_s$  represents the number of stickers or end monomers, and  $\sigma$  is the range of interaction potential between ends, to be defined below.

In order to systematically test the accuracy of theoretical understanding of the influence of cyclical structures on the thermodynamics of the system, a very simple model was developed. Each polymer chain is given an entropic spring force such that the free energy of a single chain is:

$$(3.17) \quad F = \frac{3}{2} \frac{R^2 T}{R_o^2}$$

$R_o^2$  is  $Na^2$ , where  $N$  represents the number of monomers in the chain, and  $a$  is the inter-monomer distance. A Gaussian distribution has been shown to be consistent with associating polymer chains at sufficient densities in previous simulations [74, 73]. A simple square well

interaction potential between the end monomers is used, of the following form.

$$(3.18) \quad U = \begin{cases} -\varepsilon & r < \sigma \\ 0 & r > \sigma \end{cases}$$

where  $\varepsilon$  and  $\sigma$  represent the depth and the width of the potential well with units of energy and length respectively. Because each polymer chain is assumed to be ideal, possessing no excluded volume, the locations of all the monomers in the chain do not need to be stored, only the connectivity and locations of the chain ends. Also, without excluded volume effects, phase separation will not be seen in the system. The only factors that will affect calculated properties are the competing entropic and bonding contributions.

Results of two types of simulations will be discussed. For both types of simulations, only the case of pairwise association is considered, so tree-like structures cannot be formed. This allows us to test the validity of the mean field model described in Section 3.1.2. In the first case, we simulate this theoretical model. That is, the probability  $p$  that a bond is formed if the end-monomer distance is less than  $\sigma$  is determined only by the energy of the bond and is given by:

$$(3.19) \quad p = \frac{e^{\frac{\varepsilon}{k_B T}}}{1 + e^{\frac{\varepsilon}{k_B T}}}$$

This is a two state model following the model for chemical reaction initially suggested to model the transition state between gauche and trans conformations for polymer chains [79]. It also includes the effects of bond saturation, as in hydrogen bonding. In order to ensure that detailed balance is obeyed and that the system is in true thermoreversible state of chemical equilibrium, the important additional step in Monte Carlo to ensure equilibrium is

to make sure the number of attempts to break a bond is equal to the number of attempts to make a bond. In the second type of simulation, we consider the case where a bond is always formed if it is not yet saturated. We denote this case as diffusion limited, and it corresponds to the case of physical bonding.

Resulting thermodynamic and structural properties from both types of simulations, such as the average energy per particle, the heat capacity per volume, and the fraction of loops, are compared directly with theoretical results.

### 3.2.1. Thermoreversible chemical equilibrium

The average energy per particle, the heat capacity per volume, as well the fraction of chains participating in loops as functions of reduced temperature  $T^* = \frac{k_B T}{\epsilon}$  and reduced density  $\rho^* = \rho \sigma^3$ , are directly compared with theoretical results for the case of an equilibrium chemical thermoreversible bonding interaction. In this case the reaction constant is given by

$$(3.20) \quad k = \frac{4\pi\sigma^3}{3} e^{\frac{\epsilon}{k_B T}}$$

The following results are presented for 1,000 polymer chains ( $N_m = 1000$ ), each with a length of 10 monomers, where  $a$ , the intermonomer distance, is defined to be  $\sigma$ , the width of the potential well. Averages of thermodynamic quantities were taken every 10,000 MC cycles for a total of 1,000,000 MC cycles after a 10,000 MC cycle equilibration. This was to ensure that structural quantities, such as the fraction of loops, sufficiently relax between measurements. The following a snapshot from simulations, showing the existence of a percolated cluster in the simulation box.

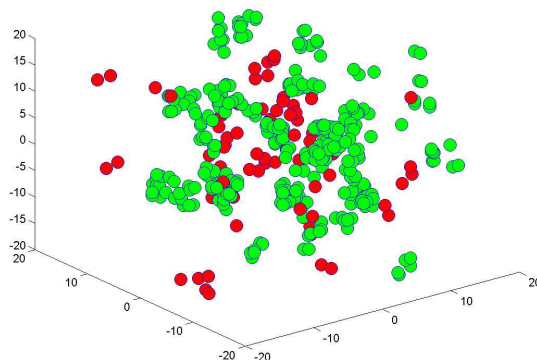


Figure 3.4. Snapshots of the simulation close to the percolation regime. The green, or lighter monomers, represent members of a percolated cluster.

Fig. 3.5 compares MC data for the average energy and heat capacity with the analytical predictions. The average energy per particle agrees more closely with analytical results as reduced density increases and the heat capacity per volume matches perfectly the results from the theoretical calculations. Notice that the magnitude of the peak in the heat capacity per volume versus temperature increases as the density increases. However, the maximum in the heat capacity per number of molecules (that is heat capacity per volume divided by density) increases as the density decreases.

Fig. 3.6 shows the probability distribution of the chain's end-to-end distance. One can clearly see the discontinuity at  $r = \sigma$ . This discontinuity results from the square well form of the interaction potential between the ends of the chain. As seen from the figure, the discontinuity goes away with increased temperature. It will also disappear with increased density of the chains. Indeed, as the density increases, less chains participate in self loop structures in agreement with Fig. 3 where it is shown that the weight averaged molecular

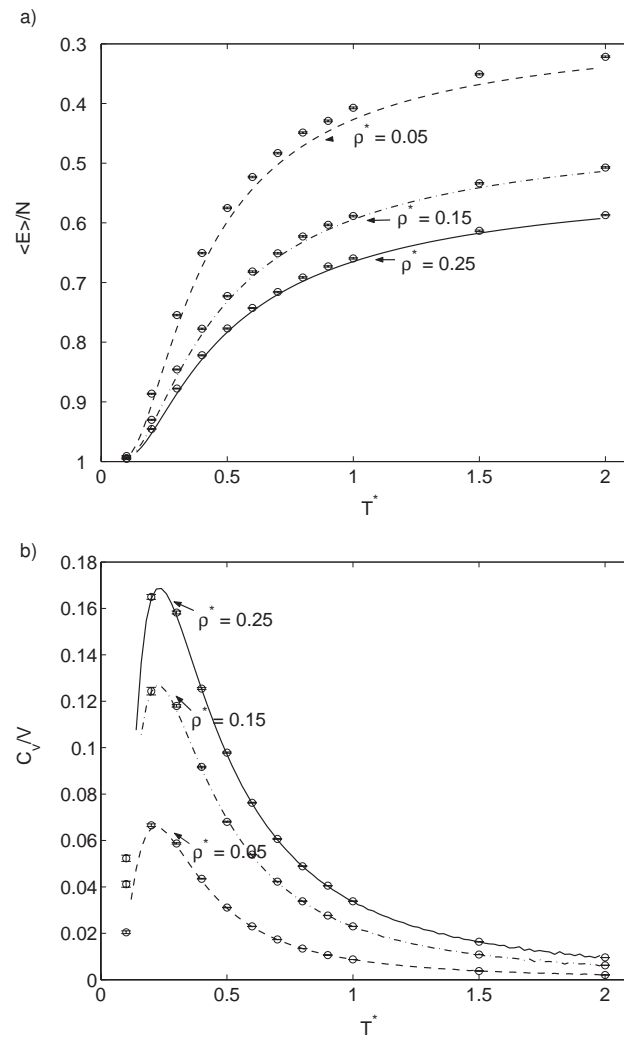


Figure 3.5. Average energy per particle (a) and heat capacity per volume (b) as functions of reduced temperature  $T^*$  at reduced densities  $\rho^* = 0.05, 0.15, 0.25$  with the theoretical results respectively marked with dashed, dot-dashed, and solid lines and the simulation results represented by circular points. Standard deviation is smaller than the width of the circular point, otherwise it is marked.

weight of the clusters increases if the density increases. This means that there will be less deviations from the predicted Gaussian distribution of the chain's end-to-end distance.

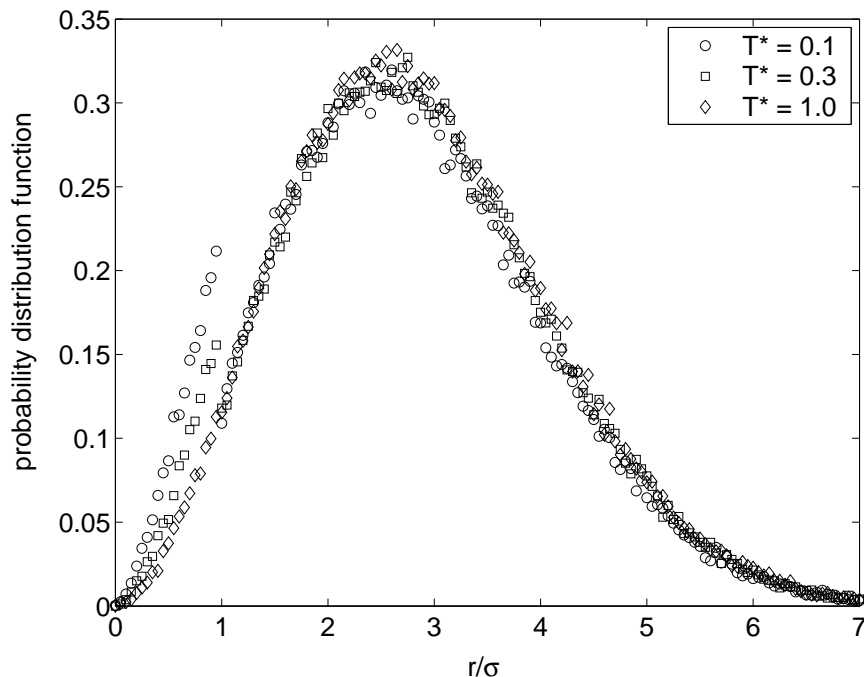


Figure 3.6. The probability of the chain end-to-end distances  $r$  in units of the width of the square potential  $\sigma$  at a reduced density  $\rho^* = 0.05$  for different effective temperatures  $T^* = 0.1, 0.3, 1.0$ . For all values of  $r/\sigma > 1$  the probability is Gaussian and it is independent of  $T^*$ . Deviations from the Gaussian distribution are observed at length scales smaller than  $\sigma$  when  $T^*$  is very low.

Next, the effects of increasing the length of the polymer chain was explored. Most notably, at a reduced density  $\rho^* = .05$  and reduced temperature  $T^* = 1.0$  as seen in Fig. 3.8, which shows the largest deviation from mean field theory results for the average energy per particle, increasing the length of polymer chain to 100 monomers from 10 monomers substantially decreases disagreement with theoretical predictions for the average particle energy. Mean field theory is a better description when the characteristic length of interactions is much less than the average distance between interacting monomers [62].

The comparison between theory and simulation, however, is not so straightforward for the case of structural quantities such as the fraction of chains that belong to loops. In Fig. 3.9,

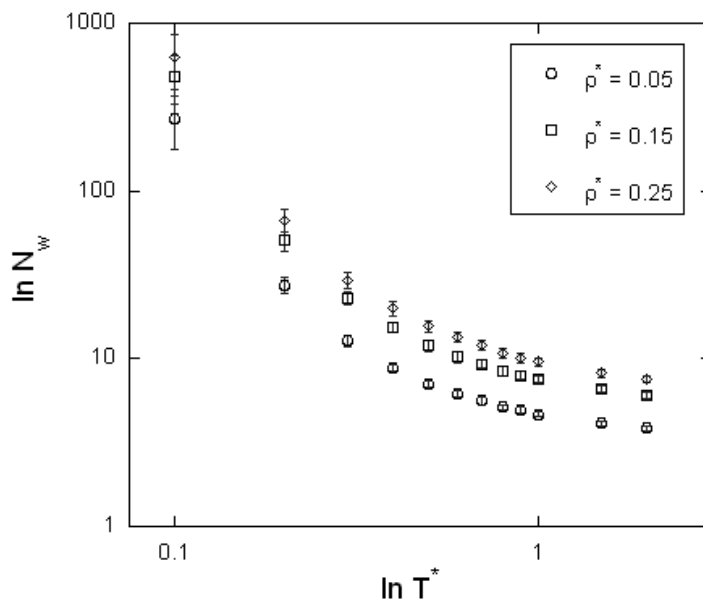


Figure 3.7. The weight average molecular weight of clusters as a function of effective temperatures  $T^*$  for various reduced densities  $\rho^* = 0.05, 0.15, 0.25$ .

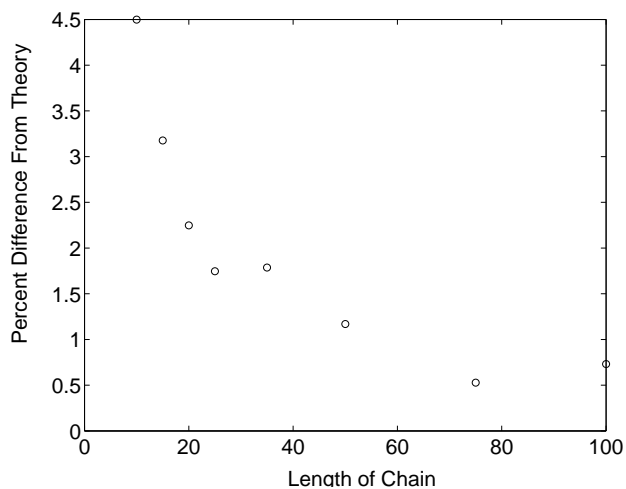


Figure 3.8. Percent difference in energy between theory and simulation at a reduced density  $\rho^* = 0.05$  and a reduced temperature  $T^* = 1.0$ . As the chain length is increased, percent difference decreases.

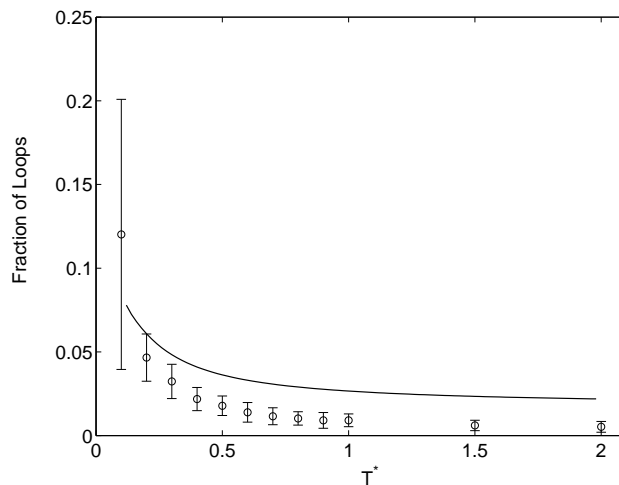


Figure 3.9. Fraction of chains that belong to loops as a function of reduced temperature  $T^*$  at several a reduced density of 0.15 ( $\rho^* = 0.15$ ). The theoretical results are marked with a solid line, while the simulation results are represented by circular points. Standard deviation is indicated. Disagreement is seen with theoretical results at both low and high temperatures.

the fraction of chains in loops as a function of reduced temperature at a reduced density of 0.15 for both theory and simulation is illustrated. The simulation underestimates the fraction of loops at high temperatures, and large fluctuations are seen at lower temperatures, which is an effect of the system size. In order to understand what is happening it is necessary to systematically study the finite size effects of the system.

Neglecting the finite size effects, the fraction of loops at low temperatures can be found as follows. Let us rewrite Eq. 3.13 for the total density of polymer chains in the form

$$(3.21) \quad \rho = \rho_{\text{linear}} + \rho_{\text{ring}}$$

where

$$(3.22) \quad \rho_{\text{linear}} = \frac{1}{2k} \frac{x}{(1-x)^2}$$

$$(3.23) \quad \rho_{\text{ring}} = \frac{1}{R_0^3} \xi(x)$$

with  $x = zk$  and function  $\xi(x)$  defined as

$$(3.24) \quad \xi(x) = \frac{1}{2} \left( \frac{3}{2\pi} \right)^{3/2} \sum_{n=1}^{\infty} \frac{x^n}{n^{3/2}}$$

For small temperatures ( $T \rightarrow 0$ ) associating constant is large ( $k \rightarrow \infty$ ) and  $\rho_{\text{ring}}$  could be explicitly found

$$(3.25) \quad \rho_{\text{ring}} = \begin{cases} \rho, & \rho < \rho_c \\ \rho_c, & \rho > \rho_c \end{cases}$$

where  $\rho_c = \xi(1)R_0^{-3} \simeq 0.43R_0^{-3}$ . The fraction of chains in rings or loops in the limit of small temperature could be readily found:

$$(3.26) \quad f = \begin{cases} 1, & \rho < \rho_c \\ \rho_c/\rho, & \rho > \rho_c \end{cases}$$

In particular, if the chain consists of 10 monomers ( $R_0 = 10^{1/2}\sigma$ ) and the density of chains is  $\rho\sigma^3 = 0.15$  then the fraction of loops at low temperatures  $f \simeq 0.09$ , which is in reasonable agreement with the simulation data shown in Fig. 3.9.

To address the finite size effects and the validity of the mean field theory in more detail we also examine fluctuations in the number of the chains that belong to loops during our simulation process. Looking at low temperatures ( $T^* = 0.1$ ) we can see from Fig. 3.10 a), as we increase the size of the system, keeping a constant density, the probability distribution

of the fraction of chains in loops becomes narrower and thus fluctuations in the number of chains that belong to loops become smaller suggesting that in the limit of a large system they would become infinitely small.

One can also notice a sudden jump in the distribution at  $f = 1$ . This effect takes place only in small systems at low temperatures and could be describe as follows. At low temperatures all the stickers should be combined in pairs. As illustrated by Eq. 3.26 the fraction of the chains that belong to loops is less than 1 if  $\rho > \rho_c$ . There is only one possibility left for the chains that do not belong to loops: they have to be connected in one big linear chain since all the stickers have to be combined in pairs in the low temperature limit. If the ends of such a linear chain meet then the fraction  $f$  becomes 1. As shown in Fig. 3.10a) for a system of 200 molecules and  $T^* = 0.1$  such event takes place with the frequency of 20%.

We conclude here that it is possible, with large enough simulation sizes, that the average fraction of loops shown in Fig. 3.10 would converge to the theoretical curve predicted by mean field theory.

### 3.2.2. Diffusion limited case

It is easy to adapt simulation algorithms to consider the case when the attraction between end-groups is diffusion limited. In this case, a bond is always formed between two end groups if it is not yet saturated. The following results are presented for 1,000 polymer chains ( $N_m = 1000$ ), each with a length of 10 monomers. Averages of thermodynamic quantities were taken every 1,000 MC cycles for a total of 100,000 MC cycles after a 1,000 MC cycle equilibration. Temperatures below  $T^* = 0.2$  are not considered due to long energy relaxation times.

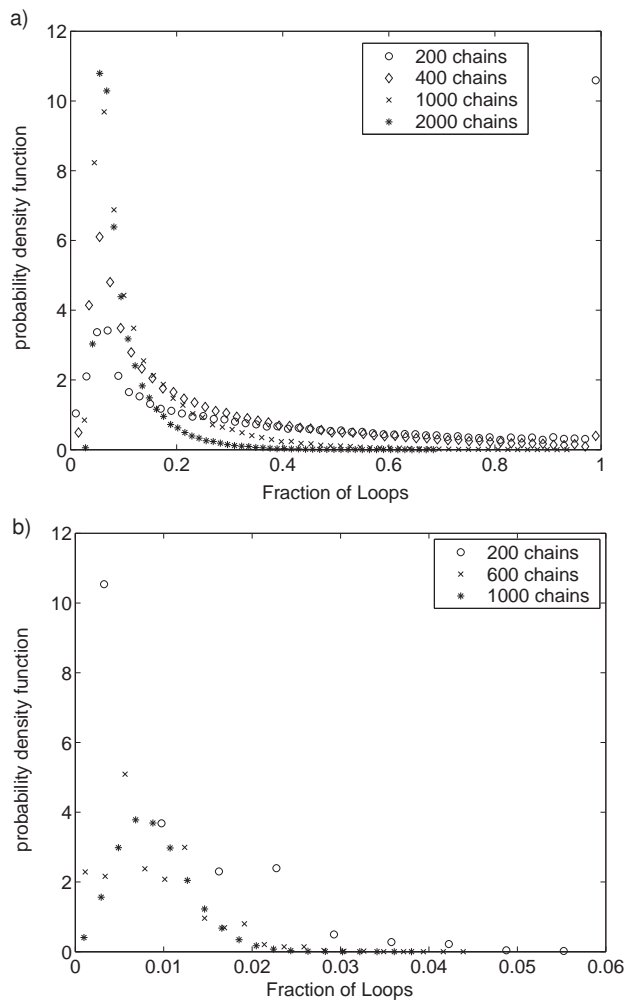


Figure 3.10. Probability of occurrence of different fractions of chains in loops at a reduced density  $\rho^* = 0.15$  and (a) a low temperature  $T^* = 0.1$ , and (b) a comparably higher temperature  $T^* = 1.0$ .

It is of interest to determine to what extent mean field theory of thermoreversible chemical association can be used to describe the system in the case where both intra and intermolecular reactions are diffusion limited. In this case, we introduce an additional fitting parameter  $k_o$ , in order to vary the statistical weight of the bond.

$$(3.27) \quad k = k_o \frac{4\pi\sigma^3}{3} e^{\frac{\epsilon}{k_B T}}$$

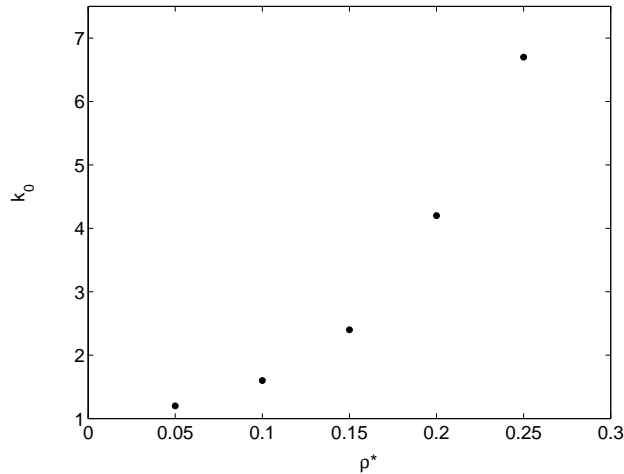


Figure 3.11. Values of  $k_o$  obtained from numeric fits to thermodynamic results obtained from simulation at several densities. As the density is increased, the value of  $k_o$  also increases.

Thermodynamic quantities including the average energy per particle (see Fig. 3.11) and heat capacity per volume are fit to numerical results. While fitting the data, a general trend is observed. As the density is increased, the parameter  $k_o$  needed to fit simulation data also increases, which is consistent with the fact that the theory of thermoreversible association cannot describe physical bonding. In the case of physical bonding, as the concentration of chains increases the correlation function assigned to the probability of forming a contact is a complex function not only of the interactions but also of the concentration of the systems, and the effect of the interactions cannot be described only by the second virial coefficient in dilute chain solutions [80].

### 3.3. Summary and conclusions

Various simulations of thermoreversible physical association and of non-reversible chemical association exist in the literature. It is well established that results of simulations of thermoreversible physical association cannot be described by the mean field model nor by

percolation theory. In this chapter, two separate models of thermoreversible association are explored with simulation, a model of chemical thermoreversible association, for which well-defined theoretical models exist, as well as a model of physical diffusion limited association. Resulting thermodynamic and structural quantities of the two models are then compared with those predicted by the classical theory of thermoreversible association. We consider only pairwise association to avoid problems associated when networks are formed. In pairwise association only linear structures and loops can exist.

We find that thermoreversible chemical association is well described by the mean field model. The fraction of linear and loop structures as a function of the number of associated chains obtained in the simulation compares well with the theoretically obtained distribution. The thermodynamic quantities are also well described by the model. Finite size scales are important at low effective temperatures. Instead, for the diffusion limited thermoreversible association model, the simulations are not described by theory. In thermoreversible physical association the units react whenever they are within a given distance. In this case, the correlation function determines the probability of interaction. It is well known that as the concentration increases it is more difficult to describe these correlations even in system without saturated physical bonds. In particular, a simplistic second virial approach cannot describe these correlations. Therefore, we expect that serious corrections need to be made in the model of thermoreversible chemical association to describe the simulation results of thermoreversible diffusion limited association. One can use a concentration dependence association constant, which can be fitted using the simulation results.

These studies provide the basics for the understanding of more complex associating systems. For example, if we include specific van der Waals interactions in the chemical thermoreversible association model analyzed here we can describe solutions of heterogeneous macromolecules with end units capable of forming hydrogen bonding with each other in different solvent conditions. In certain cases phase segregation is expected to take place in these solutions [66]. The competition of various physical interactions in the arrest of colloidal suspension undergoing gelation has been addressed recently [81, 82, 83]. In the present study we have stable solutions because we have only analyzed ideal chains. Including excluded volume would simply rescale thermodynamic quantities. In bad solvent conditions for the chain backbones, however, phase segregation is expected. Our results suggest that systems with chemically thermoreversible associating end units in bad solvent conditions can be described by the theories that address segregation in polydispersed solutions [84]. However, when tri-functional association is included, we expect more complex phase behavior [85, 86, 87].

### 3.4. Acknowledgements

Dr. Min Sun Yeom is acknowledged for guidance with Monte Carlo code. Dr. Alexander Ermoshkin is acknowledged for guidance and instruction in mean field gelation theory. Portions of this chapter also appear in: "Thermodynamics of Reversibly Associating Ideal Chains," S. M. Loverde, A. V. Ermoshkin, and M. Olvera de la Cruz, *Journal of Polymer Science, Part B: Polymer Physics*. 43, 796 (2005).

## CHAPTER 4

**A Model for Charged, Incompatible Mixtures at an Interface****4.1. Introduction and background**

Polymers at interfaces, in particular, charged polymers at interfaces have been gaining much attention recently due to potential biomedical applications. For example, DNA on the surface of cationic membranes has been shown to be an efficient method of transfection [4]. Or else, cationic antimicrobial peptides, have shown potentiality for targeting specific bacteria types [?, ?]. The type of interface may vary, such as solid liquid interfaces, soft liquid interfaces in Langmuir-Blodgett films, or else fluctuating interfaces found in membranes or bilayers. Lateral periodicity or pattern formation on the surface into separate domains or periodic microphases, is a physical behavior that is seen with many different colloidal, polymer-based, and biological systems. Polymer adsorption to the interface is a complex balance of the entropy and the potential of interaction with the surface or interface. In many cases, the forces are short range, such as van der Waals interactions with the substrate. However, depending on the surface dielectric properties, as well as the salt concentration in the medium, long range forces such as dipolar and charged interactions may play a significant effect on the equilibrium surface or interface structure.

The main discussion in the next several chapters is organized around two separate motivations: periodic pattern formation on the surface, as well as the effects of salt concentration in the surrounding solution on the surface structure. In the present chapter, a model of

competing electrostatic and short range van der Waals interactions for molecules strongly adsorbed to interfaces is outlined. In the first section, examples of pattern formation for several different interfaces, such as the solid liquid interface, liquid liquid interface, and air liquid interface, in multiple experimental systems are given. An overview of theoretical development for competing dipolar interactions on the interface is given. Within the next section, the formation of lamellar and hexagonal periodic domains is described theoretically at low temperatures using strong segregation theory. The phase behavior as a function of electrostatic strength and short range interactions is compared with scaling at high temperatures, in which a mean field approach is used to describe the density fluctuations. This chapter will provide the necessary framework for Chapter 5, in which molecular dynamics simulations will be developed, and Chapter 6, in which the effects of salt on the pattern formation of the interface will be considered. The theoretical work presented at the end of this chapter will also be extended in Chapter 7, in which the possibility of more complex phases will be examined.

#### 4.1.1. Experimental review

Some recent examples of surfactant adsorption onto solid liquid interfaces show that the resultant structures on the surface of negatively charged mica and silica, as well as hydrophobic graphite [88, 89]. The adsorption is a complex mix of surface chemistry, surfactant concentration in the bulk, solvent and screening effects, as well as the surfactant chain length. For the case of a neutral substrate, graphite, simulations of nonionic surfactants have illustrated that the morphology of the adsorbed micelle is dependent on the chain length [90]. Moreover, alkylphosphonic acid, an anionic surfactant, has been shown to form islands on

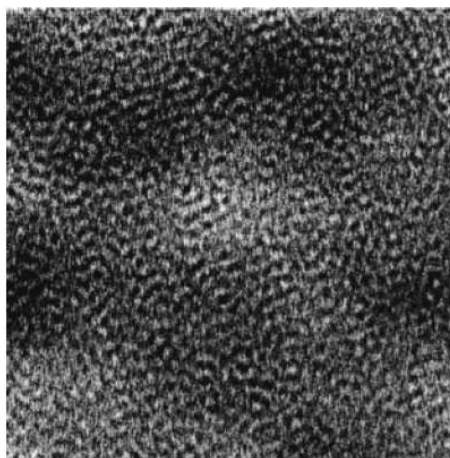


Figure 4.1. AFM images of absorbed surfactant micelles on silica at  $25C$ .  $300nm \times 300nm$ . Reproduced from Ducker et al [88].

mica. The evolution of these island structures are reminiscent of many classical materials science coarsening problems. Scaling analysis has indicated that long range forces, such as the electrostatics of the system, might be necessarily included to explain the nucleation and growth [91].

In contrast to pattern formation at the solid liquid interface which displays specific dependence on the substrate molecular interaction, behavior at the air water interface is mainly dependent on the intermolecular interactions. Pattern formation on the surface of Langmuir-Blodgett films with mixed monolayer systems has been observed using epifluorescence techniques [92, 93, 94]. Depending on various experimental conditions, such as the pH of the system [93], the compression of the lipid monolayer [92], patterns including hexagonal domains, lamellar stripes, and even more complex spirals have been observed [93]. Upon compression, the monolayer undergoes a transition between a liquid-expanded and liquid-condensed phase, regions of high and low charge density. The shapes of the domains are dependent on the fraction of neutral component, the configurations of the tails, as well as

the chirality of the molecules themselves. For example, cholesterol as a neutral component possesses an inherent chirality due to its chemical nature.

The contribution of electrostatics to the ordering and stability of the patterns has been considered in the regime in which the inverse screening length is much less the periodic domain size. In this case, for charged molecular headgroups, the contribution free energy is essentially a dipolar contribution. In addition, in terms of the contribution due to the individual dipole moment of the molecules, the dipolar contribution in plane has been analyzed in terms of the shape asymmetry for one individual domain [95, 96].

Next, consider the liquid liquid interface. Mixtures of cationic and anionic amphiphilic molecules can form thermodynamically stable structures such as micelles, membranes and multilamellar systems. These self-assembled structures have been studied as a function of the molar ratio of the oppositely charged molecules, their concentration in solution, and the ionic strength of the environment [97, 98, 99, 100]. In addition, the presence of other neutral components leads to a large variety of structures and the possibility of local organization on the surface of membranes and monolayers. In many cases, just as in monolayer systems, this gives rise to a phase coexistence between solid domains immersed in a liquid background. The shape of the domains, which can be stretched or circular, depend on the composition of the membrane and possibly the elasticity, as the screening in solution does not affect the shape of the domains themselves [101].

Such structures are important in diverse applications, such as the design of bio-sensing devices [102]. Moreover, they serve as model systems for the understanding of the properties of cell membranes; formation of structured domains is known to be crucial to cell signaling processes [8]. In addition, structure formation due to the competition between short and

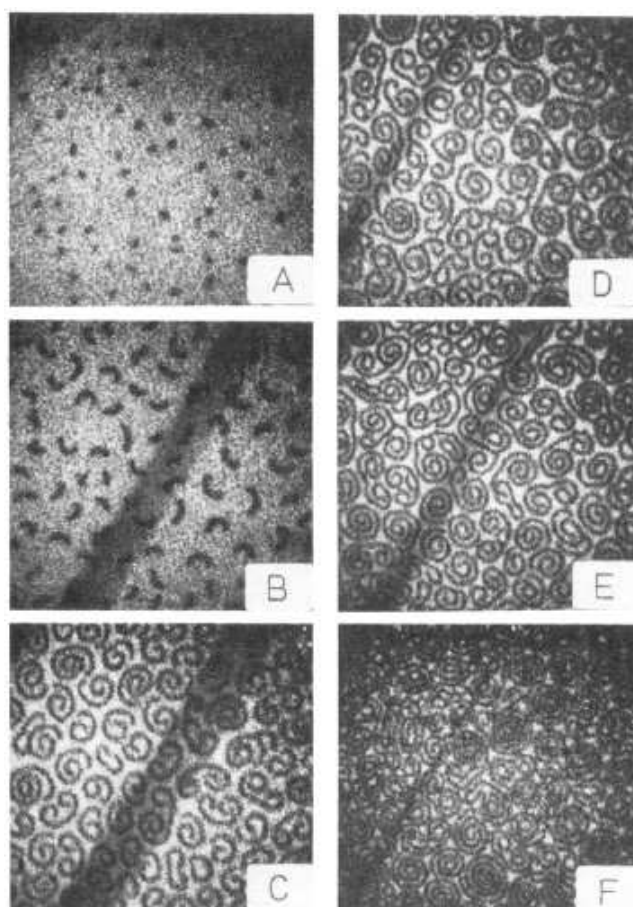


Figure 4.2. Fluorescence micrographs of a 5 mol film at pH 11 and 10 C as upon compression of langmuir monolayer. A) indicates the start of the transition. F) indicates the completion. The lighter regions represent a fluid mixed neutral and charged phase and the darker regions indicate a dense charged region. Reproduced from Heckl et al.[93]

long range interactions leads to the formation of phases with periodic structures in a large variety of systems including not only lipid mixtures [92, 103] but also in two dimensional uniaxial ferromagnets [104], reaction controlled phase segregating mixtures [105], and two dimensional electron gases in MOSFET's [106]. A summary of systems exhibiting pattern formation due to competing interactions is shown in Table 4.1.

System	Length scale	Forces	Reference
Langmuir films	$1 - 10\mu m$	Dipolar	[100-101]
Surfactant Adsorption	$50nm$	Dipolar	[88, 89]
Membranes	$10 - 100nm$	Bending elasticity, Dipolar	[92, 103]
Magnetic systems	$10\mu m$	Magnetic field	[104]
Metal alloys	$1 - 10nm$	Elasticity	[?, ?]
Semiconductors	$50nm$	Surface stress	[106]
Polymers and Polyelectrolytes	$50nm$	Covalent bonding	[107, 14]
Shrinking Gels, Gels at Interface	$\mu m$	Elasticity, Osmotic Stress	[108, 109]

Table 4.1. A variety of physical systems which display pattern formation at different length-scales due to dipolar, stress, elasticity, magnetic forces. Table adapted from Suel and Andelman [110].

#### 4.1.2. Theoretical overview

As discussed in the previous section, periodic phases due to competitive interactions on the surface, or in the bulk, are seen in a multitude of physical systems. This diverse set of systems, such as Langmuir films and adsorbates on metals, membranes or vesicles, charged diblock copolymers, polyelectrolyte solutions, all display sources of competition that gives rise to periodic patterns [110]. A plethora of questions arise, such as the dynamic and kinetic effects such as the nucleation of the domains, the effect of disclinations on pattern formation, as well as the correlation between microscopic ordering and the faceting of domains on the surface [111, 112]. However, this section will focus on studies that has been to determine the electrostatic contribution to the equilibrium shape of finite domains, considering flat or fixed interfaces.

Considering polar molecules at the interface, Andelman [95] has shown that the free energy due to the dipolar and short range interactions close to the critical point gives a periodic hexagonal or lamellar structures. He also notes the appearance of two phase coexistence regions with a gas or solid isotropic phase. The behavior of a charged headgroups, as opposed

to pure dipolar interactions, may depend on the ionic strength of the solution. For strong screening in the solution, charged headgroups may give a contribution to the free energy that looks like a dipolar contribution. For low values of screening, we can expect the formation of Wigner crystalline structures [113]. However, the behavior of the dielectric constant close to interfaces is quite complex and may give rise to long range effects, even in the presence of screening. For example, Netz has shown that in the presence of an interface, the Debye Hückel interaction is enhanced by a factor of two [114]. It is unlikely that the complete effects of a locally varying dielectric constant close to interfaces may be fully understood for some time. Recent work indicates that electrostatic coupling through a charged lipid bilayer may be enhanced by these considerations [115].

Numerical simulations studying the effects of electrostatics on pattern formation due to competing interactions show expected behaviors. The formation of charged domains on a flat square lattice due to the competition between full Coulomb  $1/r$  interactions and net short range repulsion amongst oppositely charged molecules has been explored by simulation at zero temperature [116] and also by mean field arguments at high temperatures [116, 117]. These stoichiometric mixtures develop ordered striped domains possessing a characteristic width that depends on the strength of the competing Coulomb and short range interactions at low temperatures. At high temperatures percolated structures develop that resemble a spinodal decomposition pattern during phase segregation of binary systems, but growth is restricted, as in block copolymer systems with microphase segregation [107, 14].

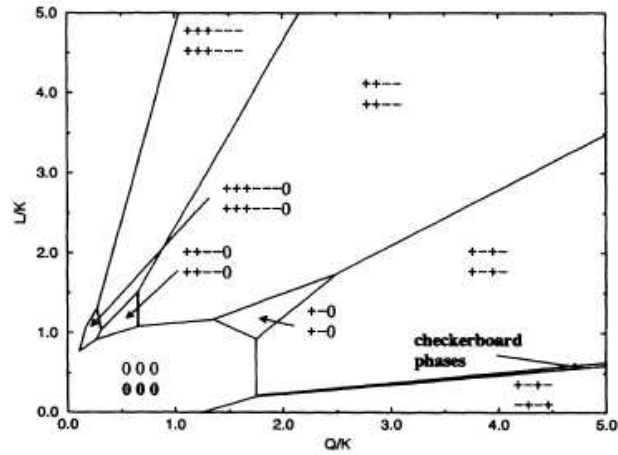


Figure 4.3. Phase diagram for a competing system of lattice spins, with short range ferromagnetic behavior with parameter  $L$ , and long range anti ferromagnetic behavior of parameter  $Q$ . Density is also introduced through the parameter  $K$ . Reproduced from Loew et al [116] Striped phase coexists at low values of  $Q$  along with a concentration of holes, represented by 0.

## 4.2. Development of a model for pattern formation

In this chapter, the possibility of charged patterns formed by molecules strongly adsorbed to interfaces, either flat surfaces of biological or synthetic membranes, or else any other neutral substrate is explored. Using analytic and simulation techniques, the competition between electrostatics and short range van der Waals, or immiscibility, between oppositely charged molecular components exhibits rich phase behavior. In the next two sections, analytic models are used to describe the phase behavior of the components at both high and low temperature regimes.

### 4.2.1. Scaling analysis at low temperatures

The phase behavior of the ionic mixture can be examined analytically in two separate regimes. At higher temperatures, small density fluctuations exist around the mean density.

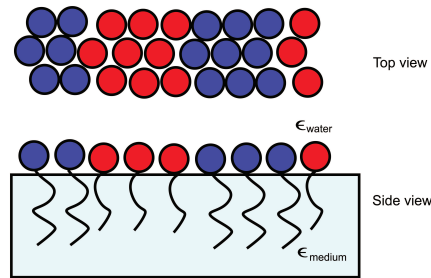


Figure 4.4. Cartoon of oppositely charged (red and blue denoting positive and negatively charged headgroups) molecules strongly absorbed to the interface. Molecules assume hexagonal close packing into periodic microphases as illustrated.

At low temperatures, when the system exhibits strongly segregated domains, the system is periodic. At low temperature values, or high values of the magnitude of short range attraction, the system exhibits well-defined periodic lamellar when the charge surface coverage of the positive and negative molecules are equal and confined to a flat surface. The free energy of the system is dominated by the electrostatic cohesive energy in addition to the interfacial contribution to the free energy, which is characterized by the line tension,  $\gamma$  per thermal energy  $k_B T$ . Within the strong segregation regime, the entropic contribution to the free energy is negligible.

Following the example of the free energy for a incompressible two dimensional system of a mixture of positive and negative components [118], the results for a coarse grained free energy scaling analysis of  $N_A$  positively and  $N_B$  negatively charged components interacting with a three dimensional Coulombic  $1/r$  potential can be generalized for a  $d$  dimensional system. The free energy can be written as sum of the total electrostatic interactions and the contribution from the line tension of each periodic segregated domain. Each charged domain is approximated by a electroneutral unit cell which has a characteristic lattice length  $L$ , dimensions  $L^d$ , and an associated charge density  $\sigma$ . The net free energy per total number of

particles  $N = N_A + N_B$ , in units of  $k_B T$ , can be written as

$$(4.1) \quad \frac{F_{NET}}{N} = \frac{F_{cell}}{N_{cell}} \approx \frac{a^d}{L^d} \left( \gamma s_1 L^{d-1} + \frac{l_B \sigma^2 s_2 (L^d)^2}{L} \right) = \left( \frac{F_o a^d}{L_o^d} \right) F.$$

Here,  $s_1$  and  $s_2$  are geometrical parameters that depend on the characteristic geometry of the underlying unit cell,  $a^d$  represents the size of the particle, and  $N_{cell}$  represents the number of particles per unit cell. The Bjerrum length  $l_B$  is given by,

$$(4.2) \quad l_B = \frac{e^2}{4\pi\epsilon\epsilon_r k_B T}.$$

$F_o$  and  $L_o$  are system dependent parameters, defined by the minimization of the free energy of the system with respect to the characteristic size of the system,  $L$ ,

$$(4.3) \quad F_o = \left( \frac{\gamma^{2d-1}}{(l_B \sigma^2)^{d-1}} \right)^{1/d}$$

and

$$(4.4) \quad L_o = \left( \frac{\gamma}{l_B \sigma^2} \right)^{1/d}.$$

The dimensionless free energy per unit area in terms of  $s_1$  and  $s_2$  is then described by

$$(4.5) \quad F = \frac{s_1}{D} + s_2 D^{d-1}$$

where  $D = L/L_o$  is the ratio of the characteristic size of the unit lattice to the length of the system. Minimizing the dimensionless free energy with respect to  $D$  gives the free energy of

the favored periodic structure as

$$(4.6) \quad F = 2 \left( (d-1)s_2s_1^{d-1} \right)^{1/d}$$

where

$$(4.7) \quad D = \left( \frac{s_1}{(d-1)s_2} \right)^{1/d}.$$

Depending on the area fraction of charge coverage,  $f$ , and the geometry of the unit lattice cell, the free energy can be calculated for different sets of crystalline structures. For an ideally symmetric system, consisting of equal components of positively and negatively charged molecules with similar head group sizes,  $f$  is 1/2. The minimum free energy in this case, for a two dimensional system, is characterized by lamellar structures.

The line tension is proportional to the immiscibility of the component molecules,  $\chi$  [119]. The Flory-Huggins parameter,  $\chi$ , is defined as the difference in the magnitudes of the short range interactions between two components as  $\chi = (\varepsilon_{12} - \frac{1}{2}(\varepsilon_{11} + \varepsilon_{22})) / k_B T$ , where the  $\varepsilon_{ij}$  represents the pair interaction energy between  $i$  and  $j$ . For a lower, or two dimensional system,  $L_o$  would be comparably larger than for a three dimensional system due not only to the  $1/d$  power law dependence but also to the decreased value of the Bjerrum length  $l_B$  for a surface in contact with water. For a surface in contact with an aqueous solution the mean permittivity of the medium is much higher than in a dense three dimensional system, which decreases the Bjerrum length  $l_B$ , and thus the magnitude of  $L_o$ , significantly. For these reasons, patterning on a surface due to the competition of electrostatic interactions with short range interactions, is considerably more feasible than the creation of charge domains in a bulk three dimensional system.

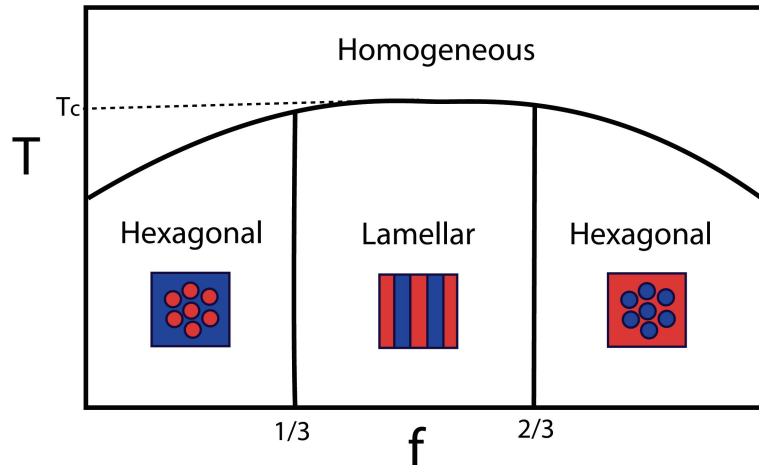


Figure 4.5. Phase diagram of the minimum free energy as a function of charge fraction,  $f$ , and temperature,  $T$ . At high temperatures the density is homogeneous. As temperature is decreased there is a transition temperature,  $T_c$ , at which a periodic phase forms. For charge fractions,  $1/3 < f < 2/3$ , the minimum free energy phase is lamellar. Outside this region the minimum free energy is hexagonal. Figure adapted from Solis et al [118].

Comparing length scales with experimental systems, consider a two dimensional system of a single layer of positively and negatively charged lipids at an interface between water and an alternate medium. The average dielectric permittivity of at the interface  $\epsilon_i \sim 40$ , in between that of the water  $\epsilon_{water} \sim 80$  and that of the dense medium  $\epsilon_{medium} \sim 1$ . This would correspond to a Bjerrum length  $l_B \sim 2nm$  in terms of the a classical electrostatic interaction between charged head groups of the lipids exposed to the aqueous interface. Considering a large magnitude of the net interaction between tails of interacting lipids at the interface ( $\chi \sim 15$ ), depending on the length of the hydrophobic tail of the molecules ( $\sim 20$  carbons) and the charge density of the head-group ( $\sim .6/nm^2$ ), this could correspond to a fairly large equilibrium domain size  $L_o$  ( $\sim 80nm$ ). Domains of this size or larger have been seen for experimental systems of competing short range and long range electrostatic interactions.

### 4.2.2. Scaling analysis at high temperatures

Next, consider the opposite, high temperature regime. Since the system does not exhibit well-defined periodic structures, the entropic contribution to the free energy cannot be ignored. In this case, linear response theory or the Random Phase Approximation for a compressible binary systems [120] is used to describe the behavior of the correlations as a function of the relative strength of the short range attraction and the electrostatic interactions. The Random Phase Approximation for a one component system was introduced in Section 2.1.3. For a general system of  $N$  components, where  $i$  and  $j$  represent components of a different type, the partition function can be written as [121, 122]

$$(4.8) \quad Z = \frac{1}{N_A!N_B!} \int \exp\left(-\frac{H(r_i^{(1)}r_j^{(2)})}{k_B T}\right) \prod_i dr_i^{(1)} \prod_j dr_j^{(2)}$$

where the Hamiltonian of the system is represented by

$$(4.9) \quad H(r_i^{(1)}r_j^{(2)}) = \sum_i \sum_j v_{ij}(r_i^{(1)} - r_j^{(2)}).$$

It is assumed that the interparticle potential can be broken up into a short range and long range electrostatic potential,  $v_{ij} = v_{ij}^{SR} + v_{ij}^{el}$ . The short range contribution is assumed to be of the form of the Fourier transform of a Gaussian potential, which has been shown to reasonably predict thermodynamic properties of binary systems [123],

$$(4.10) \quad v_{ij}^{SR}(r) = \frac{\varepsilon_{ij}}{\pi a^2} e^{-r^2/a^2}.$$

The long range potential is represented by the Debye Hückel potential,

$$(4.11) \quad v_{ij}^{el}(r) = \frac{z_i z_j l_B e^{-\kappa r}}{r}$$

where  $\kappa$ , the inverse screening length, is defined by the concentration of salt in the solution. We assume that the density is a smooth function and can be represented by the sum of its Fourier components

$$(4.12) \quad \rho^i(r) = \sum_k \rho_k^i e^{ikr}.$$

In this case, the partition function becomes

$$(4.13) \quad Z = Z_o \frac{A^{N_A} A^{N_B}}{N_A! N_B!} \int \exp \left( -\frac{1}{2A} \sum_{k \neq 0} \sum_{ij} (\mathbf{U}_k^{ij} + \rho_i^{-1} \delta_{ij}) \rho_k^i \rho_{-k}^j \right) \prod_{k>0} \prod_i \frac{d\rho_k^i}{\pi V \rho_i}.$$

where  $A$  represents the area of a two dimensional plane in a three dimensional volume  $V$ .  $Z_o$  includes the  $k$  zero and the self energy terms.  $\mathbf{U}_k^{ij}$  is the sum of the interaction energies of the system, consisting of the short range interactions due to the excluded volume and hydrophobic interactions,  $v_{ij}^{SR}(k)$ , as well as the long range electrostatic potential,  $v_{ij}^{el}(k)$ .

For an incompressible system of  $i$  same-sized components,

$$(4.14) \quad \sum_i \rho_k^i = 0.$$

For the case of a incompressible, neutral, symmetric system we also assume that  $\rho_+(k) = -\rho_-(k)$ . The electrostatic potential is the two dimensional Fourier transform of the screened

Coulomb interaction between charge density fluctuations,

$$(4.15) \quad U_{el}(k) = \int d^2r e^{ik \cdot r} \frac{\sigma z_T^2 l_B e^{-\kappa r}}{r} = \frac{1}{2} \sigma z_T^2 \frac{2\pi l_B}{\sqrt{\kappa^2 + k^2}}$$

where  $\sigma$  represents the charge density of the system and  $z_T$  represents the total positive and negative charge of the components. In this case, the inverse structure factor has the following contributions,

$$(4.16) \quad \frac{1}{S_0(k)} = U_k + \rho^{-1} = \frac{1}{\rho} + \frac{1}{1 - \rho} - 2\chi + \chi k^2 + U_{el}(k).$$

The structure function has a peak at the most probable wavevector,  $k^*$ . For the case when there is no screening the location of the peak,  $k^*$ , scales with the Bjerrum length,  $l_B$  and magnitude of short range attraction,  $\varepsilon$ , as  $k^* \sim (\varepsilon/l_B)^{\frac{1}{d+1}}$ . The scaling of the periodic order of the system changes at the transition temperature from  $-(1+d)$  at higher temperatures considering small density fluctuations to  $-d$  at lower temperatures, which is predicted using the previously described theory of strong segregation. For a two dimensional system, which is the subject of interest, the scaling is predicted to change from  $-1/3$  to  $-1/2$  as the temperature decreases.

At high temperatures, in the nearly isotropic state, the total free energy of the system per unit volume, in units of  $k_B T$ , can be written as

$$(4.17) \quad \frac{\Delta F(\phi)}{A k_B T} = \phi \ln \phi + (1 - \phi) \ln (1 - \phi) - \chi \phi^2 + F_{ele}/(k_B T),$$

where  $A$  represents the two dimensional area of a plane and  $F_{ele}/(k_B T)$  represents the one loop corrections obtained by integrating the charge density fluctuations [121]. This contribution to the free energy will be derived in Chapter 7 for charges at an interface.

### 4.3. Summary and conclusions

In this chapter, multiple examples of pattern formation for several different experimental systems which display pattern formation are given. These systems include langmuir monolayers, membranes, magnetic systems, semiconductors, and gels. In order to understand the phase behavior for systems displaying competing electrostatic and short range van der Waals interactions, an ideal model is developed of immiscible, but oppositely charged particles molecular components confined to an interface. The formation of lamellar and hexagonal periodic domains is described theoretically at low temperatures, using strong segregation theory. This is compared with scaling at high temperatures, in which a mean field approach is used to describe density fluctuations in the transition from the disordered to ordered state. In the next chapter, these theoretical results will be compared with the results of molecular dynamics simulations at intermediate temperatures.

### 4.4. Acknowledgements

I would like to gratefully acknowledge Dr. Monica Olvera de la Cruz for guidance concerning the analysis at high temperatures, Dr. Francisco Solis for the development of analytic theory at low temperatures.

## CHAPTER 5

# Molecular Dynamics of Pattern Formation

### 5.1. Introduction

In the previous chapter, a model of competing electrostatic and short range van der Waals interactions for molecules strongly adsorbed to interfaces was outlined. The formation of lamellar and hexagonal periodic domains was described theoretically at low temperatures. This was compared with scaling at high temperatures, in which a mean field approach is used to describe the density fluctuations. In the present chapter, these theoretical results will be compared with molecular dynamics simulations at intermediate temperatures, for both the formation of lamellar, as well as hexagonal domains. The formation of lamellar domains will be characterized at intermediate temperatures using molecular dynamics, including relevant thermodynamic quantities. In addition, the electrostatic contribution to the ordering of the interface between the domains is characterized. When considering the formation of hexagonal domains, at finite temperatures there are deviations from both the shape and packing within the domain structures. These quantities, as well as the effects of considering different stoichiometric charge ratios will be discussed. It is found that changing the charge ratio of the components allows for the freezing of the local inter domain structure, using the Lindemann Criterion.

## 5.2. Molecular dynamics of pattern formation at the interface

The model system is composed of a mixture of  $N_+$  positively and  $N_-$  negatively charged monomer units in a simulation box of size  $L^3$ . The molecules are confined to a two-dimensional plane perpendicular to the  $Z$  axis, with periodic boundary conditions in the  $X$  and  $Y$  directions. Each monomer unit represents a charged biological or polymeric molecule, that interacts attractively with a like monomer via hydrophobic forces. To begin with, only symmetric mixtures are considered, where the charge and radius of the positively and negatively charged monomer units are equivalent. The total system is electroneutral. We are interested in the case where the two-dimensional layer exhibits well-defined periodic patterns along the surface of the plane. Fluctuations perpendicular to the monomer plane are restricted.

N,V,T molecular dynamics simulations were performed using Espresso, a simulation code developed by the MPIP-Mainz group of Polymer Theory and Simulation. A stochastic or Langevin thermostat is used, to ensure a constant temperature, along with a Verlet algorithm to calculate particle velocities at each timestep. The unit of energy is  $\varepsilon$ , of length  $\sigma$ , and of mass  $m$ . Temperature is then defined in terms of  $\varepsilon/k_B T$  and time in units of  $\sqrt{\sigma^2 m / \varepsilon}$ . A full Coulomb potential is used for calculations of charge-charge interactions. The ELC (Electrostatic Layer Correction) method developed by Arnold et al. to sum the electrostatic energy contribution to the free energy [37, 38]. This method is a correction to the P3M Ewald summation technique, [124] in which the Fourier transform of the electrostatic contribution to the energy is summed using a mesh formulation, as described in Section 2.2.5. Table 5.1 summarizes the interaction potentials between the positive and negative component monomers in this system. The potential between charges is the full

Interactions	+	-
+	$U_C + U_{LJ}$	$U_C + U_{HC}$
-	$U_C + U_{HC}$	$U_C + U_{LJ}$

Table 5.1. Interparticle potentials

Coulomb potential,

$$(5.1) \quad U_C = \frac{l_B T q_1 q_2}{r}$$

where  $l_B$  represents the Bjerrum length of the system.

For the present simulation results,  $l_B$ 's of  $0.1\sigma$ ,  $0.2\sigma$  and  $0.5\sigma$  are considered. Considering an average dielectric permittivity of the medium ( $\epsilon_r \sim 80$ ) this corresponds to a fairly large headgroup size ( $\sim 20\text{\AA}$ ). The short range interaction between like monomers is the classic Lennard Jones potential,

$$(5.2) \quad U_{LJ} = 4\epsilon \left( \left( \frac{\sigma}{r} \right)^{12} - \left( \frac{\sigma}{r} \right)^6 \right) \quad r < r_c$$

where  $\sigma$  is the monomer radius, and the potential is cut at a radius  $r_c$  of  $2.5\sigma$ . An additional term is also added to the potential to keep the derivative continuous at  $r_c$ .  $U_{HC}$  is the same as  $U_{LJ}$ , with a cutoff radius,  $r_c$ , of  $2^{1/6}\sigma$ , including only the repulsive part of the potential, which represents the excluded volume of the molecule.

A fairly dense surface particle density,  $\rho$ , of 0.6 was examined, to compare with phase behavior predicted by strong segregation theory, while remaining sufficiently far from the two dimensional hard disc crystallization regime of approximately  $\rho = 0.89$ , as determined by previous Monte Carlo and molecular dynamics simulation studies [125]. This allows

sufficient diffusion for the system to equilibrate, as described in the next section.

$$(5.3) \quad \rho = \frac{(N_+ + N_-)\pi\sigma^2}{4L^2}$$

Phase behavior in comparison with theory at lower surface densities is slightly more complex and will be discussed in Chapter 7. In this section, the majority of simulation results are presented for a system size of 1000 charged monomers, while finite size effects are explored by increasing the system size by a factor of 2. Approximately  $10^6$  MD steps are used to equilibrate the system; the equilibration time grows increasingly longer at higher values of the Bjerrum length.

To determine if  $\rho = 0.6$  was sufficiently far from the crystallization regime, the mean square displacement as a function of MD timestep was calculated. Using the Einstein relation for linear diffusion, the magnitude of  $D$  the diffusion constant can be obtained.

$$(5.4) \quad 4D = \lim_{t \rightarrow \infty} \frac{\partial |\Delta r(t)|^2}{\partial t}$$

While diffusion is linear initially, nonlinearity starts developing at values of  $\varepsilon/k_B T \geq 4.0$ . In these cases, particles are trapped within each stripe and become caged within its boundaries. This represents the limit of the Newtonian diffusion regime. If the value of  $D$  is examined for different values of the electrostatic strength, the initial diffusion is similar, but, for higher values of  $\varepsilon$ , the system with the higher  $l_B$  has faster diffusion on the surface. However, for both systems, a regime of very small diffusion is approached as  $\varepsilon/k_B T$  increases. For the scope of this thesis, only regimes that display linear diffusive behavior are considered.

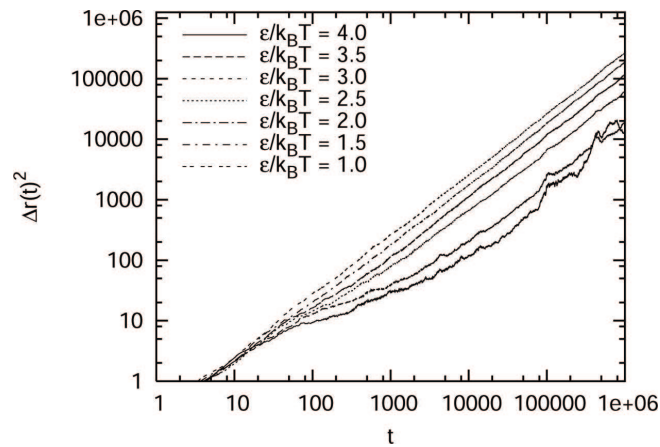


Figure 5.1. Mean square displacement as a function of timestep at  $l_B/\sigma = 0.5$  for values of  $\varepsilon/k_B T = 1.0 - 4.0$ . While diffusion is linear initially, nonlinearity starts developing at  $\varepsilon/k_B T = 4.0$

### 5.2.1. Formation of lamellar phase

At lower values of  $\varepsilon$ , domains of positive and negative component monomers appear in the system. As the magnitude of  $\varepsilon$  increases, the domains begin to increase in size in an

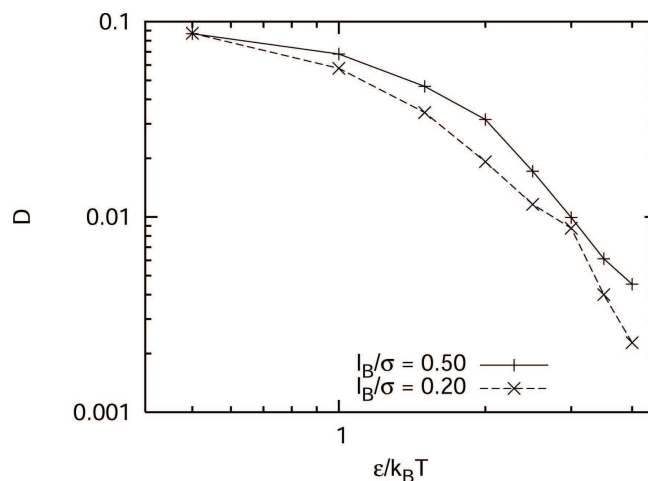


Figure 5.2. Diffusion coefficient,  $D$ , as a function of short range interaction  $\varepsilon/k_B T$ , for two comparable values of the Bjerrum length,  $l_B/\sigma = 0.2, 0.5$ . With increasing  $\varepsilon$ , faster diffusion is seen for higher values of  $l_B$ , but both systems approach a regime of very small diffusion.

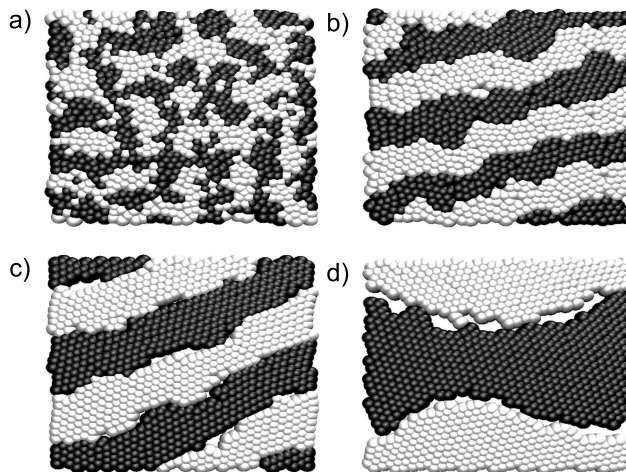


Figure 5.3. Snapshots of the system at a)  $\varepsilon = 1.0$ , b)  $2.5$ , c)  $4.0k_B T$  at a constant  $l_B$  of  $0.2\sigma$ . Introduction of  $\kappa = 20\sigma$  d) induces macroscopic phase segregation at an  $\varepsilon$  of  $4.0k_B T$ ,  $l_B$  of  $0.2\sigma$ .

isotropic manner, forming a percolated structure. As the value of  $\varepsilon$  further increases, the domains begin elongate and then to orient into well-defined lamellar, breaking the symmetry of the system. Increasing even further, the lamellar begin to widen. Average internal energy and heat capacity per particle are calculated at several values of Bjerrum length ( $l_B = 0.1\sigma, 0.2\sigma, 0.5\sigma$ ). At higher values of  $l_B$ , electrostatics plays a more important role in the equilibrium configuration of the system. The electrostatic repulsion between like charged monomers increases. In order to minimize this contribution to the free energy, the stripes become thinner.

The average internal energy ( $\langle E \rangle / N$ ) and heat capacity per particle ( $C_V$ ) are calculated at several different values of the Bjerrum length ( $l_B = 0.1\sigma, 0.2\sigma, 0.5\sigma$ ). The average internal energy is less negative at the higher value of  $l_B$  due to the increased repulsion between like charged head groups. At lower values of  $l_B$  the heat capacity displays a peak, which corresponds to the crossover from the percolated phase to the lamellar phase. The

magnitude of this peak increases and shifts to the left as the value of the Bjerrum length is decreased.

Lamellar spacing is systematically characterized by the calculation of the two dimensional structure factor,  $S(\vec{k})$ , where  $\vec{r}$  corresponds to a vector in the x,y plane.

$$(5.5) \quad S(\vec{k}) = \int g(\vec{r} - \vec{r}') e^{i\vec{k}\cdot\vec{r}} e^{i\vec{k}\cdot\vec{r}'} d^2\vec{r}$$

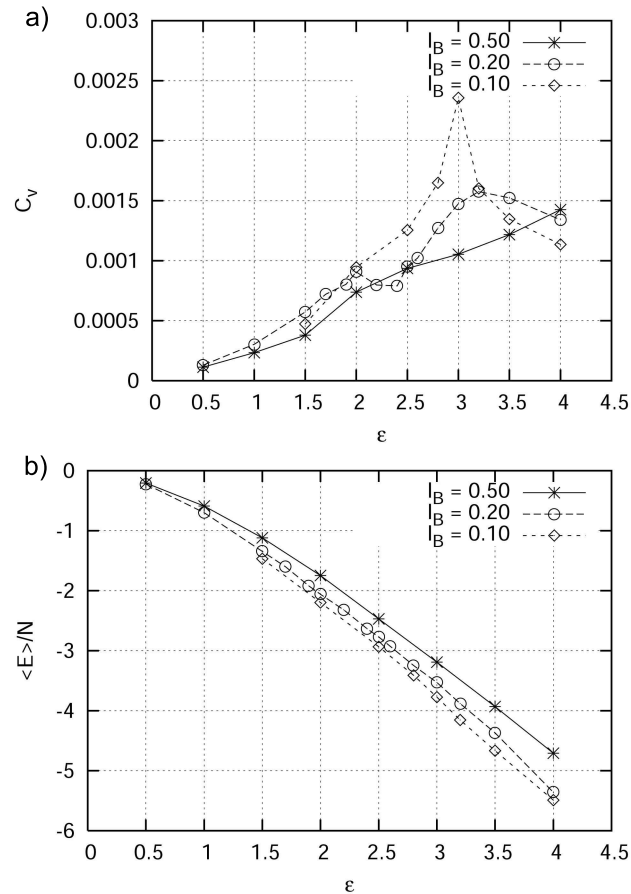


Figure 5.4. a) Heat capacity per particle ( $C_V$ ) and b) average internal energy ( $\langle E \rangle / N$ ) at several values of the Bjerrum length ( $l_B = 0.1\sigma, 0.2\sigma, 0.5\sigma$ ). The heat capacity displays a peak, which corresponds to a crossover from percolated, random domains to a lamellar phase. The magnitude of the peak increases and shifts to the left as the value of the  $l_B$  is decreased.

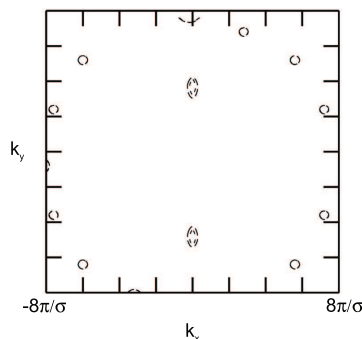


Figure 5.5. Contour plot displaying the location of the peak,  $k^*$ , in the structure factor,  $S(k)$ , for several values of short range attraction  $\varepsilon = 4.0$  and  $l_B = 0.5$ . The peaks are located at 90 degrees and 270 degrees respectively.

$S(\vec{k})$  displays a peak at  $k^*$  corresponding to the inverse lamellar spacing in the direction perpendicular to the lamellar.

As a function of  $\varepsilon$ , the peak location corresponds to scaling predictions by strong segregation theory at high values of  $\varepsilon$  ( $k^* \sim \varepsilon^{-1/2}$ ). At lower values, the location is consistent with predictions by the Random Phase Approximation ( $k^* \sim \varepsilon^{-1/3}$ ).

The orientational order of the domains can be characterized by the interfacial orientational order parameter  $g_2$  [126].

$$(5.6) \quad g_2 = \frac{1}{N} \sum_{i=1}^N \frac{1}{N_i} \sum_{j=1}^{N_i} e^{2i\theta_{ij}}$$

where  $N_i$  is the number of neighbors of opposite type of monomer at an interface and  $\theta_{ij}$  is the angle between two neighbors. A neighbor is defined as two particles of different type, within range of short range attraction ( $r_{ij} < r_c$ ). As the magnitude of short range attraction increases, the calculated order parameter increases, which corresponds to the ordering of the domains by the development of orientational order at the interface. The increase in order

of the domains, indicated by an increase in the order parameter  $g_2$ , proceeds the location of the peak in the heat capacity. Higher values of the Bjerrum length  $l_B$  correspond to a higher value of the order parameter  $g_2$  for stronger short range attraction. As the electrostatic contribution to the segregation increases, the characteristic domain size decreases, but the orientational order of the domains increases. At lower values of  $l_B$ , this initial increase is followed by a levelling off, or slight decrease, that corresponds to the formation of holes at the interface. The holes disrupt the orientational order, or the hexagonal packing, of the monomers within the segregated domains. This is equivalent to the inclusion of a ternary component with a non-selective interaction between positive and negative components. This topic will be discussed further in Chapter 7.

Examinations on the finite size effects of the system are explored to determine the effect of the periodic boundary conditions on the ordering of the more strongly segregated lamellar. Doubling the size of the system at larger values of the short range attraction ( $\varepsilon = 4k_B T$ ), quantitatively affects the ordering of the lamellar by decreasing the alignment of the domains along the boundaries of the system and increasing the fluctuations along the interface. This results in a characteristic decrease in the order parameter,  $g_2$  from .43 ( $\pm .02$ ) to .37 ( $\pm .02$ ). This leads to the conclusion that the finite size of the system may slightly promote the ordering of the interface between solid domains.

Molecular dynamics simulations of oppositely charged monomers, interacting with a short range LJ potential and confined to a two dimensional plane, are examined at different strengths of short range attraction and long range electrostatics. The system exhibits well-defined domains; the width and ordering of the domains are dependent on the depth of the LJ well,  $\varepsilon$ , and the strength of the Coulomb interactions,  $l_B$ . The length-scale of the

ordering of the system can be quantitatively characterized by the two dimensional Fourier transform of the density,  $S(\vec{k})$ , where  $\vec{k}$  is the inverse spacing of the system.  $S(\vec{k})$  has a peak  $k^*$  which scales with the line tension of the domains,  $\gamma$ . The underlying assumption of strong segregation theory is that the microphase regions of charge are well defined and periodic, with a line tension  $\gamma$  that is proportional to  $\chi$ . Since the magnitude of the short

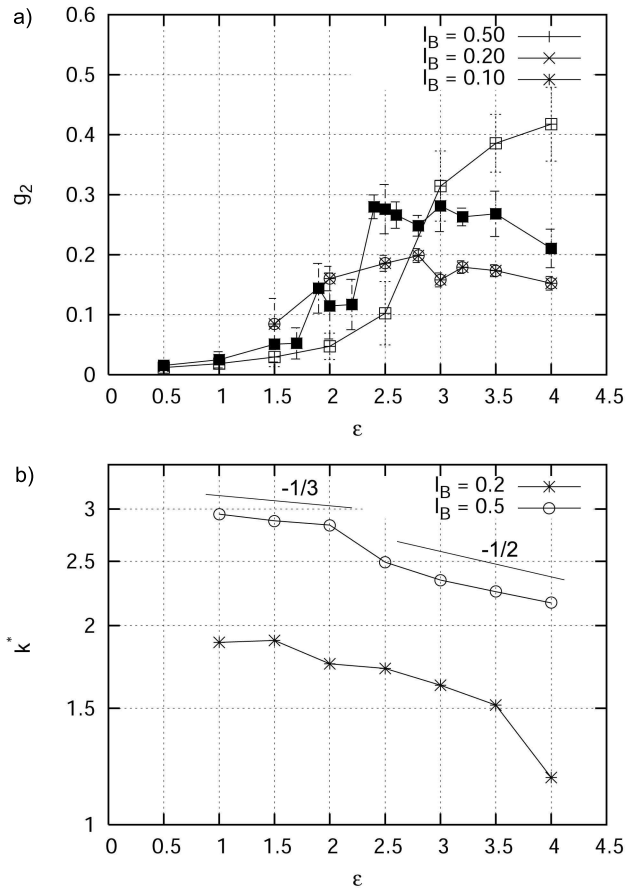


Figure 5.6. a) The interfacial orientational order parameter  $g_2$  at several values of the Bjerrum length ( $l_B = 0.1\sigma, 0.2\sigma, 0.5\sigma$ ) as a function of  $\varepsilon$ . As the orientational order of the domains increases,  $g_2$  increases from 0 to a finite value. b) The location of the peak  $k^*$  in the structure factor  $S(\vec{k})$  as a function of  $\varepsilon$ . The scaling of  $k^*$  with  $\varepsilon$  changes from  $-1/3$  to  $-1/2$ .

range attraction  $\varepsilon$  is proportional the Flory-Huggins interaction parameter  $\chi$ ,  $k^*$  should scale with  $\varepsilon$  in the regimes where strong segregation theory holds [118]. It is shown that, at higher values of  $\varepsilon$ , the scaling of  $k^*$  with  $\varepsilon$  is consistent with theory. At lower values of  $\varepsilon$ , a different scaling is found, which is consistent with that which is found using linear response theory. Electrostatics represents a more important contribution to the characterization of the interfacial line tension in this regime.

The degree of ordering can be examined by the calculation of the interfacial orientational order parameter,  $g_2$ . The transition from a random, percolated domain structure to well defined lamellar is a gradual transition, that is demonstrated by the gradual increase of the parameter  $g_2$  as a function of  $\varepsilon$ . This result is consistent with what one would exhibit with a Kosterlitz and Thouless type transition [125], in which the two dimensional ordering the system exhibits a continuous phase transition, that can be defined by a similar positional order parameter. It is clear that higher strengths of electrostatic interactions leads to higher values of interfacial order, which leads to the conclusion that the electrostatics may have a definite role in the shape and stability of the microphases.

Examinations of the finite size effects of the system indicate that the degree of ordering is slightly influenced by the periodicity of the simulation box, however, further examinations were not made due to the computational intensiveness of the electrostatic energy term. Decreasing the strength of the electrostatics in the system, by changing the charged interaction from a straight Coulomb potential to a screened Debye Hückel interaction, the ordering of the system disappears and the mixture phase segregates as shown in Fig. 5.3 d), which is consistent with analytical arguments, as will be discussed in Chapter 6.

### 5.2.2. Formation of hexagonal phase

The theory of shape asymmetry for finite two dimensional domains has been considered due to the in-plane dipolar interactions [96] and charged or dipolar interactions perpendicular to the surface for a singular domain shape [103]. For the case of a finite domain, the free energy is the sum of the charged or dipolar interactions, as well a contribution due to the line tension at the interface. It has been shown that the free energy can be written in terms of the anisotropy of the domains, such as a square, an ellipse, or a torus [127]. Moreover, the free energy can be minimized with respect to the periodic length scale of the inter domain spacing, including the electrostatic interactions between multiple domains [118], which has been demonstrated for the lamellar and hexagonal case. This is increasingly important as the density of the domains on the surface is high. As shown previously, for a symmetrically charged system, the lowest free energy state is lamellar. However, for an asymmetric ratio of positive and negative charged groups, the lowest free energy state consists of spherical domains arranged in a hexagonal lattice. The coexistence between lamellar and hexagonal phases has also been considered, in addition to superdomain structures [?].

In experimental systems, such as monolayers at an air water interface or else biomembranes, equilibrium structures between that of lamellar and hexagonal structures are also seen. This transition is presumed to be temperature and concentration dependent. In addition, the domains themselves are not perfectly spherical, but slightly elliptical [103]. In terms of langmuir monolayers, the asphericity of the domains may also result from an in-plane dipolar molecular moment [127], dependent on the specific chemistry of the lipid molecules. In this section, the asphericity of the domains is considered for different strengths of the electrostatics relative to the short range van der Waals interaction between the components

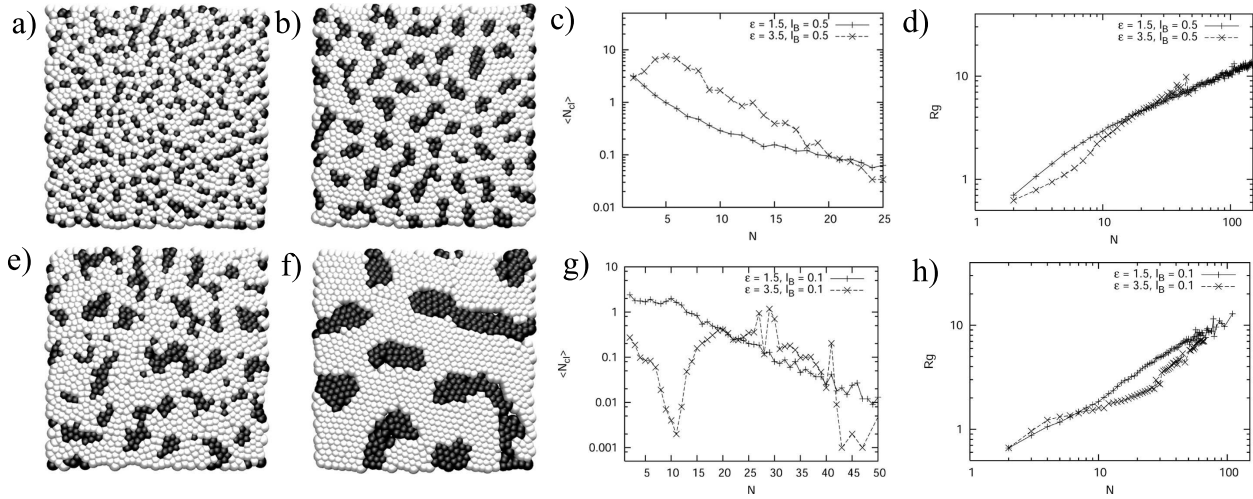


Figure 5.7. Snapshots of the equilibrium domain shapes, domain distribution,  $N_{cl}$  vs  $N$ , and radius of gyration,  $R_g$  vs  $N$  for a higher Bjerrum length a-d)  $l_B/\sigma = 0.5$ , and lower Bjerrum length e-h)  $l_B/\sigma = 0.1$ .

by using molecular dynamics simulations. In addition, the degree of crystallinity in the local structure is calculated using the Lindemann criterion, a parameter well known in solid state physics for the characterization of the melting temperature of solids [128].

Electrostatics plays a significant role in the formation of the domains, as well as the resulting equilibrium shape. In this section, the results are presented for 900  $N_+$  positively and 300  $N_{3-}$  negatively charged monomer units of charge 3-. The charge ratio is defined as  $f = \frac{N_+}{N_-} = \frac{z_-}{z_+} = 3$ . To begin with, the formation of domains at two different strengths of electrostatic interactions is presented, as shown in Fig. 5.7. The top row represents higher values of the Bjerrum length,  $l_B = 0.5$ , while the bottom row represents lower values of the Bjerrum length,  $l_B = 0.1$ . As the value of  $\epsilon$  is increased, for a constant value of the Bjerrum length, the negatively charged particles begin to cluster into domains as shown in Fig. 5.7 a) and e), the first images on the left. The size of the initial domains, as well as the distribution of domain sizes is dependent on the Bjerrum length. For stronger values of the

Bjerrum length the negatively charged particles possess less of a tendency to cluster and are more disperse (Fig. 5.7 a). For lower values of the Bjerrum length, there is a distribution of randomly ordered, as well as much larger, domains as shown in Fig. 5.7 e).

In Fig. 5.7 b) and f), the images shown immediately to the right, increasing the short range interaction  $\varepsilon$  results in the formation of finite domains. Here, in b), the domains remain small for high values of the Bjerrum length. For lower values of the Bjerrum length, in f), the resulting structures are a result of the competition between the short range interactions, which promotes the growth of the domains, with the electrostatics, which prefers an elongated interface. In certain cases, these domains also display a preference for curvature perpendicular to their axis.

Immediately to the right of these images, the cluster size distribution for these respective images are shown. Initially, the average number of clusters  $N_{cl}$  per size  $L^2$  of the simulation box is exponentially decreasing with  $N$ , the number of particles per cluster, 5.7 c) and g). As the value of  $\varepsilon$  increases, the distribution function develops a small peak at finite size  $N$ , corresponding to domain formation. This peak has much greater distribution, and for a higher number of particles, for the lower value of Bjerrum length, Fig. 5.7 g). Increasing the electrostatic strength, decreases the size of the domains.

The average radius of gyration as a function of  $N$  is plotted immediately to the right of the previous images. The interesting thing to notice is that there is a transition at a certain cluster size to different types of scaling behavior, upon increasing  $\varepsilon$ . Below this lengthscale,  $R_g$  scales like  $N^{1/2}$  which is to be expected for spherical domains. For larger clusters above this critical size,  $R_g$  scales linearly with  $N$ . This is to be expected for stretched, linear domains. This critical size transition from circular to non-circular domains has been coupled

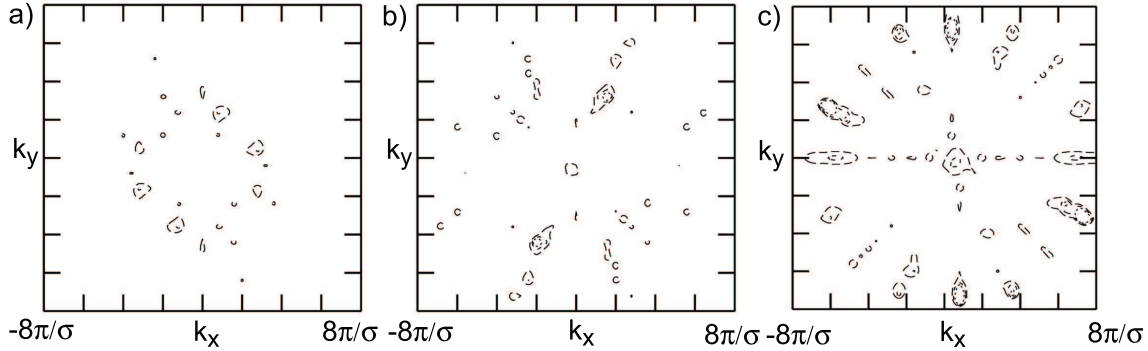


Figure 5.8. Structure factor,  $S(k)$ , for value of short range attraction ( $\varepsilon/k_B T = 4.0$ ) for different strengths of the electrostatics,  $l_B/\sigma =$  a) 0.1, b) 0.2, c) 0.5. The local ordering of the domains is not perfectly hexagonal. For higher values of the electrostatics ( $l_B/\sigma = 0.5$ ) the ordering at larger length scales displays a cubic, or square, structure, which may be a finite size effect.

theoretically with the line tension, charge density, and the area of the individual domain [103]. This is consistent with these simulation results.

The ordering of the domains on the interface can be further examined by examination of the two dimensional structure factor,  $S(k)$ , as in the lamellar case. In Fig. 5.8, contour plots of the structure factor for three different strengths of the electrostatics,  $l_B/\sigma = 0.1, 0.2, 0.5$ , are shown. The local ordering of the domains does not display perfect sixfold symmetry. Notice the ring of peaks at small values of the wave vector in the left image of Fig. 5.8, corresponding to  $l_B/\sigma = 0.1$ . The domains themselves are not perfectly spherical, as shown in the previous subsection, which does not allow for perfect hexagonal packing. For a larger system size, this ring should become more diffuse. For increasing values of the electrostatics, image in the middle and right of Fig. 5.8, the ring of peaks corresponding to the local domain structure shifts to the outside of the image, larger values of the wave vector. The ordering at larger length scales, smaller wave vectors, indicates cubic, or square, structure, close to

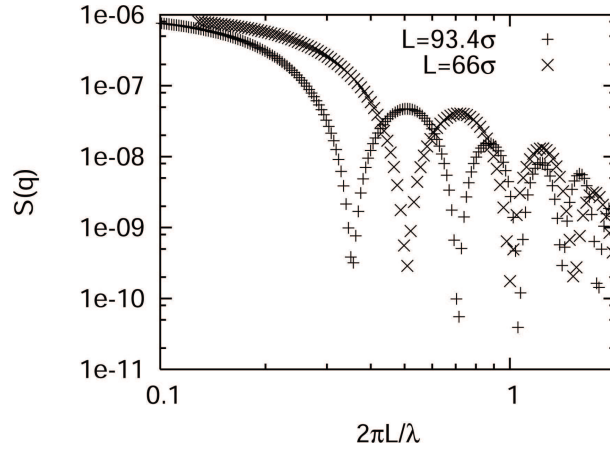


Figure 5.9. Structure factor,  $S(k)$ , for value of short range attraction ( $\varepsilon/k_B T = 4.0$ ) for strengths of the electrostatics,  $l_B/\sigma = 0.5$ . The ordering at larger length scales at an angle perpendicular to the box edges displays a cubic, or square, structure. Increasing the total area of the box by a factor of two from  $L = 66\sigma$  to  $L = 93.4\sigma$  show that these peaks shift relative to the box size.

the center of the image. Examination at larger system sizes will indicate this is a finite size effect. The structure factor,  $S(k)$ , for value of short range attraction ( $\varepsilon/k_B T = 4.0$ ) for strengths of the electrostatics,  $l_B/\sigma = 0.5$  was examined. Increasing the total area of the box by a factor of two from  $L = 66\sigma$  to  $L = 93.4\sigma$  show that these peaks shift relative to the box size as shown in Fig. 5.9. This ordering, then, is indicated to be an artifact of the box.

The local ordering of the domains can be further characterized using the Lindemann criterion. Peierls and Landau argued that there is no long range order for a two dimensional solid [129, 130, 131]. The local thermal fluctuations of the atoms induces a displacement with respect to the equilibrium position which increases logarithmically with the system size. For two dimensional Coulombic systems, it has been suggested that although long range translational order cannot exist, long range orientational order can be extended infinitely far [132]. Melting in two dimensions is synonymous with a Kosterlitz and Thouless transition

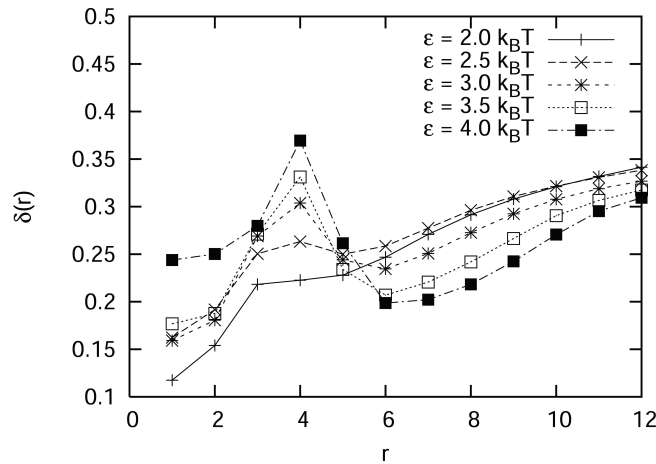


Figure 5.10. Normalized root mean square displacement,  $\delta(r)$ , of the center of masses of domains for increasing values of  $\varepsilon$ . Lindemann Criterion,  $\delta(r)$ , indicates that the local structure of the domains are liquid for these values of the parameters,  $l_B$  and  $\varepsilon$ .

[133, 134], which was further extended by Halperin and Nelson, in which the local structure melts through dislocations [135, 136]. The Lindemann criterion has been used to study melting and condensation for two dimensional Coulombic systems [137], and, in this case, is applied to the study of the underlying lattice structure of the domains of the solid phase. For two dimensional systems, the melting of the structure is when the root mean square value of the lattice fluctuations exceeds 0.1 of the lattice spacing.

The center of masses of the charged domains represent the lattice structure for the two dimensional Wigner crystal formed by the solid phase. For perfect circular domains at low temperatures, the center of masses of the neighboring domains should occupy equilibrium positions in an hexagonal lattice. The fluctuations of the center of masses of the domains about this equilibrium lattice increases with temperature, and, at a certain ratio of the fluctuation length scale relative to the periodicity of the lattice, the structure should melt. The root mean square displacement for the center of mass,  $R$ , of each cluster,  $cl$ , is defined

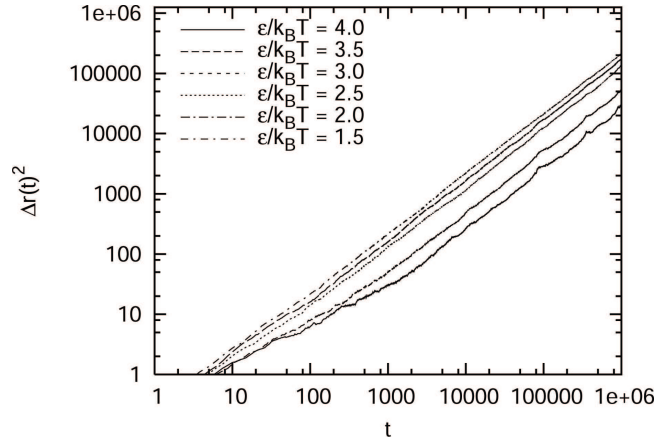


Figure 5.11. Mean square displacement as a function of timestep at  $l_B/\sigma = 0.5$  for values of  $\varepsilon/k_B T = 1.5 - 4.0$ . While diffusion is linear initially, nonlinearity starts developing at  $\varepsilon/k_B T = 4.0$

as

$$(5.7) \quad \delta(r) = \frac{1}{N_{cl,i}} \sum_{cl,i} \frac{\frac{1}{N_{cl,j}} \left( \sum_{cl,j} (R_{cl,i} - R_{cl_j})^2 \right)^{\frac{1}{2}}}{R_{cl,i} - R_{cl_j}}.$$

Upon examination of the Lindemann criterion,  $\delta(r)$ , the root mean square displacement of the domain center of masses, it is found that the local fluctuations exceed the Lindemann Criterion limit (0.1 normalized by the lattice spacing). Examining Fig. 5.10, the peak represents the first appearance of neighboring domains, followed by a minimum which indicates the local ring structure. The increase after the minimum is due to the appearance of non-neighboring domains. The minimum is coincident with the local fluctuations in the ordering of the domains. Upon increasing  $\varepsilon$ , the short range attraction, the fluctuations in the local lattice of domains is decreasing, but not enough to form a locally frozen phase. The local domain structure is thus still liquid. This agrees with the diffusion of the particles, from the mean square displacement, as a function of timestep.

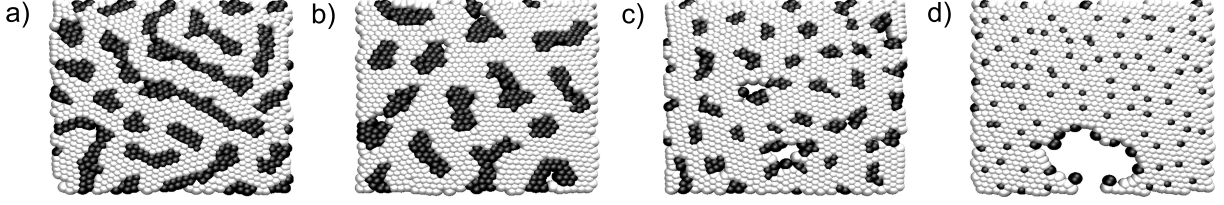


Figure 5.12. Snapshots of simulations for values of short range attraction ( $\epsilon/k_B T = 4.0$ ) for strength of the electrostatics,  $l_B/\sigma = 0.5$ , for varying charge ratios of the components. a) 2:1, b) 3:1, c) 5:1, d) 10:1.

### 5.2.3. Asymmetric charge ratios and the Lindemann Criterion

An interesting question to examine is to study the transition from the lamellar to hexagonal phases by varying the charge ratio of the components,  $f$ , while still maintaining the electro-neutrality of the system. In this section, the results are presented for  $zN_+$  positively and  $N_{z-}$  negatively charged monomer units of charge  $z-$ . The charge ratio is defined as  $f = \frac{N_+}{N_-} = \frac{z-}{z+} = z-$ . For different charge ratios of the components, the magnitude of the electrostatic and short range contributions to the free energy are shifted, so that increasing the charge asymmetry results in the freezing of the local crystalline order of the domains.

To characterize the shape transition, it is necessary to measure the magnitude of the asphericity of the individual domains as a function of the charge ratio of the components. The matrix of inertia of the domains is defined as

$$(5.8) \quad T_{x,y} = \frac{1}{N_{Cl}} \sum_i^{N_{Cl}} (r_x^i - \bar{r}_x)(r_y^i - \bar{r}_y)$$

where  $N_{Cl}$  represents the number of ions in one cluster or domain and  $r_x^i$  represents the component of the position of  $i$ th ion. The eigenvalues of the matrix represent  $Rg_{\perp}^2$  and  $Rg_{\parallel}^2$ . Taking the ratio,  $R$ , of  $Rg_{\perp}$  to  $Rg_{\parallel}$ , a value close to 1 signifies a more spherical domain. The distribution for the asymmetry of the domains changes as a function of the charge ratio of

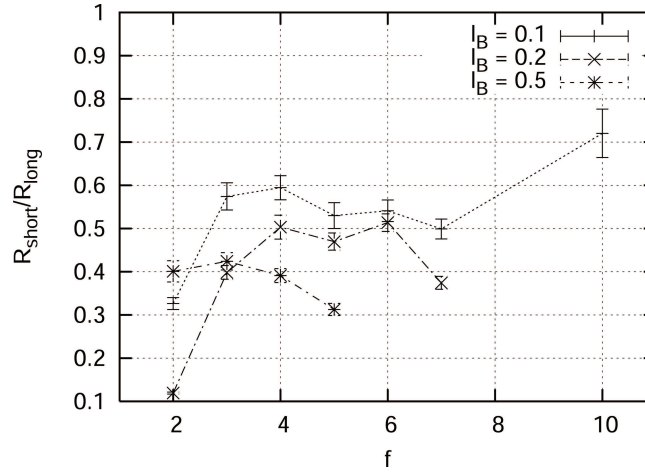


Figure 5.13. Ratio of the asymmetry of the domains as a function of the charge ratio of the components. The most spherical domains are present for charge ratios,  $f$ , close to 3 : 1, while for increasingly asymmetric mixtures, there is a gradual increase in the asymmetry of the domains.

the components, as seen in Fig. 5.13. Starting from a symmetric system, this ratio increases so that the most spherical domains are present for charge ratios,  $f$ , of 3 : 1. However, for increasingly asymmetric mixtures, there is a gradual increase in the asymmetry of the domains, until the domains are simply single particles, arranged in a hexagonal lattice.

Upon examination of the Lindemann criterion for a fixed ratio of the electrostatics to the short range interactions ( $l_B/\sigma = 0.5, \varepsilon = 4.0$ ) the root mean square fluctuations of the domain positions relative normalized by the average radius of the inter domain distances, the Lindemann Criterion is than 0.1 of the inter domain distance for values of  $f < 7$ . As in the previous figure, in Fig. 5.14 the peak represents the first appearance of neighboring domains, followed by a minimum which indicates the local ring structure. However, upon increasing the charge ratio of the components, the peak shifts to the left. The inter domain distance is shrinking. The minimum, corresponding to the fluctuations in the local ordering

of the domains, decreases until it passes under the Lindemann criterion ratio for a charge ratio between 7:1 and 10:1.

The short range order of the local hexagonal lattice is freezing as a function of increased electrostatic interactions between the minority components. At these ratios of the electrostatics, the domains mainly consist of single particles. In addition, the solid phase is compressing, so the additional empty space is expelled from the solid phase. In examining Fig. 5.12 c) this is signified by the region of empty space that is segregated from the solid phase. If the local structure is freezing or forming a glass, this should be signified in the thermodynamic quantities such as the heat capacity of the system. Indeed, as a function of the charge asymmetry of the system, the heat capacity per molecule displays a peak for charge ratios of 5:1. This indicates the onset of the freezing of the local order of the system. Upon examination of the diffusion of the particles, from the root mean square displacement, for charge ratios greater than 5:1 diffusion becomes non-linear. This indicates the formation of a glass.

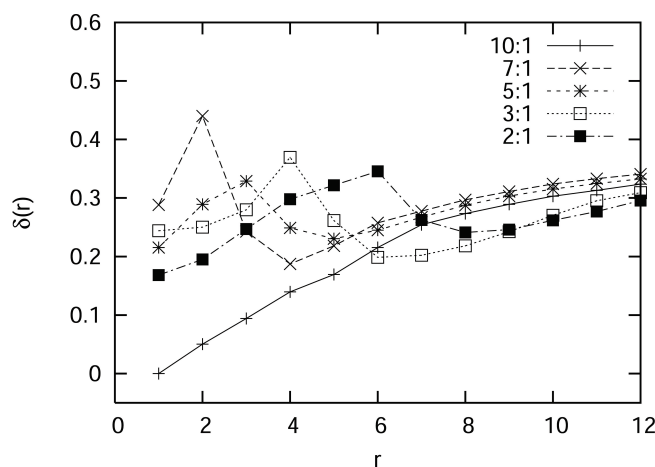


Figure 5.14. Normalized root mean square displacement,  $\delta(r)$ , of the center of masses of domains as the asymmetry of the system is changed.

The long range order of the domains can be further examined using the structure factor,  $S(k)$ . As a function of increasing charge ratio of the components, there is a clear shift from lamellar ordering to hexagonal-type ordering. In Fig. 5.17 on the left,  $S(k)$ , displays two peaks that correspond to lamellar phases at angles slightly tilted from the horizontal as seen in snapshot in Fig. 5.17 a). With increase in the charge ratio of the components, the lamellar peaks disappear and a ring of peaks reminiscent of hexagonal order appears. Cubic structure is indicated at long wavelengths, which may again consist of a finite size effect.

This transition from the lamellar to the hexagonal phase is relevant to many systems. For example, domain shape instabilities from circular domains to branched phases have been shown to be induced upon compression of langmuir monolayers [92]. The electrostatic contribution to the pattern formation in these systems, as it pertains to the monolayer films, at high densities, is decidedly relevant to the melting transitions of these films. It is

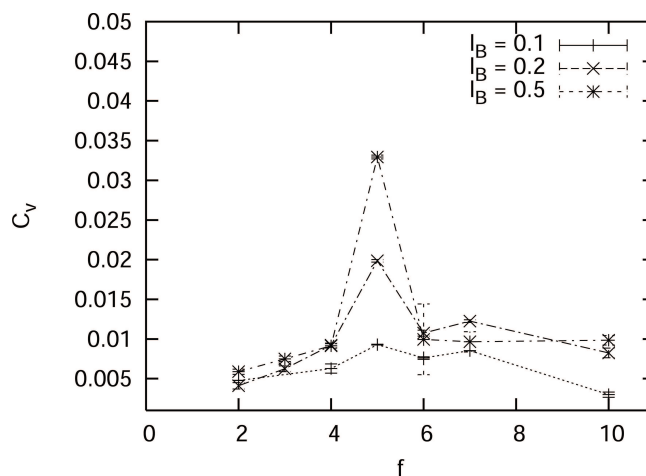


Figure 5.15. Heat capacity per particle as a function of the charge ratio of the components. Fluctuations peak for charge ratios of 5:1. This is the onset of the formation of a Wigner crystalline phase.

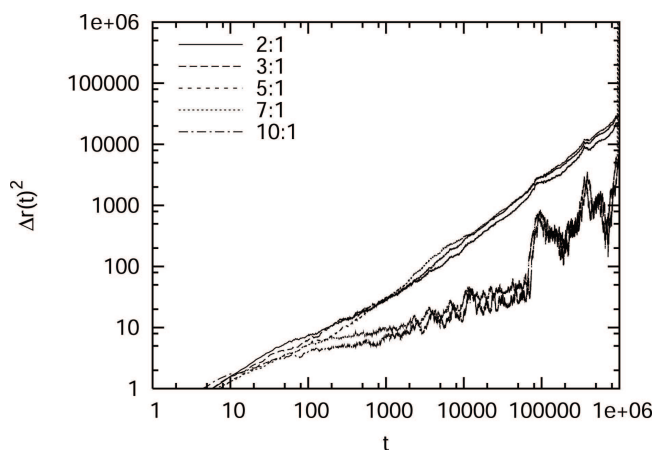


Figure 5.16. Mean square displacement as a function of timestep at  $l_B/\sigma = 0.5$  and  $\varepsilon/k_B T = 4.0$ , for increasing charge ratios of the components. For charge ratios  $> 5:1$ , diffusion becomes non-linear. This indicates the formation of a glass.

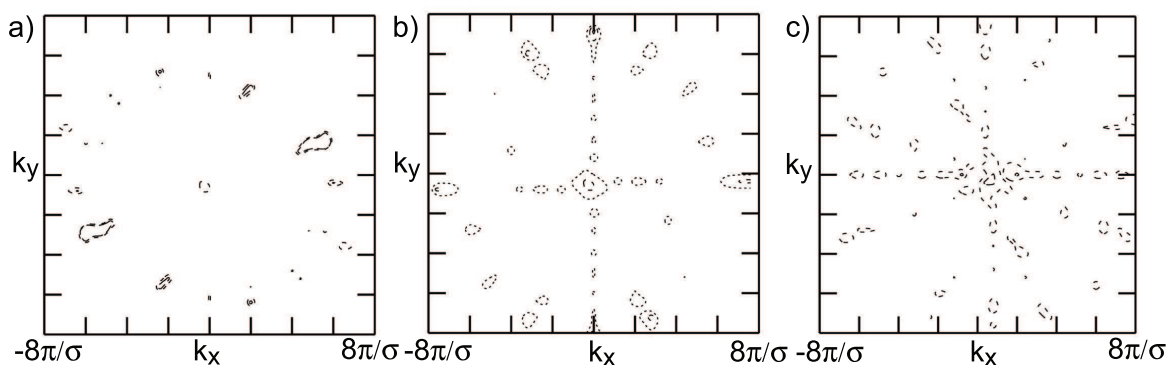


Figure 5.17. Structure factor,  $S(k)$ , for value of short range attraction ( $\varepsilon/k_B T = 4.0$ ) for strength of the electrostatics,  $l_B/\sigma = 0.5$ , for varying charge ratios of the components. From left to right, a) 2:1, b) 5:1, c) 10:1. For 2:1 mixtures, two strong peaks indicate lamellar order. With increase in charge ratio, lamellar phase is lost and ring of peaks reminiscent of hexagonal order appears. Cubic structure is indicated at long wavelengths, which is a finite size effect.

shown here that increasing the electrostatic contribution, or changing the charge ratio of the components, has the effect of freezing the local domain structure.

### 5.3. Summary and conclusions

In this chapter, theoretical results for lamellar and hexagonal phases were compared with molecular dynamics simulations at intermediate temperatures. The formation of lamellar domains was characterized, including relevant thermodynamic quantities. It is found that the electrostatic interactions contribute greatly to the interfacial ordering. When considering the formation of hexagonal domains, at finite temperatures, there are deviations from both the shape and packing within the domain structures that digress from the phase behavior described from strong segregation theory at low temperatures. A critical domain nucleus is found at which the domains change their shape from circular to noncircular behavior. Moreover, it is found that the charge ratio of the electrostatic components influences the shape asymmetry, as well as the degree of local order in the inter domain structure.

### 5.4. Acknowledgements

This work was supported by the IGERT-NSF Fellowship for Complex Systems and Dynamics awarded to S. Loverde, and by NSF grant number DMR-0414446 and DMR-0503943. I would like to acknowledge the group of Dr. Christian Holm, who is now at Frankfurt Institute for Advanced Studies, Johann Wolfgang Goethe-Universität, including Axel Arnold and Bernward Mann (†2006) for guidance learning how to use Espresso, an efficient molecular dynamics simulation code developed for charged systems. In addition, the NSEC Fellowship for international study, for enabling me to travel to Mainz.

I would especially like to acknowledge Dr. Yuri Velichko for initial guidance with molecular dynamics simulations and analysis. Portions of this chapter have also appeared in: "Competing interactions in two dimensional Coulomb systems: Surface charge heterogeneities in

coassembled cationic-anionic incompatible mixtures,” S. M. Loverde, Y. Velichko, and M. Olvera de la Cruz, *Journal of Chemical Physics*, 124, 144702 (2006).

## CHAPTER 6

## Effects of Salt

## 6.1. Introduction

Surface modification by polyelectrolytes is a well-established field [?] that possesses many applications—fabrication of nano-patterned templates for storage media, nanowires [?], or studies of cell growth and patterning [8]. One can consider the behavior of salt and macromolecular behavior near charged surfaces, as well as examine how the salt affects the pattern formation on the surface itself. The competing interactions involved are the entropy of the salt or macromolecules, in comparison with the electrostatic interaction between the molecules in solution with the surface electrostatic potential. In certain regimes, the electrostatic interaction dominates the entropy in solution and adsorption to the underlying substrate is found. For example, it has been shown that adsorption onto the surface by

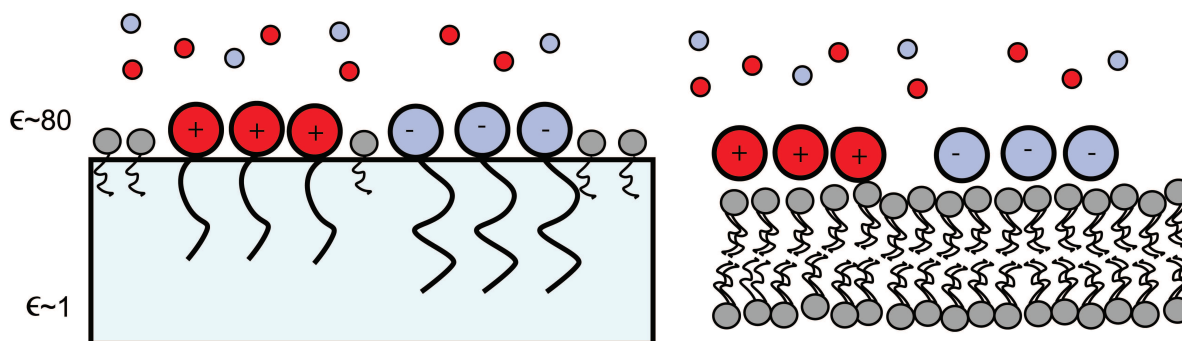


Figure 6.1. Cartoon of the interface, a microemulsion (oil water interface) or else the interface of a flat, crystalline membrane. In either case, there will be counterions or salt in the medium.

polyelectrolytes can even lead to overcompensation of the surface charge, which allows for multilayering of adsorbed layers of opposite charges [?, ?]. If the surface itself is heterogeneous, the situation is quite complex. For example, when considering a heterogeneous mixture of surfactants in a monolayer, possessing a classic binodal behavior, it is shown that considering attractions with a polymer in solution modifies the surface phase behavior [?]. In this chapter, two separate aspects of the phenomena of salt behavior near patterned interfaces are examined.

Section 6.2.1 considers implicit salt in the surrounding medium, assuming a continuous distribution of ions in solution. Next, the modified surface potential is used to examine the pattern formation on the interface. In the low temperature limit, the behavior of the system can be examined using strong segregation theory as introduced in Chapter 4, using a screened Debye Hückel potential. The transition from a patterned interface to a phase segregated state is a first order transition with respect to the inverse screening length, defined by the salt concentration in the medium. In the high temperature limit, the transition from a disordered phase to a phase segregated state is a continuous transition as described in Section 6.2.2. Using molecular dynamics simulations, but using a screened Debye Hückel potential instead of the full Coulomb potential, illustrates the melting of the periodic structure in Section 6.2.3.

The second approach discussed in Section 6.3.1 considers the distribution of multivalent salt in the surrounding medium, while assuming a fixed, patterned substrate with lamellar domains of opposite charges. At low temperatures, phase coexistence is found between a phase of condensed dipoles at the interface between the lamellar domains, as well as condensed monopoles at the center of the lamellar domains. This phase behavior is dependent

on the surface charge density, as well as the density of salt in the medium. Molecular dynamics shows that these results can be extended to intermediate temperatures in Section 6.3.2, and illustrates the possibility of more complex mixed surface phase behavior close to a fixed, patterned, heterogeneously charged substrate.

## 6.2. Salt effects on pattern formation

### 6.2.1. Low temperature Debye Hückel limit

In the low temperature limit, the behavior of the system can be examined assuming the domains are strongly segregated, but considering a screened or Debye Hückel interaction between the charged components. In this case, electrostatic repulsion between the components can be weakened enough to allow for the full segregation of the components. The ions in the outside medium effectively neutralize the charge on the surface. In the low temperature limit, the free energy of the solid phase displays a discontinuous jump from either the hexagonal or lamellar phase to the macroscopically phase segregated state. The free energy minimum with respect to cell size remains the same until the inverse screening length,  $\kappa$ , is comparable to the cell size. At this point, there is a new minimum at the infinite cell size, which corresponds to complete segregation. This is a first order transition. Full details of these calculations are found in Solis et al [118]. The resulting phase diagram for the line of first order transitions from periodic to macroscopic phase segregation on the surface is plotted in Fig. 6.2.

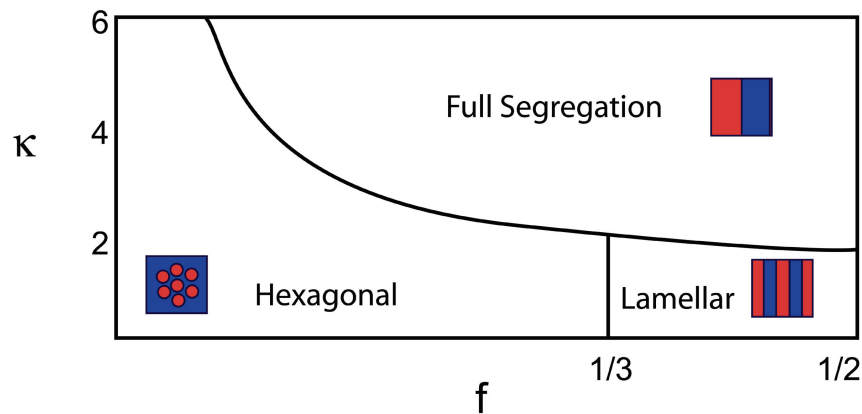


Figure 6.2. For an increase in the inverse screening length,  $\kappa$ , the system jumps from a periodic phase to a fully segregated mixture of opposite charges. Reproduced from Solis et al [118].

### 6.2.2. High temperature limit

In the high temperature limit, using a screened or Debye Hückel potential instead of the Coulomb potential for electrostatic interactions, linear response theory can be used to examine how the density fluctuations in the system behave. To determine how the peak wavevector scales with increasing external screening, the behavior of the inverse structure factor can be calculated in a regime where the scaling of the peak in the structure factor from simulation results is still consistent with linear response theory. In chapter 4, it was found that the inverse structure factor has the following contributions,

$$(6.1) \quad \frac{1}{S_0(k)} = U_k + \rho^{-1} = \frac{1}{\rho} + \frac{1}{1-\rho} - 2\chi + \chi k^2 + U_{el}(k).$$

For a symmetric system,  $\rho = 1/2$ , so that

$$(6.2) \quad \frac{1}{S_0(k)} = 4 - 2\chi + \chi k^2 + \frac{8\pi l_B}{k^2 + \kappa^2}.$$

When  $\frac{\partial S(k)^{-1}}{\partial k} = 0$ , the structure factor is a maximum, corresponding to the peak wavevector,  $q^*$ . It is found that as the magnitude of screening by the ions of solution,  $\kappa$ , increases, the value of  $q^*$  goes continuously to zero,

$$(6.3) \quad q^* = \left( -\kappa^2 + \left( \frac{4\pi l_B}{\chi} \right)^{2/3} \right)^{1/2}$$

before the structure factor diverges,  $S(k)^{-1} = 0$ , at which there is macroscopic phase segregation, as shown in in Fig. 6.3. This is in agreement with analytical predictions from the strong segregation regime, which predicts a discontinuous jump from finite sized periodic cells to an infinite cell at a value of  $\kappa$  which is inversely proportional to periodic length-scale of the system.

At higher values of short range attraction, as shown in the shaded area in Fig. 6.3 the structure factor diverges when  $q^* > 0$ . This corresponds to a region of microphase segregation, in which there is a preferred wavelength of density fluctuations, before the system jumps to the fully phase segregated state. Microphase segregation is seen for many polymer systems, including weakly charged polyelectrolytes [121] and may be applicable to the pattern formation found on the surface of cell membrane systems [138].

### 6.2.3. Melting of the lamellar phase using molecular dynamics

Introduction of electrostatic screening, or including the effects of salt on the local ordering of the system, is considered by using a screened Debye Hückel potential instead of the Coulomb potential for electrostatic interactions,

$$(6.4) \quad U_{DH} = \frac{l_B T q_1 q_2 e^{-\kappa r}}{r}$$

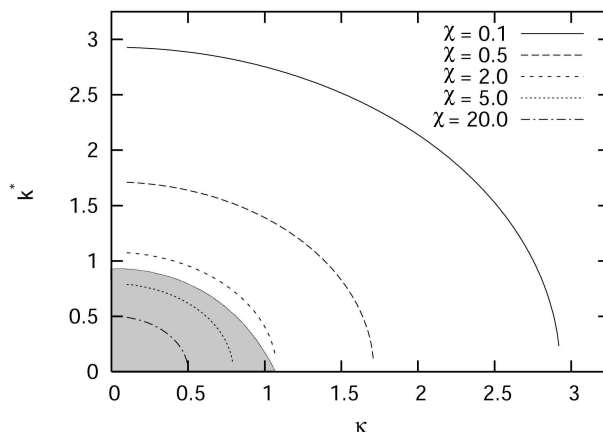


Figure 6.3. The location of the peak,  $k^*$ , in the structure factor,  $S(k)$ , as a function of  $\kappa$  as predicted by linear response theory for several values of short range attraction ( $\chi = 0.1, 0.5, 2.0, 5.0, 20.0$ ) for an intermediate strength of the electrostatics,  $l_B = 0.2$ . The shaded area indicates  $S(k)$  diverges at a finite value of  $k$ .

where  $\kappa$  represents the screening length due to the surrounding three dimensional solution of ions (see Chapter 2).

In Fig. 6.4, several snapshots are shown for increasing  $\kappa$  for fixed values of short range attraction and electrostatics. Initially, the periodicity of the lamellar stripes widens slightly as shown in Fig. 6.4 a), followed by the breaking of the periodic phase. The stripes bend to produce a percolated structure as shown in Fig. 6.4 b). The width of the stripes continues to widen, while the fluctuations along the interface grow to larger length-scales. This segregation continues until two stripes exist for the width of the box. Upon segregation, in the solid phase the short range attraction dominates the electrostatic repulsion between the charged particles Fig. 6.4 c). Near perfect hexagonal close packing exists within the domains, and nearly all of the neutral components, or empty space, is expelled to the interface between the domains.

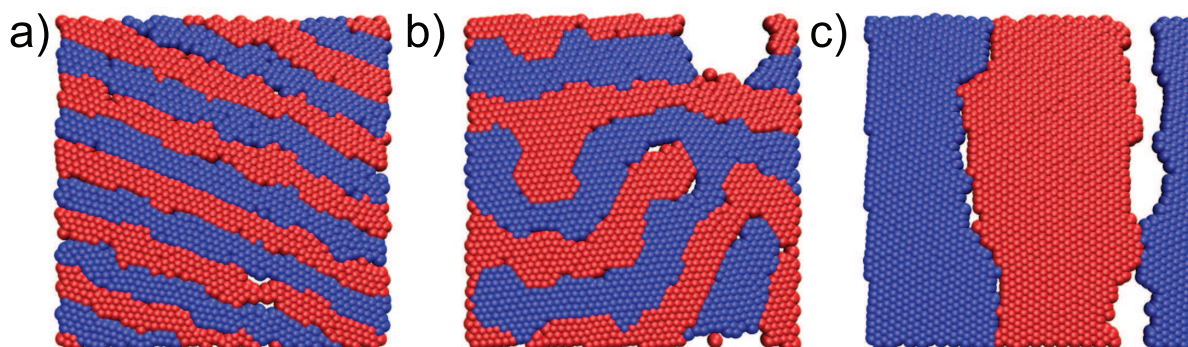


Figure 6.4. Snapshots of the system for  $\epsilon = 4.0$  and  $l_B = .5$ , showing progressive values of screening. a)  $\kappa = 0.2\sigma^{-1}$  b)  $0.4\sigma^{-1}$  c)  $1.0\sigma^{-1}$ . The system melts when  $1/\kappa \sim L$  where  $L$  is the width of the periodic domain.

Examining the peak wavevector,  $k^*$ , as a function of  $\kappa$ , the inverse screening length, from analysis of the structure factor, the peak wavevector indicates a continuous melting of the system (Fig. 6.5). For both values of the electrostatics presented ( $l_B = 0.2, 0.5\sigma$ ), the peak wavevector decreases from the maximum, which is the solution for pure Coulombic interactions, gradually until the system is segregated for the full width of the simulation box.

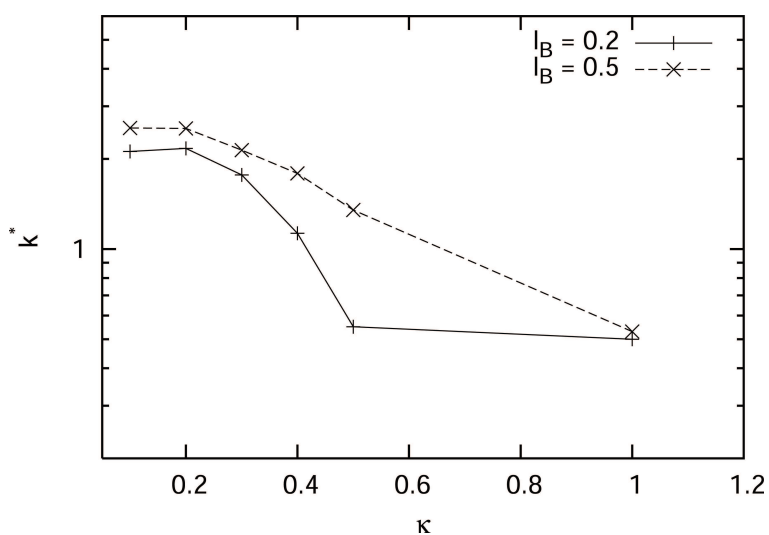


Figure 6.5. Peak wavevector,  $k^*$ , as a function of  $\kappa$ , the inverse screening length for two values of the electrostatic interactions ( $l_B = 0.2, 0.5\sigma$ ).

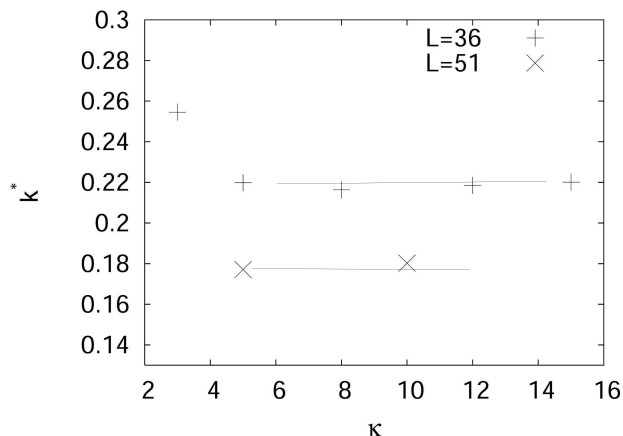


Figure 6.6. The location of the peak,  $k^*$ , in the structure factor,  $S(k)$ , as a function of  $\kappa$  from simulation results spanning a range of the screening parameter ( $\kappa = 3 - 15\sigma$ ) at an intermediate value of short range attraction ( $\epsilon = 2.0$ ). Increasing the size of the system from  $L = 36$  to  $L = 51$  decreases the average value of  $k^*$ .

At higher values of electrostatic screening ( $\kappa = 5\sigma^{-1}, 10\sigma^{-1}, 15\sigma^{-1}$ ), examining the behavior of the system with an intermediate values of short range attraction ( $\epsilon = 2.0$ ), the system phase segregates into two macroscopically charged domains of positive and negative ions. The peak in the structure factor indicates that the segregation length-scale is nearly constant as a function of the screening length. This is in agreement with analytic theory [118]. The location of the peak shifts to lower values with an increase in the characteristic size of the simulation box.

While the nature of this transition from simulation indicates a continuous transition, there are many factors to consider. Using a  $1/r$  Coulomb potential, as it was shown in Chapter 5, that increasing the strength of the electrostatics in the system leads to more ordered, elongated interfaces. At finite temperatures, when screening the electrostatics, the interface develops fluctuations at long wavelengths compared to the size of the simulation box as shown

in Fig. 6.4 b). Within the context of strong segregation theory, these density fluctuations can be incorporated into the interfacial term in order to correctly describe the melting transition at finite temperatures. In addition, as will be discussed much more thoroughly in Chapter 7, there is adsorption of the neutral component at the interface between the domains. This has a tendency to swell the interface, and changes the gradient contribution to the free energy. Also, as seen in the progression of images in Fig. 6.4, this factor changes as the inverse screening length progressively increases. At low values of screening, these interfacial modifications will need to be taken into account in order to correctly describe the system. However, for high values of screening, the two phases of immiscible components coexist separately from a third neutral phase.

In order for a transition to be first order, the symmetry of the system should be broken. As was discussed in Chapter 5, this possibility of long range order on surfaces is a topic under much debate [129, 132, 133]. The electrostatics can result in the local freezing of the domain structure, however, this was shown to be true only for strongly asymmetric systems. Melting in two dimensions is synonymous with a Kosterlitz and Thouless transition [133, 134], which was further extended by Halperin and Nelson, in which the local structure melts through dislocations, or defects in the local packing of the components [135, 136]. Defects in the lamellar ordering are seen in the melting simulations, such as the interface where two lamellar meet as shown in Fig. 6.4 b). To systematically study the melting of this transition, larger simulation sizes would be needed in order to incorporate all wavelengths of the density fluctuations. This could be examined, as in two dimensional Lennard Jones systems [?], magnetic systems [?], or charged systems [?], by studying the finite size effects.

Due to the long range nature of the Coulomb force, the systematic study of the order of this transition would be computationally quite extensive.

### 6.3. Multivalent ion condensation on patterned surfaces

#### 6.3.1. Theory of condensation

Charged surfaces and their interactions with ionic environments are particularly interesting due to the long-range nature of electrostatic interactions and its relative independence from molecular structure. The break down of the mean field Poisson Boltzmann approximation to describe adsorption of ions to charged surfaces [139] has since motivated many studies concerning this phenomena. Simple models such as a single component plasma near a neutralizing background revealed two-dimensional crystallization of adsorbed ions onto homogeneously charged surfaces [140]. That is, the electrostatic correlations between ions can result in the formation of solid phases on a highly charged surfaces. For example, this effect is speculated to describe colloidal crystallization into solid phases near oppositely charged membrane surfaces [141, 142].

In this section, the potential of a fixed lamellar surface of opposite charge is calculated analytically. From the surface potential, the energy of a condensed counterion in the center of the stripe can be calculated, as well as the energy of a condensed pair of counterions (a dipole) at the lamellar boundaries. The electrostatic potential near the striped surface (Fig. 6.7 a)) is given by

$$(6.5) \quad \Psi(\Delta y, z) = e\sigma \int_{-\infty}^{\infty} dx \int_{-\lambda/2}^{\lambda/2} dy \sum_{i=-\infty}^{\infty} \psi_i(x, y, \Delta y, z)$$

where  $e$  is the unit of electron charge,  $\sigma$  is the surface number charge density,  $\lambda$  is the width of one lamellar domain and

$$(6.6) \quad \psi_i(x, y, \Delta y, z) = \frac{(-1)^i}{\sqrt{x^2 + (y - \Delta y + i\lambda)^2 + z^2}},$$

where  $\Delta y \in [-\lambda/2, \lambda/2]$  determines the shift from the center of the stripe along the  $y$ -axis. Using the identity [143] the electrostatic potential can be calculated exactly:

$$(6.7) \quad \Psi(\Delta y, z) = \frac{8e\sigma\lambda}{\pi} \times \sum_{l=1}^{\infty} \frac{\sin^3(\pi l/2)}{l^2} \sin\left(\frac{\pi l(\lambda - 2\Delta y)}{2\lambda}\right) e^{-\frac{\pi lz}{\lambda}}.$$

The magnitude of the potential decays exponentially and has sinusoidal profile with extremum in the center of the stripes. Thus, the energy of the single charge in the center of the stripe (Fig. 6.7c) is  $v_c = -4\pi Z e^2 \sigma a \lambda / 3$  and the energy of the dipole at the interface (Fig. 6.7b) is  $v_d = -2\pi Z e^2 \sigma a^2$ . More details concerning the calculation of an exact phase diagram based on these results can be found in Ref. [?].

### 6.3.2. Adsorbed ion phases using simulation

There have been multiple Monte Carlo and molecular dynamics simulations of flexible polyelectrolytes close to the surface of patterned, heterogeneously charged surfaces [?, ?]. These simulations show that charge heterogeneities on the surface can give rise to local adsorption, and also that the polyelectrolyte configuration is sensitive to the specific patterns on the surface.

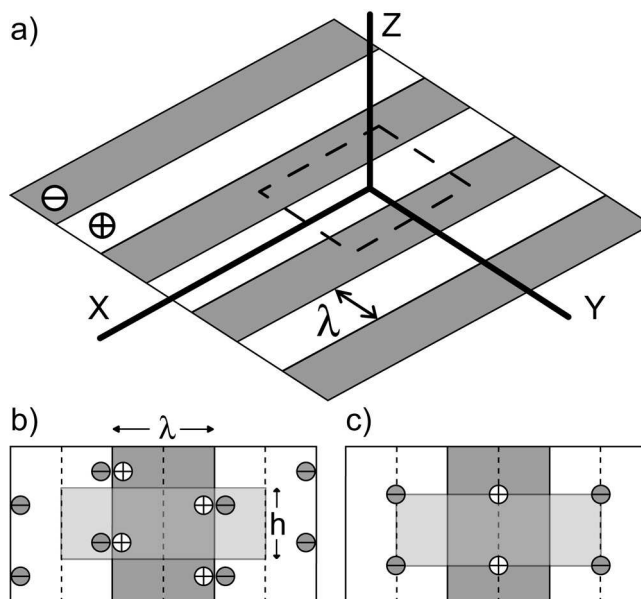


Figure 6.7. a) The schematic representation of the system. The basic Wigner lattices formed by condensed b) ions forming dipoles and c) single ions.

In this section, molecular dynamics simulations test the formation of Wigner crystalline phases described in the previous section at intermediate temperatures, using a full Coulomb interaction between particles. By assuming that the polyelectrolytes are strongly adsorbed to the surface of the interface due to strong interactions (hydrophobic, van der Waals) between the counterions and the substrate, the phase diagram can be simply explored, assuming a confined counterion layer. A perfect lamellar surface of opposite charges, with ions ordered in cubic patterns into stripes is constructed as illustrated in Fig. 6.8. Decreasing the strength of the surface potential is explored by simply moving a confined plane of multivalent ions of charge  $Z_{+/-}$  through varying distances,  $z$ , close to the constructed lamellar surface. This is equivalent to modifying the strength of the surface potential,  $\Psi(\Delta y, z)$ , by a factor of  $e^{-z}$ , as defined in Eq. 6.5.

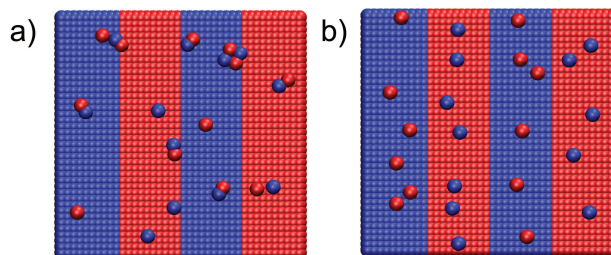


Figure 6.8. Snapshots from molecular simulation of a) mixed and b) single ion phases at  $T = 0.5k_B T$ ,  $l_B = 0.1$ . Multivalent ions possess a charge of  $Z_{+/-} = 10$ . This plane of confined counterions is moved through a distance,  $z$ , of a)  $10\sigma$  to b)  $1\sigma$  from the surface.

It is found that condensed multivalent ions ( $Z_{+/-} = 10$ ) form dipoles along the interfaces, while single ions lie in the center of the stripe. Starting from a very close distance to the lamellar plane,  $z = 1\sigma$  (Fig. 6.8 b) the strong correlation between ions, is preserved even at relatively high temperature  $T = 0.5k_B T$ . Notice how thermal fluctuations do not destroy the long range order; the ions neatly condense to form a cubic array with single monomers adsorbing in the center of the lamellar. Increasing the distance between the two planes further, the counterions progress through the single ion phase until there is a transition to a mixed phase at  $z = 10\sigma$  (Fig. 6.8 a), where an adsorption of dipoles at the interface between stripes occurs. In addition to dipoles at the interface, chain clusters and paired dipoles form suggesting rather complex phase behavior previously found mostly in the bulk [144, 145].

#### 6.4. Summary and conclusions

In this chapter, two aspects of the salt effects on the pattern formation of a charged, patterned surface, are considered. If the counterions in solution possess a continuous distribution, one can determine the modified phase behavior for pattern formation on the interface. Both low and high temperature approaches are outlined, after which molecular

dynamics simulations illustrate the melting to a phase segregated state. Simulations suggest that, when considering the screening of the Coulomb interactions, interfacial fluctuations become more prevalent. In addition, dislocations or defects in the lamellar patterning are seen, which is consistent with mechanisms of melting of local two dimensional order.

While considering the behavior of multivalent salt close to a fixed, heterogeneously charged substrate, the phase diagram is dependent on the surface charge density. At low surface charge densities, salt should condense first at the interface between the domains. With a progressively increasing charge density, this phase behavior should shift, until condensation is mainly at the center of one locally charged region. With further increase, it is speculated that hexagonal packing of the counterions will be observed in the center of the domains. These results are consistent with previous simulations, but also suggest that if the initial adsorption should in fact occur at the interface between two strongly charged domains. Molecular dynamics shows that these results can be extended to intermediate temperatures in Section 6.3.2, and illustrates the possibility of more complex mixed phases.

## 6.5. Acknowledgements

I would like to gratefully acknowledge Dr. Francisco Solis and Dr. Yuri Velichko for their analytic work on the ion condensation. Portions of this chapter may also appear in: "Ion condensation on charged patterned surfaces," Y. Velichko, F. Solis, S. M. Loverde, and M. Olvera de la Cruz.

In addition, I would also like to acknowledge Dr. Graziano Vernizzi and Kevin Kholdstedt for useful discussions.

## CHAPTER 7

**Phase Segregation on the Surface****7.1. Introduction**

Phase separation phenomena and pattern formation at surfaces [146, 147] are both areas of great scientific interest. Several recent studies have shown that mixtures of immiscible oppositely charged molecules can form regular periodic nanostructures [118, 141, 142]. The competition of short range immiscibility and long range attractions leads to the formation of periodic structures in a multitude of systems, as discussed in the previous chapter. As in the previous chapter, charged microphases may be formed by molecules adsorbed onto biological membranes, and other neutral surfaces. It is well known that minority components adsorb to interfaces [148] and, when oppositely charged components are adsorbed, ionic domains reminiscent of biological rafts may form. However, the effects of decreasing the total molecular charge density plays a critical role in the surface phase behavior. Neutral components act to decrease the line tension between charged domains, and may allow for the coexistence of a condensed, or solid phase, as well a liquid phase. Understanding the formation of the between these two regions is critical to understanding the surface behavior of charged mixtures, as well as their interaction with other macromolecules. For example, it has been shown that proteins which are nonselective between a liquid condensed and liquid expanded phase display preferential adsorption to the interface [?].

Phase coexistence has been considered theoretically for competing short range and electrostatic interactions, in certain limits. In the bulk solution, the phase behavior for oppositely charged, incompatible polyelectrolytes has been examined using the one loop approximation. It is shown that, for the limit of low screening, electrostatics can overcome the net incompatibility in order to produce microphase segregation, and even condensation, for low values of immiscibility [149]. On the surface, for incompatible mixtures of competing dipoles, at

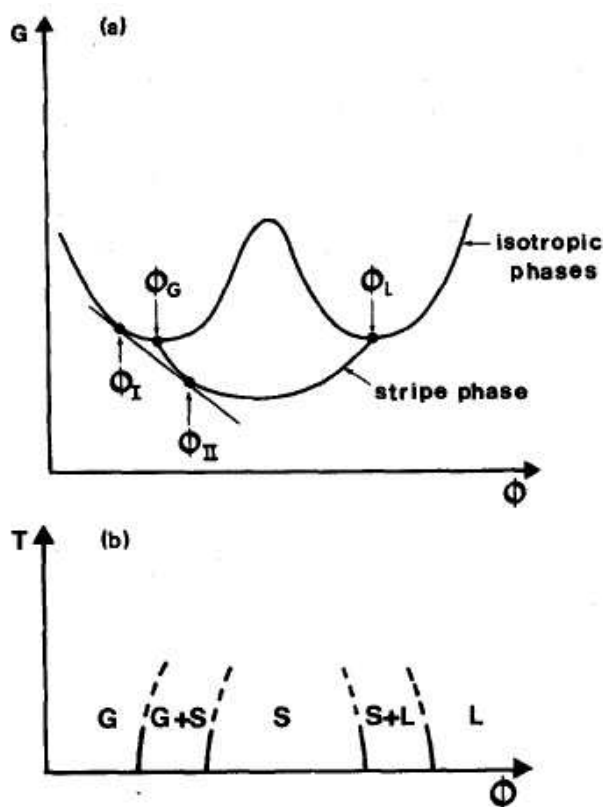


Figure 7.1. a) Schematic free energy at low temperatures. The isotropic free energy has two minima, corresponding to solid and gas phases. When the dipolar interactions are included, the possibility of two phase coexistence between isotropic and striped phase appears. b) Schematic phase diagram constructed from energy shown above. The stripe shows coexistence regions with gas and solid phases. This phase diagram can also be extended to incorporate hexagonal phases. Reproduced from Andelman et al [95].

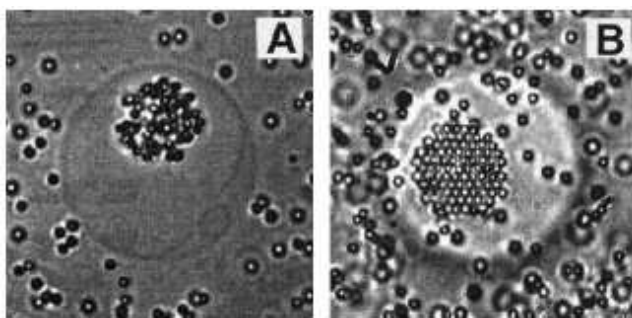


Figure 7.2. a) Disordered and b) more ordered rafts of negatively charged colloidal particles adsorbed to the surface of a tense vesicle, composed of a mixture of cationic and neutral surfactants. Reproduced from Ramos et al [141].

low temperatures, Andelman has demonstrated the possibility of phase coexistence between a periodic, striped phase with an isotropic (liquid or gas) phase. The two phase coexistence regions are constructed by minimizing the free energy difference between the isotropic and stripe phases, as shown in Fig. 7.1. In this chapter, using the same general methods for construction of a two phase region, the boundaries of the coexistence region between a periodic solid phase and isotropic gas phase will be determined. However, the electrostatic contribution to the gas phase phase density will also be considered.

The contribution of electrostatics to phase segregation on interfaces is a general problem, and may be applicable to a variety of experimental systems. As shown in the review in the Chapter 4, the compression of langmuir monolayer mixtures results in the coexistence of a liquid condensed, or gel state, with a liquid expanded state. The liquid expanded state possesses a low charge density compared with the liquid condensed state [93]. In addition, recent experiments have shown the possibility of the aggregation of negatively charged colloidal particles on the surface of vesicles composed of a mixture of charged and neutral phospholipids [141, 142]. While this experimental system is much more complicated than

the ideal system that will be discussed in this chapter, the resulting solid phase of hexagonally close packed molecules at an interface, within a low density gas phase, are overwhelmingly similar in their structure as shown in the images reproduced from Ramos et al in Fig. 7.2. The underlying physics behind this, and similar, systems, has been the cause of much discussion [?].

## 7.2. Theoretical model of phase segregation on the surface

In this chapter, the possibility of phase segregation formed by a mixture of charged molecular components strongly adsorbed on biological membranes, and other neutral surfaces is explored. This includes liquid interfaces, such as emulsions when cationic and anionic surfactants are adsorbed onto the interface. Many simplifications to the model are made compared to experimental systems. In this model, specific interactions with the interface or substrate with the adsorbed molecules are not considered. In addition, the fluctuations in the shape of the interface are ignored. The phase behavior is accurate when the interface of interest is non-fluctuating, when the bending modulus is sufficiently high so that equilibrium fluctuations are less than  $k_B T$ . The electrostatic contribution to the bending elasticity for the case of microemulsions [?], or membranes [150, 151], is just beginning to be investigated. The model presented here is only applicable to flat, crystalline membranes or microemulsion with sufficiently low curvature.

The coexistence of two possible phases is considered at low temperatures. One phase consists of a dense, patterned solid formed by the charged components. Its free energy is analyzed by assuming the formation of microphase regions of constant particle and charge density as first described in Section 4.2.1. The second phase consists of an isotropic gas of

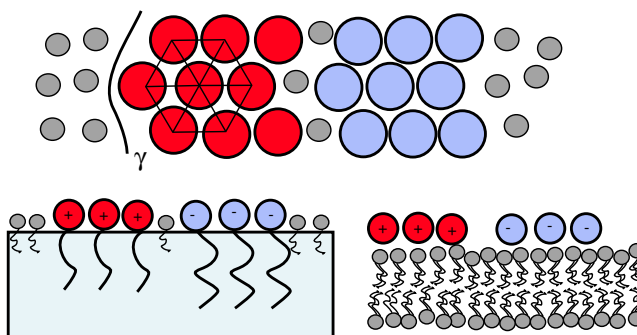


Figure 7.3. Schematic of neutral and charged components strongly adsorbed to a liquid interface, such as an emulsion or the surface of a bilayer. The charged components segregate into a periodic solid phase with line tension  $\gamma$  within a homogeneous background.

charged particles; its free energy can be calculated using linear response theory by means of the one loop approximation or Random Phase Approximation (RPA) [120, 152] at the interface as first described in Section 2.1.3 and Section 4.2.2.

### 7.2.1. Free energy of the solid phase

Within strong segregation theory, as first described in Section 4.2.1, the equilibrium phase is determined by the charge ratio of the molecular components. The solid phase possesses elongated domains with a lamellar periodicity, for mixtures of equally charged molecular components. For asymmetrically charged molecular components, the solid phase possesses circular domains with a hexagonal periodicity. The average absolute value of the charge density in the solid phase is  $\psi = f_+ \psi_+ + f_- |\psi_-|$  where  $f_{+/-}$  represents the area fraction of the components and  $\psi_{+/-}$  is their respective charge density. The free energy of the solid microphase, per area  $A$  with periodicity  $L$ , has the form

$$(7.1) \quad \frac{F_m}{Ak_B T} = \gamma \frac{s_1}{L} + l_B \psi^2 s_2 L.$$

The Bjerrum length is  $l_B = \frac{e^2}{4\pi\epsilon k_B T}$ ,  $k_B$  is the Boltzmann constant,  $T$  is the temperature,  $\epsilon$  is the dielectric permittivity of the medium, and the line tension between microdomains is  $\gamma$ . The coefficients  $s_1$  and  $s_2$  are dimensionless quantities that depend on specific shape of the microdomains.  $s_1$  is the ratio of the microdomain interface length within a unit cell to the size of the cell.  $s_2$  is the integral of the dimensionless Coulombic potential over the whole space, averaged over a unit cell. These values are calculated following Ref [118]. Minimizing the free energy with respect to the size  $L$ , there exists an optimal characteristic length  $L_{min} = (s_1/s_2)^{1/2}L_0$ , with  $L_0 = (\gamma/(l_B\psi^2))^{1/2}$ . Evaluation of the free energy density at that point results on a value of  $2(s_1s_2)^{1/2}\frac{f_0}{L_0}$ , where  $f_0 = (\gamma l_B\psi^2)^{1/2}$  [118, 153].

The complete free energy of the solid phase also includes the cohesive energy that arises from segregation of the charged molecules from the neutral component. The cohesive energy consists of the sum of the short range attractive contacts (of magnitude  $\epsilon$ ) per component in the solid phase. At low temperatures, a constant density given by the hexagonal close packing packing of spherical molecules of radius  $\sigma$  can be assumed. This corresponds to a constant density  $\rho_{solid} = \frac{1}{\sqrt{3}\sigma^2}$ . The effective cohesive energy per unit area can then be written in terms of  $\epsilon$ , which corresponds to the net interaction between components, with 6 contacts between neighbors. The line tension is, from geometrical packing arguments,  $\frac{\sqrt{6}\epsilon}{\sigma}$ . Inclusion of the cohesive energy, leads to a total free energy for the solid phase as:

$$(7.2) \quad \frac{F_s(\rho_{solid})}{A} = -3\epsilon\rho_{solid} + 2(s_1s_2)^{1/2}f_0/L_0^2.$$

### 7.2.2. Free energy of the gas phase

The free energy of the gas phase is calculated using the Random Phase Approximation [120] as a function of the relative strength of the short range attraction,  $\varepsilon$ , and the electrostatic interactions,  $l_B$ . The method involves an expansion of the free energy of the system in terms of density fluctuations, neglecting all terms of larger than second order. For a general system of interacting  $i, j$  charged monomers, the partition function is written as

$$(7.3) \quad Z = Z_o \frac{V^N}{N!} \int \exp \left( - \sum_{k \neq 0} \sum_{ij} \frac{\mathbf{A}_k^{ij} \rho_k^i \rho_{-k}^j}{2V} \right) \prod_{k>0} \prod_i \frac{d\rho_k^i}{\pi V \rho_i}.$$

where  $\mathbf{A}_k^{ij} = \mathbf{U}_k^{ij} + \rho_i^{-1} \delta_{ij}$ . Here,  $\rho_i$  represents the density of the  $i$ th component and  $\rho_k$  is the Fourier transform of the component densities.  $Z_o$  includes the  $k = 0$  and self energy terms.  $\mathbf{U}_k^{ij}$  is the sum of the interaction energies, consisting of the short range interactions due to the excluded volume and hydrophobic interaction, as well as the long range contributions due to the electrostatic energy. The electrostatic contribution to the internal energy matrix uses the two dimensional Fourier transform of the screened Coulomb interaction,  $E_{el}^{ij} = 2\pi z_i z_j l_B (k^2 + \kappa_{out}^2)^{-1/2}$ .  $\kappa_{out}$  is the screening length defined by the concentration of ions in the surrounding solution.

The free energy is then

$$(7.4) \quad F = \sum_{ij} \frac{N_i(N_j - \delta_{ij})}{2V} U_o^{ij} + \sum_i N_i \ln \frac{\rho_i}{e} \\ + \sum_{k>o} \left[ \ln \frac{\det |U_k^{ij} + \rho_i^{-1} \delta_{ij}|}{\det |\rho_i^{-1} \delta_{ij}|} - \sum_i \rho_i U_k^{ii} \right].$$

where  $U_0^{ij}$  includes only the short range excluded volume of the components, as the electrostatic contribution vanishes due to charge neutrality. The second term is a standard entropic term. The third term is the electrostatic contribution due to density fluctuations, calculated by integrating over the possible values of  $k$  from 0 to  $2\pi/a$ , where  $a$  is the molecular size. The interaction matrix,  $U_k^{ij}$ , is

$$(7.5) \quad U = \begin{pmatrix} U_{11} & U_{21} \\ U_{21} & U_{22} \end{pmatrix} \\ = \begin{pmatrix} \frac{1}{\rho_1} + \nu_{11} + \frac{2\pi z_1^2 l_B}{\sqrt{k^2 + \kappa^2}} & \nu_{12} + \frac{2\pi z_1 z_2 l_B}{\sqrt{k^2 + \kappa^2}} \\ \nu_{12} + \frac{2\pi z_1 z_2 l_B}{\sqrt{k^2 + \kappa^2}} & \frac{1}{\rho_2} + \nu_{22} + \frac{2\pi z_2^2 l_B}{\sqrt{k^2 + \kappa^2}} \end{pmatrix}.$$

In the present case, the electrostatic energy  $E_e l^{ij} \gg \nu_{ij}$ , where  $\nu_{ij}$  consists of the short range, or the effective excluded volume of the monomers. In this case, the short range contribution due to density fluctuations is negligible and  $U_{ij}$  consists of only the electrostatic contribution due to the fluctuations. This term is designated  $F_{ele}$ . The resulting expression corresponds to the Debye Hückel correction to the free energy [120] as introduced in Section 2.1.2, but in the two dimensional limit.

The free energy can be broken up into parts. The first portion includes the  $k = 0$  short range and electrostatic terms and the entropic contribution to the free energy,  $F_0$ . The second portion,  $F_{ele}$ , includes  $X$ , the electrostatic correction to the energy due to the density

fluctuations, as well as  $Y$ , the self energy contribution. This can be written as

$$(7.6) \quad F = F_0 + F_{ele}$$

$$F = \frac{N_1(N_1 - 1)U_0^{11}}{2V} + \frac{2N_1N_2U_0^{12}}{2V} + \frac{N_2(N_2 - 1)U_0^{22}}{2V}$$

$$+ N_1 \ln \frac{\rho_1}{e} + N_2 \ln \frac{\rho_2}{e} + \sum_{k>0} \left( \frac{X}{\rho_1\rho_2} - Y \right)$$

First, consider the  $k = 0$  terms,

$$(7.7) \quad F_0 = \frac{N_1(N_1 - 1)U_0^{11}}{2V} + \frac{2N_1N_2U_0^{12}}{2V} + \frac{N_2(N_2 - 1)U_0^{22}}{2V} + N_1 \ln \frac{\rho_1}{e} + N_2 \ln \frac{\rho_2}{e}$$

The free energy per unit volume is then

$$(7.8) \quad \frac{F_0}{V} = \frac{N_1}{2V} \left( \frac{N_1 - 1}{V} \right) U_{0,SR}^{11} + \frac{N_1 N_2}{V V} U_{0,SR}^{12} + \frac{N_2}{2V} \left( \frac{N_2 - 1}{V} \right) U_{0,SR}^{22}$$

$$+ U_{0,ele} + \frac{N_1}{V} \ln \frac{\rho_1}{e} + \frac{N_2}{V} \ln \frac{\rho_2}{e}$$

The  $k = 0$  electrostatic term vanishes due to charge neutrality,

$$(7.9) \quad U_{0,ele} = \int \left( \frac{z_1^2 q l_B \rho_1^2}{2V} + 2z_2^2 q^2 l_B \rho_2^2 + \frac{\rho_1 z_1 z_2 q^2}{r} \right) d^3r$$

$$= \int \frac{1}{2} \frac{(z_1 \rho_1 + z_2 \rho_2)^2}{r} d^3r = 0.$$

For a large system, the number of particles,  $N \rightarrow \infty$ , so that 7.8, the free energy per unit volume, becomes

$$(7.10) \quad \frac{F_0}{V} = \frac{\rho_1^2}{2} U_{0,SR}^{11} + \rho_1 \rho_2 U_{0,SR}^{12} + \frac{\rho_2^2}{2} U_{0,SR}^{22} \\ + U_{0,ele} + \rho_1 \ln \frac{\rho_1}{e} + \rho_2 \ln \frac{\rho_2}{e}$$

The short range energy can be expanded for low densities using the virial theorem, as described in Section 2.1.1 of the background chapter. Including only the two body interaction terms,

$$(7.11) \quad U_{0,SR}^{ij} \cong v_{ij} = - \int \exp(-U_{0,SR}^{ij} - 1) d^2r.$$

Next, consider the  $k > 0$  terms. Evaluating  $F_{ele}$  due to the first portion,  $X$ , of the electrostatic free energy terms,

$$(7.12) \quad F_{ele,X} = \sum_{k>0} \ln \left[ \rho_1 \rho_2 \left( \left( \frac{1}{\rho_1} + \nu_{11} + \frac{2\pi z_1^2 l_B}{\sqrt{k^2 + \kappa^2}} \right) \left( \frac{1}{\rho_2} + \nu_{22} + \frac{2\pi z_1^2 l_B}{\sqrt{k^2 + \kappa^2}} \right) \right. \right. \\ \left. \left. - \left( \nu_{12} + \frac{2\pi z_1 z_2 l_B}{\sqrt{k^2 + \kappa^2}} \right)^2 \right) \right]$$

After some algebraic manipulation, this simplifies to

$$(7.13) \quad F_{ele,X} = \frac{1}{(2\pi)^2} \int 2\pi k dk \ln \left( 1 + \frac{\kappa_{in}^2}{\sqrt{k^2 + \kappa_{out}^2}} \right)$$

$\kappa_{in}$  is defined as the screening due to the ions in the plane,

$$(7.14) \quad \kappa_{in}^2 = 2\pi l_B (\rho_1 z_1^2 + \rho_2 z_2^2).$$

To begin with, consider the limit of no screening due to ions in the surrounding solution ( $\kappa_{out} \rightarrow 0$ ) to match of strong segregation theory. It has been shown that the presence of salt does not change the periodicity significantly [118] in strong segregation theory up to when the screening length is of the order of the domain size when the periodic phase decomposes into two macroscopically segregated phases of charges.

The electrostatic contribution is found to be, for the limit of no external screening due to the surrounding ions in solution,

$$(7.15) \quad \frac{F_{el}}{k_B T} = \frac{1}{4\pi} \left[ \frac{2\pi^2 \ln\left(1 + \frac{a\kappa_{in}^2}{2\pi}\right)}{a^2} + \frac{\pi\kappa_{in}^2}{a} - \frac{1}{2}\kappa_{in}^4 \ln\left(1 + \frac{2\pi}{a\kappa_{in}^2}\right) \right].$$

Including the external screening of the ions in the surrounding solution, the electrostatic contribution is a function of  $\kappa_{out}$ . After some rearrangement, it is found to be,

$$(7.16) \quad \frac{F_{el}}{k_B T} = \frac{1}{4\pi} \left[ \ln \left( \frac{\kappa_{in}^2 + \kappa_{out}}{\kappa_{in}^2 + \sqrt{\frac{4\pi^2}{a^2} + \kappa_{out}^2}} \right) \kappa_{in}^4 - \kappa_{in}^2 \kappa_{out} + \kappa_{out}^2 \ln \left( \frac{\kappa_{out}}{\kappa_{in}^2 + \kappa_{out}} \right) + \kappa_{in}^2 \sqrt{\frac{4\pi^2}{a^2} + \kappa_{out}^2} + \left( \frac{4\pi^2}{a^2} + \kappa_{out}^2 \right) \ln \left( \frac{\kappa_{in}^2 + \sqrt{\frac{4\pi^2}{a^2} + \kappa_{out}^2}}{\sqrt{\frac{4\pi^2}{a^2} + \kappa_{out}^2}} \right) \right]$$

First, consider the limit of no screening due to ions in the surrounding solution ( $\kappa_{out} \rightarrow 0$ ). The above equations simplify when considering the charge neutrality constraint,  $z_+\rho_+ = z_-\rho_-$ . The total free energy per unit area for the gas phase, for no external screening (using

$F_{el}$  from 7.15), in terms of  $\rho$  where  $\rho = \rho_+ + \rho_-$ , is then

$$(7.17) \quad \frac{F_{gas}}{Ak_B T} = \frac{\rho}{\alpha} \ln \left[ \frac{\rho}{\alpha e} \right] + \frac{\rho}{\beta} \ln \left[ \frac{\rho}{\beta e} \right] \\ + \frac{v_{11}}{2} \left( \frac{\rho}{\alpha} \right)^2 + \frac{v_{22}}{2} \left( \frac{\rho}{\beta} \right)^2 + v_{12} \frac{\rho^2}{\alpha\beta} + \frac{F_{el}}{k_B T}$$

where  $\alpha = 1 - \frac{z_+}{z_-}$  and  $\beta = 1 - \frac{z_-}{z_+}$ . The virial terms are  $v_{ij} = - \int e^{-U_{ij}/k_B T} - 1$  where  $U_{ij}$  is a hard core potential from  $0 < r < \sigma$  and a classic 6-12 Lennard Jones potential from  $\sigma < r < 2.5\sigma$ .

### 7.2.3. Construction of the two phase coexistence boundaries

To determine the phase coexistence of the solid, patterned phase and the dilute gas, one can use the common tangent rule [154] The total free energy per area is the sum of the area

x	1-x	NVT
$\mu_{gas}$	$\mu_{solid}$	
$P_{gas}$	$P_{solid}$	
$\rho_{gas}$	$\rho_{solid}$	

Figure 7.4. The chemical potentials and partial pressures of the solid and gas phase are equivalent. The density of the solid phase is fixed.

fraction in each phase,

$$\begin{aligned}
 \frac{F_{total}}{V}(\rho) &= x \frac{F_{gas}}{V}(\rho_{gas}) + (1-x) \frac{F_{solid}}{V}(\rho_{solid}) \\
 (7.18) \quad \rho &= x \rho_{gas} + (1-x) \rho_{solid} \\
 F_{total}(\rho) &= x F_{gas} \left( \frac{\rho - (1-x) \rho_{solid}}{x} \right) + (1-x) F_{solid}(\rho_{solid})
 \end{aligned}$$

where  $x$  represents the area fraction of the gas phase. The chemical potentials and of the gas and solid phase are equivalent in coexistence,

$$\begin{aligned}
 (7.19) \quad \mu_{gas} &= \mu_{solid} \\
 \left. \frac{\partial F}{\partial \rho} \right|_{\rho_{gas}} &= \left. \frac{\partial F}{\partial \rho} \right|_{\rho_{solid}}
 \end{aligned}$$

as well as the partial pressures,

$$\begin{aligned}
 (7.20) \quad P_{gas} &= P_{solid} \\
 \left. \frac{F_{gas}}{V} - \rho_{gas} \frac{\partial(\frac{F_{gas}}{V})}{\partial \rho} \right|_{\rho_{gas}} &= \left. \frac{F_{solid}}{V} - \rho_{solid} \frac{\partial(\frac{F_{solid}}{V})}{\partial \rho} \right|_{\rho_{solid}}
 \end{aligned}$$

For a fixed solid phase density, the condition of equivalent pressures and chemical potentials is equivalent to the condition of a minimum free energy,  $\partial F/\partial x = 0$ .

Since the density of the solid phase is assumed fixed, the equation

$$(7.21) \quad \frac{F_{solid}(\rho_{solid})}{A} = \frac{F_{gas}}{A} + (\rho_{solid} - \rho_{gas}) \left. \frac{\partial F_{gas}}{\partial \rho} \right|_{\rho_{solid}}$$

can be solved for the gas phase density at equilibrium,  $\rho_{gas}$ .

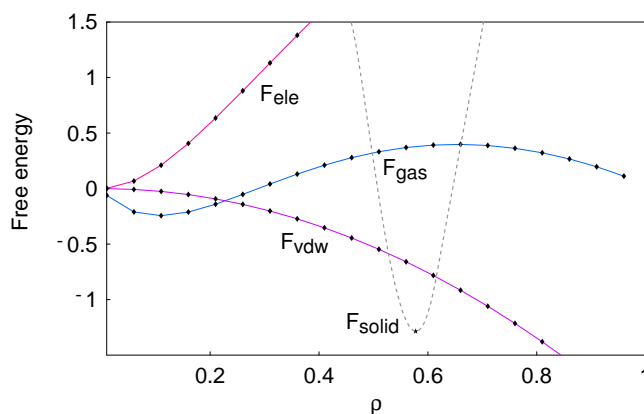


Figure 7.5. Free energy for  $\epsilon = 2.0$ ,  $l_B = 0.5$ . The repulsive electrostatic free energy is balanced by an attractive Van der Waals component. The total free energy displays a stable gas phase density, which is in coexistence with a solid periodic phase. The dashed gray line represents the theoretical free energy of the solid phase, which has been simplified by assuming a fixed solid phase density.

The fixed density of the solid phase is an assumption that can be corrected for by allowing for adsorption of the neutral components at the interfaces between domains in the solid phase, as will be discussed later in this chapter.

Fig. 7.6 shows the boundary of the coexistence region for low values of the gas phase density. The figure refers to the case of equal charge density  $z_+/z_- = 1$ . The phase diagram shape depends of course on the relative strengths of the Coulomb interaction (through the charge density) and on cohesive/immiscibility parameter  $\epsilon$ . With increasing strength of the electrostatics,  $l_B/\sigma$ , the transition to a periodic microphase occurs at lower temperatures, while increasing values of the net interaction,  $\epsilon/T$ , requires higher temperatures. At higher surface densities, nonlinear corrections including short range correlations and ion association are necessary [155, 152].

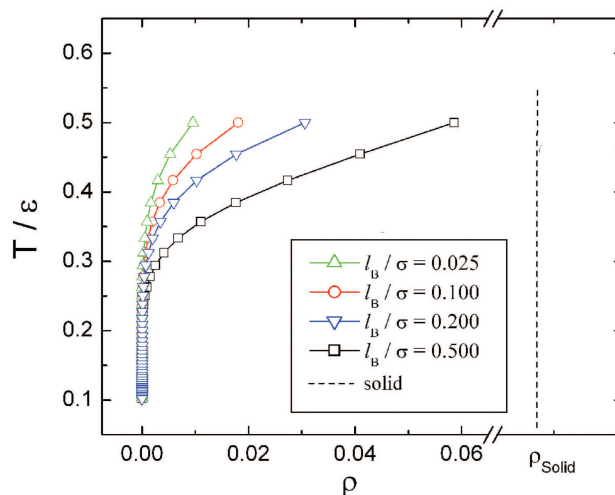


Figure 7.6. Phase diagram of the mixture. Location of solid-gas coexistence curves in  $\rho - T$  plane is shown for several different values of the Bjerrum length,  $l_B/\sigma$ . Increasing the Bjerrum length requires higher values of short range interactions,  $\varepsilon/T$ , for phase coexistence. The solid phase has constant density  $\rho_{solid}$ . The figure refers to the case of equal charge density  $z_+/z_- = 1$ , which forms a lamellar microphase.

For the coexistence of hexagonal solid domains with a gas phase, the free energy of the solid and gas phase slightly shift positions, so that the corresponding boundaries to the coexistence region are wider. This is because the free energy of the solid phase is correspondingly lower for asymmetric charge ratios. In Fig. 7.7 the boundaries for the asymmetric 3:1 case and symmetric 1:1 case are compared for different strengths of electrostatic interactions. However, this is not what is seen with molecular dynamics. The reasons for this discrepancy between theoretical results and simulations will be discussed later in this chapter.

And finally, consider the effect of external screening due to the salt in the outside solution,  $\kappa_{out}$ , for the symmetric system. The boundaries for this coexistence region are plotted in Fig. 7.8. In comparison with the coexistence of a lamellar phase with no external screening as shown in Fig. 7.6, the corresponding boundaries to the coexistence region are wider, so the

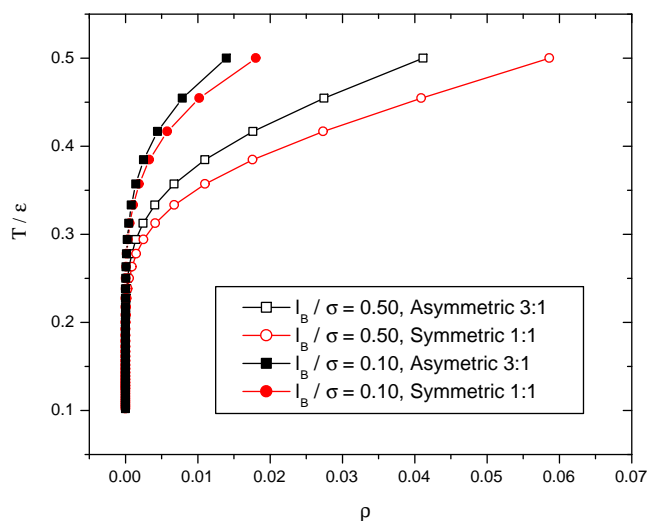


Figure 7.7. Phase diagram of asymmetric 3:1 and symmetric 1:1 mixtures for two different Bjerrum lengths. Increasing the asymmetry of the mixture requires lower values of short range interactions,  $\varepsilon/T$ , for phase coexistence. The solid phase has constant density  $\rho_{solid}$ .

external screening of the outside solution close to an interface actually favors the formation of multiple faces on the surface. This is an interesting result, which means that screening in the external solution will favor the creation of an interface between the solid and gas phases.

### 7.3. Molecular dynamics of phase coexistence

Coarse grained simulations have indicated liquid order disordered phases when considering the dipolar nature of the molecule [156], or else phase coexistence for mixed lipid bilayer systems (and subsequent effects on membrane curvature) [?, 157]. For constricted area interfaces, such as langmuir monolayers, evidence of a liquid vapor type coexistence has also been seen in simulations [158]. In this case, the competition between the electrostatics and short range van der Waals are both essential components to the model. Van der Waals

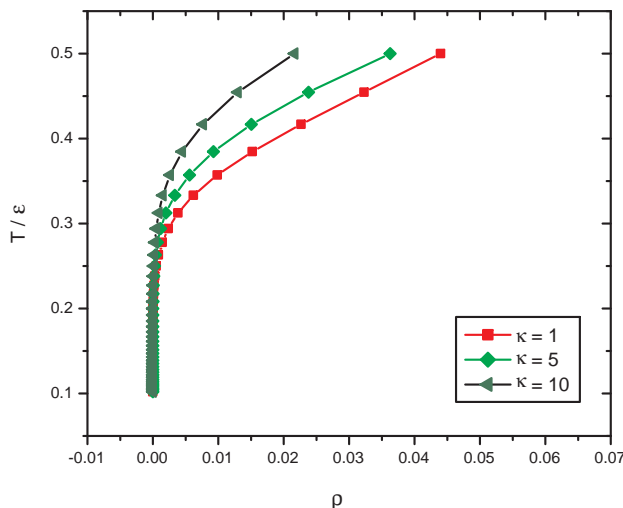


Figure 7.8. Phase diagram of for a symmetric 1:1 mixture for increasing values of  $\kappa$ , inverse screening length. Increasing  $\kappa$  requires lower values of short range interactions,  $\varepsilon/T$ , for phase coexistence. The solid phase has constant density  $\rho_{solid}$ .

interactions are described by the classic 6-12 Lennard Jones potential

$$(7.22) \quad U_{LJ} = 4\varepsilon \left( \left( \frac{\sigma}{r} \right)^{12} - \left( \frac{\sigma}{r} \right)^6 + C \right) \quad r < r_c$$

where the potential is cut at a radius  $r_c = 2.5\sigma$  and unshifted ( $C = 0$ ) for similarly charged molecules and the potential is shifted ( $C = \frac{1}{4}$ ) and cut at  $r_c = 2^{\frac{1}{6}}\sigma$  (allowing only for the repulsive part of the potential) for oppositely charged molecules, where  $\sigma$  is an effective molecular radius. The depth of the potential well,  $\varepsilon$ , entails a net immiscibility of magnitude  $\varepsilon$  between oppositely charged species. We consider a neutral and nonselective homogenous background and choose to model only the charged components. In this manner, multiple simulations of the phase behavior can be run that exactly incorporate the electrostatics. The model systems used are composed, in the symmetric case, of a mix of  $N_+ = 1000$  positively charged and  $N_- = 1000$  negatively charged units in a simulation box of size  $D^3$ ,

with  $D = 66\sigma$ . In the asymmetric case, the number of particles used were  $N_+ = 900$  and  $N_{3-} = 300$  particles. The molecules are confined to a plane perpendicular to the Z axis, with periodic boundary conditions in the X and Y directions. Constant N,V,T simulations were performed using the *Espresso* simulation package [159, 160]. Regions of the phase diagram at surface densities of  $\rho = \frac{(N_++N_-)\pi\sigma^2}{4D^2} = 0.36$  are explored. The potential between charges is a full Coulomb potential,  $U_C = \frac{l_B T q_1 q_2}{r}$ , calculated using the ELC method [37], which is a two dimensional correction to the P3M Ewald summation technique [124]. A Langevin thermostat is used to ensure constant temperature.

Late-time snapshots (after  $10^5$  MD timesteps, with  $\tau = .0125$ ) are shown in Fig. 7.10.

### 7.3.1. Phase coexistence and scaling

At small values of  $\varepsilon$  or low Bjerrum lengths (high temperature), positive and negative domains develop on the surface and, as the temperature decreases, the domains increase in size. In all the simulations, the individual molecular components exhibit a hexagonally close-packed structure (as was assumed in the analytical approach), with density fluctuations dependent on the temperature. For asymmetric charge ratios, at  $\rho = 0.10$ ,  $\frac{z_+}{z_-} = 1/3$ , in Fig. 7.10 a) note the formation of a hexagonally patterned 'island'. For larger densities, as in Fig. 7.10 b) the solid phase occupies a larger fraction of the space, but exhibits more clearly the ordering.

As shown in Fig. 7.10 c-d), for symmetric charge ratios,  $\frac{z_+}{z_-} = 1$  the preferred microstructure is lamellar. At the values of the parameters used, we observe as well the phase separation between solid patterned and neutral regions. The magnitude of  $\varepsilon$  increases from snapshot *c* to *d*, clearly modifies the fluctuations of both types of interfaces: between charged regions,

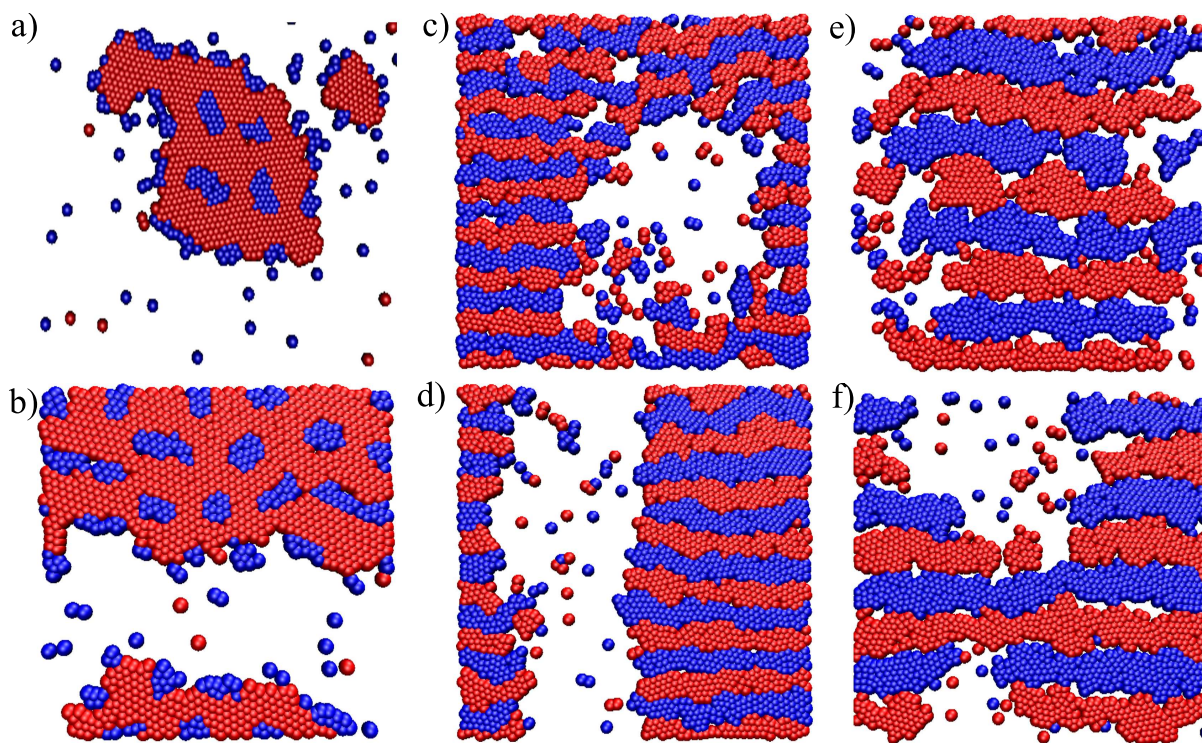


Figure 7.9. Simulation snapshots for systems with charge ratios, a-b)  $z_+/z_- = 1/3$  and c-f)  $z_+/z_- = 1$ . Frames a-b illustrate hexagonal order for different densities  $\rho_a = 0.10, \rho_b = 0.36$ . Frames c-d show the effect of increased immiscibility  $\varepsilon_c = 3.4k_B T, \varepsilon_d = 3.7k_B T$ , for a fixed Bjerrum length,  $l_B/\sigma = 0.5$ . Frames e-f show the transition from a homogeneous microphase to a phase segregated state for  $\varepsilon_e = 2.6k_B T, \varepsilon_f = 2.8k_B T$  for  $l_B/\sigma = 0.1$ .

and between the solid and neutral phases. At higher values (Fig. 7.10 d) the interfaces are much sharper and exhibit smaller shape fluctuations. A note and an interesting feature of the solid-gas interface: the orientation of the lamella is perpendicular to the interface. While the charged domains have symmetric interactions with the neutral region, the alignment must be a result of minimization of the local electrostatic energy. To some extent, this feature also appears in the asymmetric case, Fig. 7.10 a-b), where charged domains appear at the interface with the neutral domain.

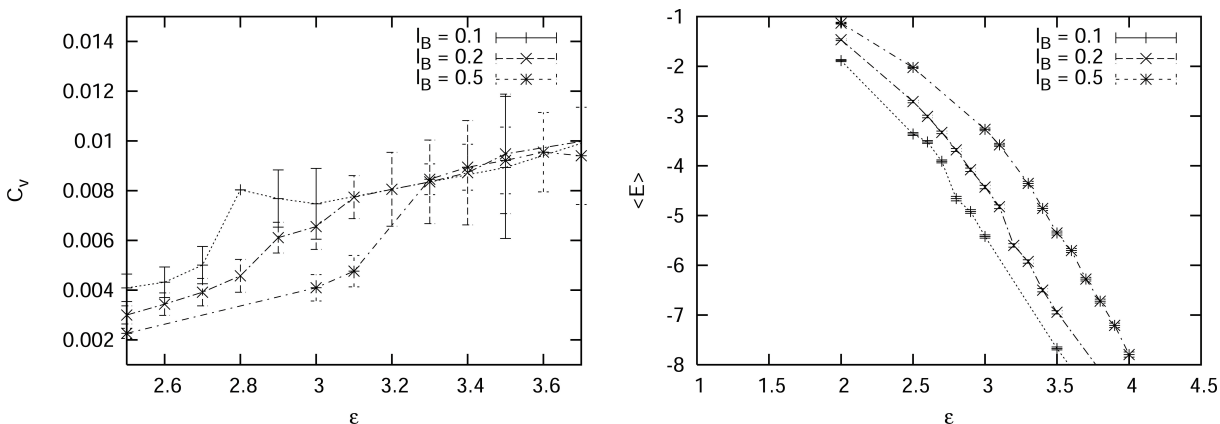


Figure 7.10. Heat capacity and average energy per particle for Bjerrum lengths ( $l_B/\sigma = 0.1, 0.2, 0.5$ ) as a function of  $\varepsilon$ . Peak in heat capacity corresponds with phase segregation of the mixture into periodic solid phase and low charge density gas phase.

Fig. 7.10 e-f) show the transition from a solid to a solid-gas coexistence phase for symmetric charge ratios, but for weaker electrostatic interactions. At low values of the cohesive energy  $\varepsilon$  the system shows the lamellar patterning but has large voids between the charged domains. An effective neutral component is attracted to the interfaces where it can reduce the effective line tension between domains. On further increase in the cohesive parameter, the coexistence region is reached, and the neutral regions segregate to form their own phase, as shown in Fig. 7.10 f). The lower values of the Bjerrum length in these cases produce larger lamellar sizes, compared with those of Fig. 7.10 c-d).

Upon examination of the phase behavior as in Fig. 7.10 f), one will notice that vacancy or minority components adsorb at the interface to decrease the interfacial energy [161, 162]). To compare the behavior observed in the simulations to theoretical results, this effect must be corrected for in the line tension. The density of the solid phase is calculated from simulations as shown in Fig. 7.11. With increasing short range attraction,  $\varepsilon$ , the density continuously

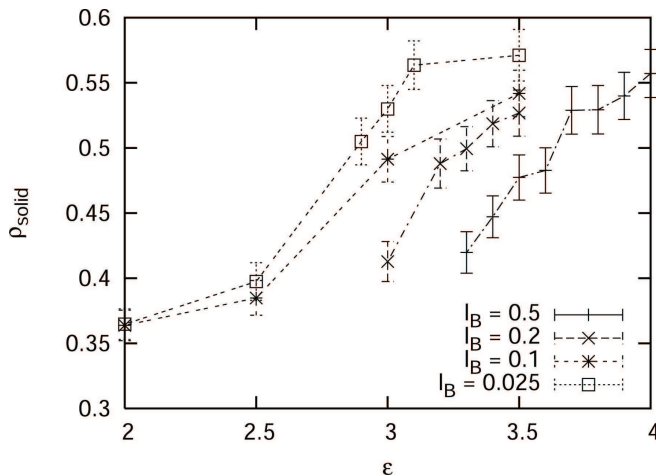


Figure 7.11. Surface density of the solid phase for a range of Bjerrum lengths,  $l_B/\sigma = 0.025 - 1$ , that correspond with values of interparticle attraction,  $\epsilon$ , after phase segregation has occurred in the system.

increases, but does not reach the value determined by the hexagonal close packing, if the distance between the particles is at the minimum in the interparticle potential. This factor needs to be accounted for.

At last, the assumption of a solid phase density fixed by the molecular radius, is abandoned. One can consider a line tension,  $\gamma$ , that scales with the particle density, proportional to the charge density, as  $\psi^{1/2}$ . Thus, the periodic length scale of the domains scales with the charge density as  $L = (\gamma/(l_B\psi^2))^{1/2} \sim (\epsilon/(l_B\psi^{3/2}))^{1/2}$ . This rescaling factors in the effect of vacancy adsorption at the interface at intermediate temperatures.

To study the scaling of the domain size in the symmetric case, the peak in the structure factor  $S(\vec{k}) = \langle \rho_k \rho_{-k} \rangle$ , is examined and compared with the behavior predicted by theory. The structure factor is the two dimensional Fourier transform of the correlation function of the charged components.  $S(\vec{k})$  displays a peak at values  $k^*$  corresponding to the inverse lamellar spacing in the direction perpendicular to the lamellas. The peak wavevector, for

the late stages of a number of simulations within the phase segregated state, over a wide range of  $l_B/\sigma \sim .01 - 1.$ , must scale as  $k^* \sim (\varepsilon/(l_B\psi^{3/2}))^{-1/2}$ . Indeed, in the simulations, the position of the peak wavevector can be fit through a line of slope  $-.47 \pm .02$  when plotted against the group  $\varepsilon/(l_B\psi^{3/2})$ , as shown in Fig. 7.12.

#### 7.4. Summary and conclusions

This chapter combines analytic techniques, both the Random Phase Approximation and strong segregation theory, to demonstrate the clear possibility of coexistence of structured ionic domains with a low charge density homogeneous phase. In addition, molecular dynamics simulations show that, with a simple rescaling of the line tension,  $\gamma$ , with charge density  $\psi^{1/2}$ , low temperature results can be extrapolated to intermediate temperature regimes. The competition between electrostatic and van der Waals interactions at the interface provides a guideline to generate well-controlled, self-assembled surface patterns. Phase segregation

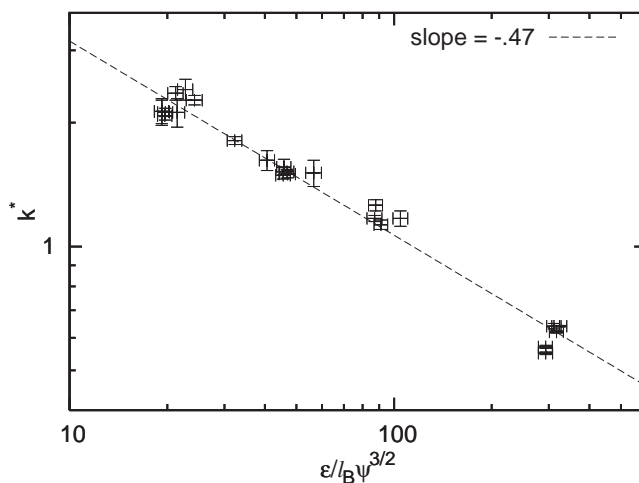


Figure 7.12. The location of the peak  $k^*$  in the structure factor  $S(\vec{k})$  as a function of  $\varepsilon/(l_B\psi^{3/2})$ . The linear fit shows agreement with the scaling predicted by strong segregation theory of power  $-0.5$ .

phenomena on surfaces and interfaces exhibits rich behavior. Ionic domains may be crucial to increase reaction rates among adsorbed biomolecules at liquid interfaces, a useful tool in biotechnology [163, 8] and important in some models of the origin of life [164].

### 7.5. Acknowledgements

I would again like to acknowledge Dr. Yuri Velichko for guidance with molecular dynamics simulations and analysis, and Dr. Francisco Solis for the development of the outline for analytic theory for phase coexistence. Portions of this chapter also appear in: "Charged particles on surfaces: Coexistence of dilute phases and periodic structures at interfaces," S. M. Loverde, F. Solis, and M. Olvera de la Cruz, *in review*, Physical Review Letters.

## CHAPTER 8

**Summary and Extension of Work to More Complex Systems****8.1. Summary**

During the course of this thesis, two topics concerning the self-assembly of polymers and polyelectrolytes are investigated. Polymer gels and polyelectrolyte self assembly on surfaces are both areas of research that display great promise for applications in the materials science community. As these areas of research continue to evolve and specialize, a greater degree of understanding concerning the self-organizational behaviors of polymers and polyelectrolytes will be necessary. In this thesis, computer simulation techniques are used in complement with theory to better understand their self-assembly behavior.

In an initial study, mean field theory and Monte Carlo techniques are used to gain insight into a classical theory of thermoreversible gelation. Two separate models of association are explored with Monte Carlo, a model of chemical association, for which well-defined theoretical models exist, as well as a model of physical association. Resulting thermodynamic and structural quantities of the two simulation models are then compared with those predicted by a mean field model of thermoreversible association. It is found that chemical association is well described by the mean field model, while, for the diffusion limited association model, the simulations results are not described well by theory.

In the following chapters, a model of competing electrostatic and short range van der Waals interactions for molecules strongly adsorbed to interfaces is explored. At low temperatures, the resulting phase diagram is shown in Fig. 8.1. For symmetric mixtures of immiscible, oppositely charged molecular components, strongly adsorbed to an interface, the minimum free energy corresponds to lamellar domains of oppositely charged components. For asymmetric mixtures, the minimum free energy consists of hexagonal domains. At high temperatures, by studying the transition from the ordered to the disordered state, different scaling is found for the size of the domains with respect to the strength of the electrostatics, and degree of immiscibility between the components.

Molecular dynamics simulations show that the periodic phases are stable at intermediate temperatures, and demonstrate that the electrostatics promotes interfacial ordering. Studying the formation of hexagonal domains, it is shown that at finite temperatures, the domains do not form in an isotropic manner. While at shorter length scales, the domains grow isotropically, the shape of the domains with larger areas grow in a linear manner. Upon examination of the structure factor,  $S(k)$ , the peak due to the local domain structure appears at shorter wavelengths, while at longer wavelengths there are some indications of finite size effects on the ordering of the domains. The fluctuations of the local inter domain structure are analyzed, using the Lindemann Criterion, and it is found that the local lattice structure is still liquid. However, upon changing the charge ratio of the molecular components, it is found that the fluctuations in the in the local domain structure decreases.

Next, the salt effects on pattern formation of a charged, patterned surface, as well as the effect of the charged surface on the concentration of multivalent salt in the medium, are examined. Both low and high temperature approaches are outlined, after which molecular

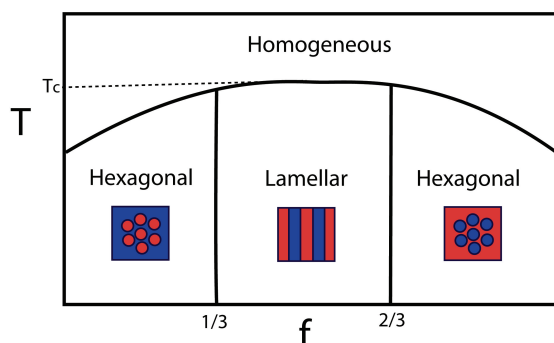


Figure 8.1. Phase diagram of the minimum free energy as a function of charge fraction,  $f$ , and temperature,  $T$ . At high temperatures the density is homogeneous. As temperature is decreased there is a transition temperature,  $T_c$ , at which a periodic phase forms. For charge fractions,  $1/3 < f < 2/3$ , the minimum free energy phase is lamellar. Outside this region the minimum free energy is hexagonal. Figure adapted from Solis et al.

dynamics simulations illustrate the melting to a phase segregated state. Simulations show that, when screening the Coulomb interactions, interfacial fluctuations become more prevalent. In addition, dislocations in the lamellar patterning are seen, which is consistent with mechanisms of melting predicated for systems displaying two dimensional order, known as the Kosterlitz Thouless Halperin Nelson and Young (KTHNY) transition. When considering the behavior of multivalent salt close to a fixed, heterogeneously charged substrate, one can consider the formation of a Wigner crystalline type phase, with adsorption at the center of the charged domains, as well as the interface between charged domains. Molecular dynamics show that these results can be extended to intermediate temperatures in Section 6.3.2, and illustrate the possibility of more complex mixed phases of salt near heterogeneous, patterned surfaces.

To investigate the phase behavior at low charge surface densities, both the Random Phase Approximation and strong segregation theory, are utilized. The boundaries of the two

phase coexistence region are constructed using the common tangent rule, for coexistence of a low charge density gas phase with a periodic, solid phase. The possibility of phase coexistence is explored with molecular dynamics simulations. It is indicated that, at intermediate temperatures, the neutral components, or vacancies, act to modify the interfacial region. In addition, molecular dynamics simulations show that, with a simple rescaling of the line tension with charge density, low temperature results can be extrapolated to intermediate temperature regimes.

The competition between electrostatic and van der Waals interactions at the interface provides a guideline to generate well-controlled, self-assembled surface patterns. These patterns, or microphases, can exist within a low density charged phase. The contribution of electrostatics to this possibility has been examined and determined to significantly affect the degree of interfacial ordering and the local structure of the domains. When examining the interactions of asymmetrically charged mixtures on the surface, such as a mixed group of polyelectrolytes, functionalized colloids, proteins, or surfactants, the electrostatic interactions, in addition to the immiscibility, may give rise to new length scales of self-assembly on the surface.

## 8.2. Extension of work to more complex systems

There are a multitude of directions to go with this work. One simple direction would be to consider the contribution to electrostatics for immiscible, charged mixtures for asymmetrically shaped or sized mixtures of polyelectrolytes. This would be directly applicable to the phase behavior of functionalized charged polystyrene spheres that have been found to form hexagonal phases on the surface of charged synthetic vesicles [141]. In these systems,

there are many degrees of freedom, including the degrees of freedom of the counterions, the polystyrene spheres, as well as the lipid diffusion and phase behavior on the surface of the vesicle [?]. While it would be interesting to see if the calculations in this work could be extending for these types of systems, in particular the possibility of phase coexistence, it is also necessary to understand the contribution of bending elasticity to these systems.

Extension of this work to incorporate the bending elasticity of an interface of membrane, would incorporate another contribution of the free energy of the interface. The elastic contribution to the free energy for a fluctuating, liquid membrane is well known to be [165, ?],

$$(8.1) \quad F_{elastic} = \int d^2r \left( \sigma + \frac{1}{2} \kappa_b (J - 2c_0)^2 + \kappa_g K \right),$$

where  $J = 1/R_1 + 1/R_2$ ,  $K = 1/(R_1 R_2)$ ,  $R_1$  and  $R_2$  are the radiuses of curvature.  $\kappa_b$  and  $\kappa_g$  are the bending modulus and the saddle splay modulus,  $\sigma$  is the surface tension, and  $c_0$  is the spontaneous curvature of the membrane. If the different molecular components display an affinity for different curvature regions, the local concentration will be coupled with the curvature. M. Seul and D. Andelman have considered what effects this will have on phase behavior in the weak segregation limit for a general system of competing interactions, and the resulting distortions this may have on the interface [110].

The phase behavior presented in this thesis is accurate when the interface of interest is non-fluctuating, when the bending modulus is sufficiently high so that equilibrium fluctuations are less than  $k_B T$ . When considering fluctuations, especially when incorporating electrostatic interactions, the situation gets more complex. For fluid membranes, the flexibility depends on the the specific interactions of the lipids, such as tail length, tilting, and

composition [166]. For mixed cationic and anionic lipids, pure Coulombic interactions are found to decrease the bending and Gaussian rigidity of membranes [150].

However, before tackling the behavior of cationic and anionic mixed membrane systems, it is necessary first to investigate the effects of electrostatics on bending elasticity with a single charged lipid composition. Mean field theory, without electrostatic correlations, indicates an increase in the bending rigidity [151]. Calculations considering electrostatic correlations of multivalent counterions on the surface of the membrane itself indicate that the formation of a Wigner crystalline phase on the surface can decrease the bending rigidity [167]. For multilayer membranes, the system is a complex mix of counterion effects, layer elasticity and flexibility, and electrostatic interactions [168]. Furthermore, it is indicated that the bending modulus is also dependent on lamellar spacing, with different scaling for different limits of the surface charge density [169]. These multilayer complexes would be extremely interesting to study, and have been gaining much attention recently.

Polyelectrolyte complexes, such as the complexation of oppositely charged polyelectrolytes as well as surfactants, have numerous biomedical and materials applications [3]. In particular, cationic lipid and DNA supramolecular assemblies have gained much attention in the polymer and materials science community [4, 170]. Recently, several additional highly charged biological macromolecules, such as F-actin [171] and the M13 virus, as well as molecularly engineered polypeptides [172] have been shown to form similar complexes. The stability of these complexes close to the isoelectric point has been considered theoretically [173, 174]. Moreover, the elastic properties of the underlying membrane have also been considered within mean field theory [175].

However, one key ingredient to the successful understanding of these systems, consists of accurate representation of the dielectric behavior of the medium close to the membrane surface. Several new methods [30, 31] exist that incorporate this possibility into Monte Carlo and molecular dynamics simulations, and it is of utmost importance to integrate these new techniques into the present simulations of polyelectrolyte self assembly.

### 8.3. Acknowledgements

Although the results are not discussed here, I would like to gratefully acknowledge Dr. Mark Stevens at Sandia National Laboratory, for guidance concerning the simulations of more complex multilamellar systems briefly discussed at the end of this chapter.

## References

- [1] J. Israelachvili. *Intermolecular and Surface Forces*. Academic Press, 1992.
- [2] D. Boal. *Mechanics of the Cell*. Cambridge University Press, 2002.
- [3] A. F. Thuenemann, Martin Mueller, Herbert Dautzenberg, Jean-Francois Joanny, and Hartmut Loewn. *Adv. Polym. Sci.*, 166:113, 2004.
- [4] C. R. Safinya. *Curr. Opin. Struct. Biol.*, 4:440, 2001.
- [5] E. Raspaud, I. Chaperon, A. Leforestier, and F. Livolant. *Biophys. J.*, 77:1547, 1999.
- [6] L. K. Sanders, C. Guáqueta, T. E. Angelini, J. W. Lee S. C. Slimmer, E. Luijten, and G. C. L. Wong. *Phys. Rev. Lett.*, in press.
- [7] R. Parthasarathy, P. A. Cripe, , and J. T. Groves. *Phys. Rev. Lett.*, 95:048101, 2005.
- [8] J. Groves. *Sci. STKE*, pe45, 2005.
- [9] M. Dubois, B. Deme, T. Gulik-Krzywicki, J. C. Debieu, C. Vautrin, E. Perez, and T. Zemb. *Nature*, 411:672, 2001.
- [10] M. Biesalski, R. Tu, and M. V. Tirrell. *Langmuir*, 21:5663–5666, 2005.
- [11] E. Kaler, K. Herrington, and A. Murthy. *Journal of Physical Chemistry*, 96:6698–6707, 1992.
- [12] D. C. Pozzo and L. M. Walker. *Macromolecular Symposia*, 227:203–210, 2005.
- [13] J. D. Hartgerink, E. Beniash, and S. I. Stupp. *Science*, 294:1684–1688, 2001.
- [14] M. D. Lefebvre, M. Olvera de la Cruz, and K. R. Shull. *Macromolecules*, 37:1118–1123, 2004.
- [15] A. E. Gonzalez. *Polymer*, 24:77, 1983.

- [16] P. J. Flory. Statistical mechanics of dilute polymer solutions. *Jour. Chem. Phys.*, 17:1347–1348, 1949.
- [17] M. Deserno. *Counterion Condensation for Rigid Linear Polyelectrolytes*. PhD thesis, Johannes Gutenberg-Universität, 2000.
- [18] R. N. Netz and D. Andelman. Neutral and charged polymers at interfaces. arXiv:cond-mat/0203364.
- [19] M. Rubinstein and A. V. Dobrynin. *Trends in Polymer Science*, 5:181–186, 1997.
- [20] A. M. Mayes and M. Olvera de la Cruz. Equilibrium domain spacing in weakly segregated block copolymers. *Macromolecules*, 24:3795, 1991.
- [21] M. Olvera de la Cruz.
- [22] D. Frenkel and B. Smit. *Understanding Molecular Simulation: From Algorithms to Applications*. Academic Press, 1996.
- [23] A. R. Leach. *Molecular Modelling: Principle and Applications*. Pearson Education Limited, 2001.
- [24] M. P. Allen and D. J. Tildesley. *Computer Simulation of Liquids*. Oxford Science Publications, 1987.
- [25] T. Soddeman, B. Dunweg, and K. Kremer. Dissipative particle dynamics: A useful thermostat for equilibrium and nonequilibrium molecular dynamics simulations. *Phys Rev E*, 68:046702, 2003.
- [26] G. S. Grest and K. Kremer. Molecular dynamics simulation for polymers in the presence of a heat bath. *Phys Rev A*, 33:3628–3631, 1986.
- [27] M. R. Hitchcock and C. K. Hall. Solid-liquid phase equilibrium for binary lennard-jones mixtures. *Journal of Chemical Physics*, 110:11433, 1999.
- [28] H. Friedman. *Molecular Physics*, 29:1533, 1975.
- [29] B. Hess, C. Holm, and N. van der Vegt. *Physical Review Letters*, 96:147801, 2006.
- [30] A. C. Maggs and V. Rossetto. *Physical Review Letters*, 88:196402, 2002.
- [31] Jorg Rottler and A. C. Maggs. *Physical Review Letters*, 93:170201, 2004.

- [32] S. W. de Leeuw, J. W. Perram, and E. R. Smith. Simulation of electrostatic systems in periodic boundary conditions. 1. lattice sums and dielectric constants. *Proceedings of the Royal Society of London Series A*, 373:27–56, 1980.
- [33] P. P. Ewald. *Ann. Rev.*, 1921, volume =.
- [34] T. Darden, D. York, and L. Pedersen. *J. Chem. Phys.*, 98:10089, 1993.
- [35] D. Parry. *Surf. Sci.*, 49:433, 1975.
- [36] R. Strebler and R. Sperb. *Mol. Simul.*, 27:61, 2001.
- [37] A. Arnold, J. Joannis, and C. Holm. *J. Chem. Phys.*, 117:2496–2502, 2002.
- [38] J. Joannis, A. Arnold, and C. Holm. *J. Chem. Phys.*, 117:2503–2512, 2002.
- [39] J. Lehn. Toward self-organization and complex matter. *Supramolecular Chemistry and Self-Assembly*, 295:2400–2403, 2002.
- [40] A. ten Cate and R.P. Sijbesma. Coils, rods and rings in hydrogen-bonded supramolecular structures. *Macromolecular Rapid Communications*, 23:1094–1112, 2002.
- [41] W. H. Binder, M. J. Kunz, C. Kluger, G. Hayn, and R. Saf. Synthesis and analysis of telechelic polyisobutylenes for hydrogen bonded supramolecular pseudo-block copolymers. *Macromolecules*, 37:1749–1759, 2004.
- [42] M. J. Kunz, G Hayn, R. Saf, and W. H. Binder. Hydrogen-bonded supramolecular poly(ether ketones)s. *Journal of Polymer Science Part A-Polymer Chemistry*, 42:661–674, 2004.
- [43] R. P. Sijbesma, F. H. Beijer, and L. Brunsveld. Reversible polymers from self-complementary monomers using quadruple hydrogen bonding. *Science*, 278:1601–1604, 1997.
- [44] L. Z. Rogovina and G. L. Slonimskii. Formation, structure, and properties of polymer gels. *Russian Chemical Reviews*, 43:503–523, 1974.
- [45] Z. Zhong, P. J. Dijkstra, J. Feijen, Y. Kwon, Y. H. Bae, and S. W. Kim. Synthesis and aqueous phase behavior of thermoresponsive biodegradable pol(d,l-3-methylglycolide)-block-poly(ethyleneglycol)-block-poly(d,l-3-methylglycolide) triblock copolymers. *Macromolecular Chemistry and Physics*, 203:1797–1803, 2002.

- [46] B. Jeong, Y. H. Bae, and S. W. Kim. Thermogelling biodegradable polymers with hydrophilic backbones:peg-g-plga. *Macromolecules*, 33:8317–8322, 2000.
- [47] Y. Chung, K. L. Simmons, A. Gutowska, and B. Jeong. Sol-gel transition temperature of plga-g-peg aqueous solutions. *Biomacromolecules*, 3:511–516, 2002.
- [48] J. Berret, D. Calvet, A. Collet, and M. Viguier. Fluorocarbon associative polymers. *Current Opinion in Colloid and Interface Science*, 8:297–306, 2003.
- [49] E. A. Fogleman, W. C. Yount, J. Xu, and S. L. Craig. Modular, well-behaved reversible polymers from dna-based monomers. *Ang. Chem. Int. Ed.*, 41:4026–4028, 2002.
- [50] A. Lendlein and R. Langer. Biodegradable, elastic shape-memory polymers for potential biomedical applications. *Science*, 296:1673–1676, 2002.
- [51] R. A. L. Jones. *Soft Condensed Matter*. Oxford University Press, 2002.
- [52] M. Daoud, E. Bouchaud, and G. Jannink. Swelling of polymer gels. *Macromolecules*, 19:1955–1960, 1986.
- [53] D. Stauffer and A. Aharony. *Introduction to Percolation Theory*. Taylor and Francis.
- [54] P. G. de Gennes. *Scaling Concepts in Polymer Physics*. Cornell University Press, 1979.
- [55] W. H. Stockmayer. Theory of molecular size distribution and gel formation in branched-chain polymers. *J. Chem. Phys.*, 11:45–55, 1943.
- [56] P. J. Flory. Molecular size distribution in three dimensional polymers. ii. trifunctional branching units. *Journal of the American Chemical Society*, 63:3091–3096, 1941.
- [57] H. Jacobson and W. H. Stockmayer. Intramolecular reaction in polycondensations. i. the theory of linear systems. *J. Chem. Phys.*, 18(12):1600–1612, 1950.
- [58] P. J. Flory. Molecular size distribution in three dimensional polymers. i. gelation. *Journal of the American Chemical Society*, 63:3083–3091, 1941.
- [59] A. N. Semenov and M. Rubinstein. Thermoreversible gelation in solutions of associative polymers. 1. statics. *Macromolecules*, 31:1373–1385, 1998.
- [60] F. Tanaka. Thermodynamic theory of network-forming polymer solutions. 2. equilibrium gelation by conterminous cross-linking. *Macromolecules*, 23:3790–3795, 1990.

- [61] A. V. Ermoshkin and I. Erukhimovich. Towards a statistical theory of associating telechelics: Equilibrium molecular structural distribution and one-cluster scattering. *J. Chem. Phys.*, 110:1781–1793, 1999.
- [62] I. Erukhimovich and A. V. Ermoshkin. Phase diagrams classification of thermoreversibly associating systems with due regard for mesoscopic cyclization effects. *J. Chem. Phys.*, 116:368–383, 2002.
- [63] M. Ishida and F. Tanaka. Theoretical study of the postgel regime in thermoreversible gelation. *Macromolecules*, 30:3900–3909, 1997.
- [64] I. Erukhimovich. Statistical theory of the sol-gel transition in weak gels. *JETP*, 81:1004–1030, 1995.
- [65] I. Erukhimovich, M. V. Thamm, and A. V. Ermoshkin. *Macromolecules*, 34:5653–5674, 2001.
- [66] J. Dudowicz, K. Freed, and J. F. Douglas. *Physics Review Letters*, 92:045502, 2004.
- [67] J. Dudowicz, K. Freed, and J. F. Douglas. *J. Chem. Phys.*, 119:12645–12666, 2003.
- [68] A. V. Dobrynin. *Macromolecules*, 37:3881–3893, 2004.
- [69] P. G. Khalatur et al. Molecular dynamics study of the solution of semiflexible telechelic polymer chains with strongly associating end-groups. *J. Chem. Phys.*, 110(6039-6049), 1999.
- [70] S. K. Kumar and J. F. Douglas. Gelation in physically associating polymer solutions. *Physical Review Letters*, 87:188301–1, 2001.
- [71] B. Bedrov, G. D. Smith, and J. F. Douglas. Influence of self-assembly on dynamica and viscoelastic properties of telechelic polymer solutions. *Europhysics Letters*, 59:384–390, 2002.
- [72] C. Chen and E. E. Dormidontova. Ring-chain equilibrium in reversibly associated polymer solutions: Monte carlo simulations. *Macromolecules*, 37:3905–3017, 2004.
- [73] J. P. Wittmer, A. Milchev, and M. E. Cates. Dynamical monte carlo study of equilibrium polymers: Static properties. *J. Chem. Phys.*, 109:834–845, 1998.
- [74] A. Milchev and D. P. Landau. Monte carlo study of semiflexible living polymers. *Physical Review E*, 52:6431–6441, 1995.

- [75] J. P. Wittmer, P. van der Schoot, A. Milchev, and J. L. Barrat. Dynamical monte carlo study of equilibrium polymers. ii. the role of rings. *J. Chem. Phys.*, 113:6992–7005, 2000.
- [76] A. Milchev, J. P. Wittmer, and D. P. Landau. Dynamical monte carlo study of equilibrium polymers: Effects of high density and ring formation. *Physical Review E*, 61:2959–2966, 2000.
- [77] P. J. Flory, U. W. Suter, and M. Mutter. Macrocyclization equilibria. 1. theory. *Journal of the American Chemical Society*, 98:5733–5739, 1976.
- [78] I. M. Lifshitz. Some problems of the statistical theory of biopolymers. *JETP*, 28:1280–1286, 1969.
- [79] D. Chandler. *J. Chem. Phys.*, 68:2959–2970, 1978.
- [80] J. P. Hansen and I. R. McDonald. *Theory of Simple Liquids*. Academic Press, 1986.
- [81] A. M. Puertas, M. Fuchs, and M. E. Cates. *Physics Review Letters*, 88:098301, 2002.
- [82] E. Zaccarelli, G. Foffi, K.A. Dawson, S. V. Buldyrev, F. Sciortino, and P. Tartaglia. *Phys. Rev. E*, 66:041402, 2002.
- [83] A. Yethiraj and A. van Blaaderen. *Nature*, 421:513, 2003.
- [84] M. Fasolo and P. Sollich. *Physics Review Letters*, 91:0683013, 2003.
- [85] K. Kroy, M. E. Cates, and W. C. K. Poon. *Physics Review Letters*, 92:148302, 2004.
- [86] F. A. Escobedo and J. J. De Pablo. Molecular simulation of polymeric networks and gels: Phase behavior and swelling. *Physics Reports*, 318:85–112, 1999.
- [87] Y. B. Huang, I. Szleifer, and N. A. Peppas. *Macromolecules*, 35:1373–1380, 2002.
- [88] J. F. Liu and W. A. Ducker. *J. Phys. Chem. B*, 103:8558, 1999.
- [89] G. S. Grest and K. Kremer. Growth of double-chained cationic surfactant films on mica. *A. Blom, G. G. Warr, and E. J. Wanless*, 59:381–385, 2006.
- [90] G. Srinivas, S. O. Nielsen, P. B. Moore, and M. L. Klein. Molecular dynamics simulations of surfactant self-organization on the solid-liquid interface. *Jour. American Chem. Soc.*, 128:848–853, 2006.

- [91] D. K. Schwartz. Mechanism and kinetics of self assembled monolayer formation. *Annu. Rev. Phys. Chem.*, 2001.
- [92] M. Seul and M. J. Sammon. *PRL*, 64:1903–1906, 1990.
- [93] W. M. Heckl, D. A. Cadenhead, and H. Mohwald. *Langmuir*, 4:1352–1358, 1988.
- [94] V. T. Moy, D. J. Keller, and H. M. McConnell. *Jour. Phys. Chem.*, 92:5233–5238, 1988.
- [95] D. Andelman, F. Brochard, and J. Joanny. *Physical Review Letters*, 86:1151–1157, 1987.
- [96] H. M. McConnell. *PNAS*, 86:3452–3455, 1989.
- [97] P. Jokela, B. Jónsson, and A. Khan. *J. Phys. Chem.*, 91:3291, 1987.
- [98] E. W. Kaler, K. L. Herrington, A. K. Murthy, and J. A. N. Zasadzinski. *J. Chem. Phys.*, 96:6698, 1992.
- [99] L. Brasher, K. Herrington, and E. Kaler. *Langmuir*, 11:4267, 1995.
- [100] T. Zemb, M. Dubois, B. Demé, and T. Gulik-Krzywicki. *Science*, 283:816, 1999.
- [101] P. A. Beals, V. D. Gordon, Z. Zhao, S. U. Egelhaaf, and W. C. K. Poon. *J. Phys: Condens. Matter*, 17:S3341, 2005.
- [102] M. Biesalski, R. Tu, and M. Tirrell. *Langmuir*, 21:5663, 2005.
- [103] D. J. Keller, J. P. Korb, and H. M. McConnell. *J. Phys. Chem.*, 91:6417–6422, 1987.
- [104] T. Garel and S. Doniach. *Phys. Rev. B.*, 26:325–329, 1982.
- [105] S. C. Glotzer, E. A. Di Marzio, and M. Muthukumar. *Physical Review Letters*, 74:2034–3036, 1995.
- [106] R. Jamei, S. Kivelson, and B. Spivak. *Physical Review Letters*, 94:056805, 2005.
- [107] L. Leibler. *Macromolecules*, 13:1602–1617, 1980.
- [108] T. Yamaue, T. Tanaguchi, and M. Doi. The simulation of the swelling and deswelling dynamics of gels. *Molecular Physics*, 102:167–172, 2004.

- [109] J. Maskawa, T. Takeuchi, K. Maki, K. Tsujii, and T. Tanaka. Theory and numerical calculation of pattern formation in shrinking gels. *Journal of Chemical Physics*, 110:10995–10998, 1999.
- [110] M. Seul and D. Andelman. Domain shapes and patterns: The phenomenology of modulated phases. *Science*, 267:476–483, 1995.
- [111] S. Schneider and G. Gompper. *Europhysics Letters*, 70:136, 2005.
- [112] R. Lipowsky and R. Dimova. *J. Phys: Condens. Matter*, 15:S31, 2003.
- [113] P. Pieranski. *Phys. Rev. Lett.*, 45:136, 1980.
- [114] R. Netz. Debye hueckel theory for interfacial geometries. *Physical Review E*, 60:3174–3182, 1999.
- [115] A. J. Wagner and S. May. *arXiv:cond-mat/0607733*, 2006.
- [116] U. Loew, V. J. Emery, K. Fabricius, and S. A. Kivelson. *Physical Review Letters*, 72:1918–1921, 1994.
- [117] Y. S. Velichko and M. Olvera de la Cruz. *Phys. Rev. E*, 72:041920, 2005.
- [118] F. J. Solis, S. I. Stupp, and M. Olvera de la Cruz. *J. Chem. Phys.*, 122:054905, 2005.
- [119] P. M. Chaikin and T. C. Lubensky. *Principles of Condensed Matter Physics*. Cambridge University Press, 1995.
- [120] P. Gonzalez-Mozuelos and M. Olvera de la Cruz. *J. Chem. Phys.*, 100:507–517, 1994.
- [121] B. Y. Borue and I. Y. Erukhimovich. *Macromolecules*, 21:3240–3249, 1988.
- [122] M. Olvera de la Cruz, L. Belloni, M. Delsanti, J. P. Dalbiez, O. Spalla, and M. Drifford. *J. Chem. Phys.*, 103:5781–5791, 1995.
- [123] S. Prestipino, F. Saija, and P. V. Giaquinta. *Physical Review E*, 71:050102, 2005.
- [124] R. W. Hockney and J. W. Eastwood. *Computer Simulation Using Particles*. A. Hilger, 1988.
- [125] A. Jaster. *Physical Review E*, 59:2594–2602, 1999.
- [126] A. D. Stoycheva and S. J. Singer. *Physical Review Letters*, 84:4657–4660, 2000.

- [127] H. M. McConnell and V. T. Moy. *J. Phys. Chem.*, 92:4520–4525, 1988.
- [128] J. M. Ziman. *Principles of the Theory of Solids*. Cambridge University Press, 1972.
- [129] R. E. Peierls. *Helv. Phys. Acta*, 177:81, 1923.
- [130] R. E. Peierls. *Ann. Inst. Henri Poincare*, 5:177, 1935.
- [131] L. D. Landau. *Phys. Z. Sowjet.*, 11:26, 1937.
- [132] N. D. Mermin. *Physical Review*, 176:250, 1968.
- [133] J. M. Kosterlitz and D. J. Thouless. Long range order and metastability in two dimensional solids and superfluids. *J. Phys C.*, 5:L124, 1972.
- [134] J. M. Kosterlitz and D. J. Thouless. Ordering, metastability, and phase transitions in two-dimensional systems. *J. Phys. C.*, 6:1181, 1973.
- [135] B. I. Halperin and D. R. Nelson. Theory of two-dimensional melting. *Physical Review Letters*, 41:121, 1978.
- [136] D. R. Nelson and B. I. Halperin. Dislocation-mediated melting in two dimensions. *Physical Review B*, 19:2457, 1979.
- [137] X. H. Zheng and J. C. Earnshaw. On the lindemann criterion in 2d. *Europhysics Letters*, 41:635, 1998.
- [138] J. Liu, S. Qi, J. T. Groves, and A. K. Chakraborty. *J. Phys. Chem. B.*, 109:19960–19969, 2005.
- [139] R. Kjellander and S. Marcelja. Correlation and image charge effects in electric double layers. *Chem. Phys. Lett.*
- [140] I. Rouzina and V. Bloomfield. Macroion attraction due to electrostatic correlation between screening counterions. 1. mobile surface-adsorbed ions and diffuse ion cloud. *J. Phys. Chem.*
- [141] L. Ramos, T. C. Lubensky, N. Dan, P. Nelson, and D. A. Weitz. *Science*, 286:2325, 1999.
- [142] J. A. Zasadzinski, E. Kisak, and C. Evans. *Current Opinion in Colloid and Interface Science*, 6:85, 2001.
- [143] R. Sperb. *Mol Sim.*, 20:179, 1998.

- [144] Y. Levin and M. E. Fisher. *Physica A*, 225:164, 1996.
- [145] Q. Yan and J. de Pablo. *Phys. Rev. Lett.*, 88:095504, 2002.
- [146] S. L. Veatch and S. L. Keller. *Physical Review Letters*, 89:268101, 2002.
- [147] D. Zhang, M. A. Carignano, and I. Szleifer. *Physical Review Letters*, 96:028701, 2006.
- [148] C. Huang and M. Olvera de la Cruz. Adsorption of a minority component in polymer blend interfaces. *Phys. Rev. E.*, 53:812, 1996.
- [149] M. Castelnovo and J. F. Joanny. *Eur Phys. J. E.*, 6:377, 2001.
- [150] A. W. C. Lau and P. Pincus. *Physical Review Letters*, 81:1338, 2004.
- [151] M. Winterhalter and W. Helfrich. *J. Phys. Chem.*, 96:327, 1992.
- [152] A. V. Ermoshkin and M. Olvera de la Cruz. *Macromolecules*, 36:7824–7832, 2003.
- [153] S. M. Loverde, Y. S. Velichko, and M. Olvera de la Cruz. *J. Chem. Phys.*, 124:144702, 2006.
- [154] C. H. P. Lupis. *Chemical Thermodynamics of Materials*. North-Holland, 1983.
- [155] P. Gonzalez-Mozuelos and M. Olvera de la Cruz. *Journal of Chemical Physics*, 118:4684–4691, 2003.
- [156] L. Saiz and M. L. Klein. Electrostatic interactions in a neutral model phospholipid bilayer by molecular dynamics simulations. *Journal of Chemical Physics*, 116:3052, 2002.
- [157] I. A. Cooke and M. Deserno. Coupling between lipid shape and membrane curvature. *Biophysical Journal*, 91:487, 2006.
- [158] S. O. Nielson, C. F. Lopez, P. B. Moore, J. C. Shelley, and M. L. Klein. Molecular dynamics investigations of lipid langmuir monolayers using a coarse-grain model. *J. Phys. Chem. B.*, 107:13911, 2003.
- [159] ESPResSo-homepage, <http://www.espresso.mpg.de>, 2002-2005.
- [160] H. J. Limbach, A. Arnold, B. A. Mann, and C. Holm. *Comp. Phys. Comm.*, 174:704, 2006.
- [161] C. Huang, P. W. Voorhees, and M. Olvera de la Cruz. *Acta Mater*, 47:4449, 1999.

- [162] C. Huang. *Studies of Phase Separation Dynamics and Interfaces in Ternary Systems*. PhD thesis, Northwestern University, 1996.
- [163] A. Goldar and J. L. Sikorav. *European Physical Journal E*, 14:211, 2004.
- [164] L. Onsager. *The Collected Works of Lars Onsager: with commentary*. World Scientific Publishing Co, 1996.
- [165] W. Helfrich. *Z. Naturforsch*, 28:693–703, 1973.
- [166] M. J. Stevens. *Journal of Chemical Physics*, 121:11942, 2004.
- [167] T. T. Nguyen, I. Rouzina, and B. I. Shklovskii. *Phys. Rev. E.*, 60:7032, 1999.
- [168] D. Harries, R. Podgornik, V. A. Parsegian, E. M. Mar-or, and D. Andelman. *J. Chem. Phys.*, 124:224702, 2006.
- [169] C. Holm, P. Kekicheff, and R. Podgornik, editors. *Electrostatic Effects in Soft Matter and Biophysics*. Kluwer Academic Publishers, 2001.
- [170] I. Koltover, K. Wagner, and C. R. Safinya. *PNAS*, 97:14046, 2000.
- [171] G. C. L. Wong et al. Hierarchical self-assembly of f-actin and cationic lipid complexes: Stacked three-layer tubule networks. *Science*, 288:2035–2039, 2000.
- [172] I. Koltover, S. Sahu, and N. Davis. *Angew. Chem. Int. Ed.*, 43:4034, 2004.
- [173] D. Harries, S. May, W. M. Gelbart, and A. Ben-Shaul. *Biophysical Journal*, 75:159–173, 1998.
- [174] R. Bruinsma. *Eur. Phys. J. B.*, 4:75, 1998.
- [175] A. Shafir and D. Andelman. *Soft Matter*, 2007.

## Vita

Sharon Marie Loverde, was born in Chicago, IL on July 5, 1979. Her mother, Joyce Anne Loverde (maiden name Gazdic), and father, Michael Salvatore Loverde, were also born in Chicago, IL. In fact, both the Loverde and Gazdic family tree have a long Chicago history, with two grandparents attending Depaul University and one attending University of Illinois, Urbana-Champaign. She has one younger sister, Gina Marie Loverde, and one younger brother, David Michael Loverde, both of whom she is very proud. She attended James B. Conant High School in Schaumburg, IL, graduating in June of 1997 as Salutatorian. In May of 2001, Sharon graduated from University of Illinois in Urbana-Champaign with a B.S. in Physics and a Minor in Math. Still staying close to home, Sharon decided to switch to an engineering program and began working on her PhD in Materials Science and Engineering at Northwestern University with her advisor Monica Olvera de la Cruz. In her first year, she obtained a background in genetic engineering and molecular biology. Switching gears a bit, Sharon began studying the art of computer simulations, and, extended previous knowledge of statistical mechanics by learning about charged systems. During the last several years of her thesis research, Sharon learned several things—her love of travel, as well as the importance of both creativity and persistence in science and engineering. After completing her PhD work, Sharon remains optimistic and inspires to continue research at the postdoctoral level, for the first time in a zip code outside Illinois. As for the future beyond that, she desires the

continued presence of both creativity and science in her life. She also imagines she might need to work a bit more on her Turkish.